CANCER CELL ENCAPSULATION

Yaride Pérez Pacheco

UNIVERSITAT ROVIRA i VIRGILI

CANCER CELL ENCAPSULATION

Yaride Pérez Pacheco

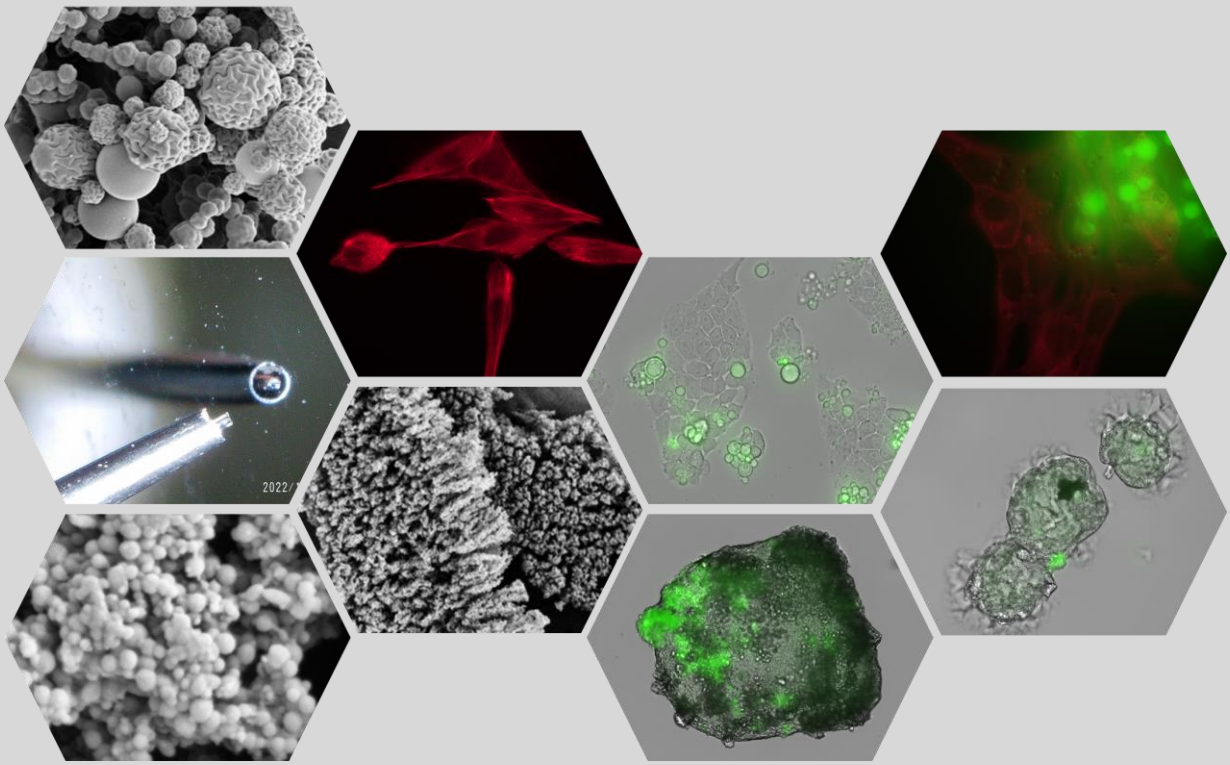

DOCTORAL THESIS
2023

Yaride Pérez Pacheco

CANCER CELL ENCAPSULATION

DOCTORAL THESIS

Department of Chemical Engineering

UNIVERSITAT ROVIRA i VIRGILI

Tarragona, Spain

2023

CANCER CELL ENCAPSULATION

DOCTORAL THESIS

Supervised by

Dr. Ricard Garcia Valls

Dr. Joan Rosell Llompart

Dr. Bartosz Tylkowski

Department of Chemical Engineering

UNIVERSITAT ROVIRA i VIRGILI

Tarragona, Spain

2023

UNIVERSITAT ROVIRA i VIRGILI

Departament d'Enginyeria Química
Campus Sescelades
Avda. Països Catalans, 26
43007 Tarragona
Tel.: 977 55 97 87
Fax: 977 55 96 21

Ricard Garcia Valls, Director of EURECAT and Associate Professor at Rovira i Virgili University, Departament d'Enginyeria Química.
Joan Rosell Llompart, ICREA Research Professor at Rovira i Virgili University, Departament d'Enginyeria Química.
Bartosz Tylkowski, Head of encapsulation and membrane technologies at chemical Technologies Unit at Eurecat.

WE STATE that the present study, entitled "Cancer Cell Encapsulation", presented by Yaride Pérez Pacheco for the award of the degree of Doctor, has been carried out under our supervision at the chemical Engineering Department at Rovira i Virgili University, and that it fulfils all the requirements to be eligible for Doctor International Mention.

Tarragona, August 2023

Supervisors of the Thesis

Dr. Ricard Garcia Valls

Dr. Joan Rosell Llompart

Dr. Bartosz Tylkowski

ACKNOWLEDGEMENTS

I would like to express my heartfelt gratitude to my supervisors, Prof. Dr. Ricard Garcia Valls, Dr. Miquel Sisteré, Dr. Bartosz Tylkowski and Prof. Joan Rosell-Llompart for their invaluable expertise, insightful ideas, constructive feedback, and unwavering support throughout the completion of this thesis.

I extend my warmest thanks to all the members of the MEMTEC group, as well as my office colleagues and friends, Dr. Marta Giamberini, Dr. Antonio Reina, Dr. Alberto Puga, Dr. Ania T., Dr. Adriana, Dr. Magda, Dr. Xavier, Dr. Monica, Belén, Yousefe, Anna, Jonas, Tahere, Tiziano, Jordi, Your collaboration and camaraderie have been truly appreciated.

I am deeply grateful for the support and assistance provided by the DEW group members, office colleagues, and friends, including Dr. Eszter Bodnár, Elena Barbero, Dr. Laura Escorihuela, Paula Martínez, María Laura and Deepak Parajuli.

I would like to express my sincere appreciation to Tiziano Alimandi for his contribution to Chapter 2. Elena Barbero and Eszter Bodnár for their contributions to the experiments corresponding to Chapters 3, as well as to Dr. Łukasz Kaźmierski and Dr. hab. Małgorzata Maj for their assistance with the experiments in Chapters 4.

I am also thankful to the Servei Tecnic of URV for their kindness and support during my doctoral research, which greatly enhanced my knowledge and experience. Special thanks to Mariana, Rita, Merce, Nuria, and Sergí.

I would like to acknowledge Núria Juanpere and Prof. Alex Fragoso for making this journey more enjoyable and memorable.

I want to thank to my unconditionally friends Ángel, Deysi, Carlos Bathuel, Carlos Jesús, Elena, Nerea, Oriana and all those people who I enjoy their company. Also, to my flat mates Kata, Shean and Blanca for their emotional supporting during writing.

Special thanks go out to all the individuals who believed in me along this path.

I want to recognize the use of software to create chemical structures using ACD/ChemSketch (Freeware) free Version Copyright© 1994-2008, Product version: 11.02 (Build 25941, 21 May 2008). Software medusa Make Equilibrium diagrams Using Sophisticated Algorithms, windows interface to the MS-DOS versions of INPUT SED and PREDOM (FORTRAN programs drawing chemical equilibrium diagrams). The plots were generated using OriginPro 8.5.0 SRI b161 Copyright© 1991-2010. Additionally, artificial intelligence software was used to correct grammar.

I am grateful to the Spanish Government for providing funding for this project through grants.

Lastly, I want to express gratitude to myself for never giving up and persevering in pursuit of my dreams and passions. It is through my determination and commitment that I have been able to overcome challenges and keep moving forward. I will continue to embrace my aspirations, knowing that hard work and perseverance are the keys to achieving success and fulfillment.

THIS WORK IS DEDICATED TO

My mom Fanny Pacheco Jiménez.

My father Manuel Salvador Pérez Pérez, siblings, nieces and nephews.

The cherished memory of my nephew Nicolás Ascanio Pérez, whose aspirations to become a scientist were cut short. However, his unwavering spirit of curiosity and ambition lives on, forever inspiring us and reminding us of the potential that lies within each of us.

.

CONTENTS

SUMMARY

This thesis shows a general view of the investigation of the production and evaluation of chitosan/sodium tripolyphosphate (CS/TPP) microcapsules and nanocapsules for further characterizations in simulated physiological environments in order to study the interaction of some of the capsules with the normal and cancer cell lines. Several important findings were obtained from the research, providing valuable insights into their physicochemical properties and potential applications.

Two methodologies to produce CS/TPP capsules were used. Firstly, regarding the production of CS/TPP microcapsules using a spray drier, it was observed that the method resulted in a broad size distribution ranging from 0.8 µm to 50 µm. To optimize the size distribution, parameters such as nozzle size, atmospheric gas, and pressure could be further optimized. The inlet temperature during the spray drying process was found to significantly affect the properties of the microcapsules. Low air inlet temperatures led to high-density membranes, high moisture content, low fluidity, and ease of agglomeration. On the other hand, extremely high inlet temperatures above 170 °C caused vaporization and membrane cracks, leading to premature degradation of the microcapsule integrity.

The behavior of CS/TPP microcapsules in different pH solutions was investigated, and it was found that the presence of TPP crosslinker provided stability across a wide range of pH values up to pH 4.5. In contrast, chitosan capsules alone were more pH-sensitive and prone to dissolution at low pH values. The protonation of chitosan's amino groups under acidic conditions increased the electrostatic repulsion between polymer chains, making them more soluble and susceptible to dissolution. However, the physical crosslinking of CS chains in the presence of TPP contributed to the microcapsules' ability to maintain their structure in response to pH changes below 6.5.

The surface charge and release behavior of CS/TPP microcapsules containing folic acid (FA) were also examined. It was found that the surface charge of the microcapsules was pH-dependent, with higher zeta potential at low pH values, indicating increased surface charge and enhanced dispersion stability. The presence of FA on the microcapsule surface further increased the surface charge due to its cationic nature, improving dispersion stability. The release profile of FA was influenced by the surrounding media. In phosphate buffer solution, FA exhibited a higher release rate, while in lactate buffer solution, the microcapsules retained their swollen state and exhibited a lower release rate. This suggested that the attachment of FA to the CS/TPP crosslinked chains was more effective in the presence of lactate buffer.

Secondly, during the development of this thesis we decided to explore the production of CS/TPP nanocapsules using electrospray, due to several advantages over spray drying, like high production efficiency, controlled size dispersion, tailor morphology. Several approaches and techniques were employed to produce nanoparticles and enhance crosslinking between CS and TPP by conservation, ionotropic gelation and spraydrier. A methodology of coaxial electrospray was developed to achieve homogeneous and CS/TPP crosslinked nanocapsules which was the first time achieved with this technique. The shape of the Taylor cone, protrusion, and nozzle configuration were improved to maintain stability and enhance crosslinking. The resulting nanocapsules exhibited a spherical morphology and low size distribution and size, and demonstrated prolonged stability in solution.

In vitro experiments involving BJ (normal) and SCLII (cancer) cell lines and the CS/TPP nanocapsules and microcapsules were conducted to investigate their effects on cell viability and interactions. The cell lines showed a high survivability rate when treated with the capsules, indicating their compatibility and resilience. The interaction between the capsules and cells varied depending on the experimental setup. In 2D cell growth systems, the interaction was less pronounced, while in 3D

cell growth systems using spheroids, the capsules demonstrated remarkable attachment to the cells, mimicking in vivo conditions and enhancing the physiological relevance of the model. The capsules influenced cellular behavior and fate, leading to various outcomes such as cell expansion, mitosis, and cell death.

LIST OF PUBLICATIONS AND CONFERENCES

Publications

X. Montané, K. Matulewicz, K. Balik, P. Modrakowska, M. Łuczak, Y. Pérez Pacheco, B. Reig Vano, J.M. Montornés, A. Bajek and B. Tylkowski "Present trends in the encapsulation of anticancer drugs" Physical Sciences Reviews 8, no. 2 (2023): 327-344. https://doi.org/10.1515/psr-2020-0080

Yaride Pérez-Pacheco, Tiziano Alimandi, Bartosz Tylkowski, Miquel Sisteré, Ricard García-Valls. Chitosan-TPP microcapsules for controlled drug reléase. journal Afinidad IQS. To be submited.

Patent application

Patent application P202330717. Reception date: August 28, 2023. Receiving office: OEPM Madrid. Reference: 2021/33580. Title: COMPOSITION OF CATIONIC POLYMER AND TRIPOLYPHOSPHATE NANOPARTICLES FOR USE AS A MEDICINAL PRODUCT AND MANUFACTURING PROCEDURE OF NANOPARTICLES “COMPOSICIÓN DE NANOPARTÍCULAS DE POLIMERO CATIÓNICO Y TRIPOLIFOSFATO PARA SU USO COMO MEDICAMENTO Y PROCEDIMIENTO DE FABRICACIÓN DE LAS NANOPARTÍCULAS”. Country Spain. Applicants: Yaride Pérez Pacheco, Ricard Garcia Valls, Joan Rosell Llompart, Miquel Sisteré and Eszter Bornár.

Book chapter

X. Montané, K. Matulewicz, K. Balik, P. Modrakowska, M. Łuczak, Y. Pérez Pacheco, B. Reig Vano, J.M. Montornés, A. Bajek and B. Tylkowski, Present trends in the encapsulation of anticancer drugs, in book Medical Physics, Models and Technologies in Cancer Research, Eds. by A. Bajek, B. Tylkowski, 2021, ISBN: 9783110662290, De Gruyter, Berlin, Boston, pp. 193-212, https://doi.org/10.1515/9783110662306-008

Conferences

- **Pérez Pacheco Yaride, Sisteré Miquel, Tylkowski Bartosz, García Valls Ricard.** CHITOSAN FOR FUTURE CANCER CELL ENCAPSULATION IN TME. [Poster, P-365]. at the EACR-AACR-ASPIC 2020 Conference: Tumor. Microenvironment. (2020). Lisbon, Portugal.
- **Pérez Pacheco Yaride, García Valls. Ricard, Tylkowski Bartosz, Sisteré Miquel.** CAPSULES OF CHITOSAN A TAILOR DRUG DELIVERY SYSTEM WITH CONTROLLED RELEASE FOR SPECIFIC ORGANS. [Oral Presentation]. At 14th Mediterranean Congress of Chemical Engineering (MeCCE-14) held virtually (2020).
- **Pérez Pacheco Yaride**, **Alimandi Tiziano, Tylkowski Bartosz, Sisteré Miquel**, **García Valls. Ricard.** CHITOSAN-TPP MICROCAPSULES FOR CONTROLLED DRUG RELEASE. [Oral Presentation]. At 15th Mediterranean Congress of Chemical Engineering. (2023). Barcelona, Spain.

Awards

- **Pérez Pacheco. Yaride, Sisteré Miquel, Joan Rosell-Llompart García Valls. Ricard.** Ajuts del Consell Social a les millors idees emprenedores Convocatòria del curs 2020-21. Projecte "Tractament del càncer basada en la inanició cel·lular" Import atorgat: 6.000 €. Universitat Rovira i Virgili.
- **Pérez Pacheco. Yaride, Sisteré Miquel, Joan Rosell-Llompart García Valls. Ricard.** Premis Emprèn 2021. Acreditació inici activitat NOSTRUMNATURALAB. Import atorgat: 1.000 €. Diputació de Tarragona.

Initiation of additional investigative activity: «Prueba de concepto» en el marco del programa estatal para impulsar la investigación científico-técnica y su transferencia, del plan estatal de investigación científica y técnica y de innovación 2021-2023. Convocatoria 2022.

LIST OF FIGURES

LIST OF TABLES

NOMENCLATURE

Symbols

Symbols	Meaning	Units
I	Electrical current	nA
k	Electric conductivity	µS/cm
Q	Flow rate	µL/min
V	Voltage	Kv
µ	Ionic strength	Adimentional
Gy	ionizing radiation dose	$J \cdot kg^{-1}$
σ	Surface tension	mN/m
ρ	Density	g/cm^3
MW	Molecular weigh	kDa

Abbreviations

Abbreviations	Meaning
EMV	Extracellular microenvironment
CS	Chitosan
TPP	Tripolyphosphate
DD	Degree of deacetylation
DA	Degree of acetylation
EtOH	Ethanol
AcOH	Acetic acid
ACN	Acetonitrile
DMSO	Dimethyl sulfoxide
PBS	Phosphate-buffered saline
FESEM	Field emission scanning electron microscopy
SEM	Scanning electronic microscope
FTIR	Fourier transformed infrared spectrometry
DLS	Dynamic light scattering

SD	Spray drier
ES	Electrospray
HV	High Voltage
HVPS	High Voltage Power Supply
HPLC-DAD	High Performance Liquid Chromatography with Diode-Array Detection
OD	Outer diameter
ID	Inner diameter
TEM	Transmission electron microscopy
FITC	Fluorescein isothiocyanate
FBS	Fetal Bovine Serum
LDA	Laser Doppler Anemometry
FA	Folic acid
PB	Buffer phosphate
LB	Buffer lactate
SD	Standard deviation
EMEM	Eagle's Minimum Essential Medium
FBS	fetal bovine serum
EDTA	Ethylenediaminetetraacetic acid
ZP	Zeta Potential
LDA	Laser Doppler Anemometry

1 INTRODUCTION AND AIMS

.

"The task is…,
not so much to see what no one has yet seen;
but to think what nobody has yet thought,
about that which everybody sees."
_Erwin Schrödinger. What is Life?

1.1 PHYSIOLOGICAL EXTRACELLULAR TUMOR MICROENVIRONMENTS

Cancer cells are characterized by accelerated growth and division, allowing the cells to invade nearby tissues, and spread to other organs. In order to support their growth, cancer cells create a new microenvironment around them by altering the chemical signals that govern cellular reproduction, as well as modifying tissue scaffolds, organ structure, and electrical signals (Narayan Bhattarai, 2005). They also suppress mechanisms that control cellular growth and prevent cell death, thereby allowing for uncontrolled replication. Cancer cells have also the ability to induce the formation of new blood vessels (angiogenesis) by reprogramming the metabolic pathways through which they obtain energy, making cancer cells gain a survival advantage over normal cells. They can invade and metastasize to other organs by avoiding detection by the immune system. In short, cancer cells are characterized by a range of molecular and cellular changes that allow them to evade normal cellular regulation, promoting the spread of disease (Pengfei Lu, 2021).

The Warburg effect describes the metabolic pathway of cancer cells, where high glycolytic rates are one of the contributing factors to excessive cancer cell growth. This process involves the use of high levels of glucose to release adenosine triphosphate (ATP) required for the cell's energy demands (Xiao Dong Xu, 2015; Vladimir Gogvadze, 2010).

The release of abundant secondary metabolites into the extracellular microenvironment (EMV) causes a significant shift in pH levels, oxygen

concentrations, ion balances, and a decrease in extracellular pH due to elevated levels of CO_2 and lactic acid. The heightened glycolytic rate leads to increased production of lactate (Yasumasa Kato, 2013; Franziska Hirschhaeuser, 2011). The activities of glucose metabolism had an important impact on the surface charge level of the cancer cells as shown in **Figure 1-1**. The transport of residues induces modifications in the electric charge of the double lipid bilayer, thus distinguishing cancer cell membranes from those of healthy cells (Bingdi Chen, 2016; Vladimir Gogvadze, 2010).

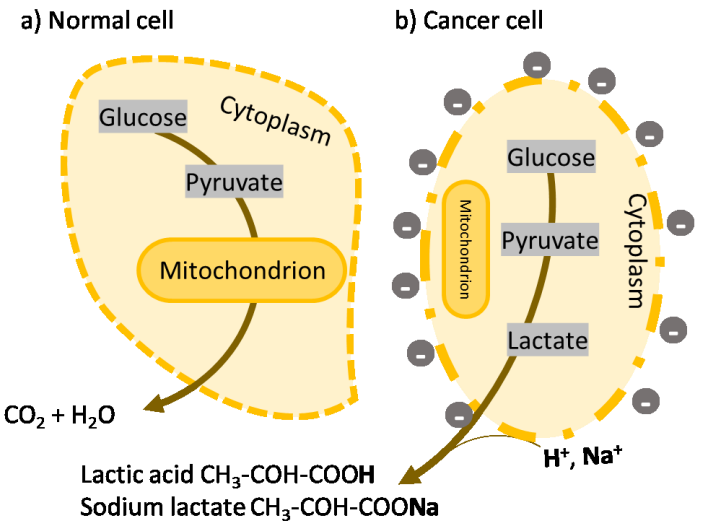

Figure 1-1. Schematic illustration of the glucose metabolism in a) normal cell and in b) cancer cell leading to lactate anion secretion and cations reduction on the membrane an increase in negative charges.

Solid tumor tissue is primarily characterized by low extracellular pH levels (Yasumasa Kato, 2013). Lactic acid, produced mainly through glycolysis in hypoxic conditions, is also generated in aerobic conditions as opposed to oxidative phosphorylation for energy production. Lactate is transported to the extracellular microenvironment (EMV) to reduce acidity levels, maintaining intracellular pH at physiological levels (pH 7.2–7.5) while decreasing extracellular pH to 4.5-6.9. The low intracellular pH caused by lactic acid enhances the activation of some lysosomal

enzymes, modifying the expression of genes involved with pro-metastatic factors. Furthermore, low extracellular pH levels inhibit T-cell activity, resulting in immune deficiency. (Yasumasa Kato, 2013; Shreya Thakkar, 2020).

1.1.1 Anticancer drugs depending on pH

The effectiveness of chemotherapeutic drugs for cancer treatment is heavily dependent on the extracellular pH levels of cancer cells (Natarajan Raghunand R. J., 2000; V. Vukovic, 1997). Some vasodilators, like hydralazine and captopril, reduce tumor growth rate by decreasing tumor blood flow. Vasodilating drugs with weak acidic pK_a values, such as 5-fluorouracil and cyclophosphamide, may be more effective at low pH levels (3.5 to <7.3) (Yasumasa Kato, 2013).

However, drugs with weak base pKa values, such as doxorubicin (pKa around 8.2-8.5), vinblastine (pK_a around 8.4-9.1), Paclitaxel (pKa around 8.2-8.6), methotrexate (pKa around 4.8-5.3), and imatinib (pKa around 5.75-6.65), may lose effectiveness due to low pH levels of the tumor microenvironment (Natarajan Raghunand B. P., 2003; V. Vukovic, 1997; Daniele R. Nogueira-Librelotto L. E., 2016). These drugs can bind to negatively charged components in the extracellular microenvironment, such as glycosaminoglycans present in the extracellular matrix, limiting their distribution and effectiveness in reaching cancer cells. Low extracellular pH (3.5 to <7.3) levels can also increase the positive charge of these drugs, making them more likely to bind to negatively charged components and reduce their bioavailability. This ultimately reduces their cytotoxicity and effectiveness in treating cancer cells. (Yasumasa Kato, 2013; Tannock, 1997; Natarajan Raghunand a. R., 2000).

High levels of lactate can contribute to radiotherapy resistance because lactate has antioxidant properties (Franziska Hirschhaeuser, 2011). However, cancer treatments face not only low pH but also the challenge of limited drug delivery to hypoxic areas, which are less responsive to chemotherapy (Barbara Muz, 2015). Furthermore, the absence of oxygen free radicals reduces the effectiveness of

radiation therapy by limiting DNA damage to cancer cells. As a result, it's essential to develop techniques for delivering effective chemotherapeutic drugs. (Yasumasa Kato, 2013; Shreya Thakkar, 2020).

1.1.2 Cellular interactions with nanomaterials

The field of nanomaterials is rapidly growing alongside the study of their interactions with cells. Their unique size, comparable to cellular organelles, presents opportunities to influence biological pathways and processes. Physicochemical properties, including shape, surface charge, surface interactions (hydrophilicity) (Yu Zhang, 2008), and protein corona, play crucial roles in these interactions. Understanding these interactions is essential for designing effective nanodevices and manipulating cell behavior in biomedical applications. As the potential of nanomaterial-cell interactions becomes evident, new materials are being developed to achieve specific cellular interactions in medicine. The design of nanodevices is tailored to achieve desired interactions with cells, such as targeting, drug delivery, and cell attachment promotion, while minimizing undesired side effects such as oxidative stress and cell death (Rawal Tejal, 2018).

The size of nanoparticles plays a critical role in their cellular uptake. Understanding the impact of size on cellular interactions is of utmost importance. While the optimal size for efficient internalization varies across cell types, 50 nm has been suggested as a suitable size based on experimental findings with various nanoparticles (Li Tang, 2013). Size-dependent toxicity has been observed in different nanoparticles, with smaller nanoparticles below 2 nm often exhibiting higher toxicity to cells compared to larger ones (Francisca Villanueva-Flores A. C.-L., 2020).

Mathematical models and experimental evidence support the relationship between nanoparticle size and cellular uptake. Smaller nanoparticles can penetrate deeper into tumor spheroids, whereas larger ones are quickly endocytosed without prior

accumulation on the plasma membrane. It is worth noting that different shapes and sizes of nanomaterials interact with cells in distinct ways, although most studies have focused on spherical nanoparticles. When measuring nanoparticle size, it is essential to use the same medium or solvent employed in biological experiments to account for factors like ionic strength, pH, and the formation of a protein corona, which can significantly affect nanoparticle size in serum (Mauro Sousa de Almeida, 2021). Moreover, nanoparticle size has been linked to sublethal effects and alterations in cellular functions.

The behavior of nanoparticles in biological environments is significantly influenced by their surface charge. The surface charge of nanoparticles can be affected by factors such as pH and biomolecule adsorption (Yu Zhang, 2008). Research demonstrates that cationic nanoparticles are more effectively internalized than neutral and anionic nanoparticle. The interaction between the surface charges of cells and nanoparticles results in unique Zeta potential patterns, enabling differentiation between normal breast cells (MCF10A) and cancer breast cells (MCF7). The findings indicate that changes in Zeta potential are influenced by both nanoparticle binding and internalization, affecting the overall uptake process (Yu Zhang, 2008). Experimental evidence suggests that nanoparticle around 100 nm in size preferentially undergo endocytosis. The interactions between nanoparticle surfaces and cells give rise to diverse biological effects (Mauro Sousa de Almeida, 2021).

1.1.3 Tumor targeting strategies by pH-sensitiveness

The significant challenge in cancer diagnosis is to identify molecular biomarkers that are specific to cancer cells while also being universally applicable across all types of cancer. The pH, ion concentration, specific metabolites, and temperature of pathological sites in the human body can vary significantly, making these environmental factors crucial for cancer identification and triggers for drug delivery carriers (Morteza Bahram, 2016).

Drug delivery carriers can be designed with degradable structures, offering the ability to control and adjust the degradation rate and profile (Daniele R. Nogueira-Librelotto L. E., 2020). Stimuli-responsive polymers are particularly desirable in this regard, as they exhibit a volume phase transition that allows their properties to be tailored to specific requirements (Morteza Bahram, 2016). These carriers, often referred to as environment-sensitive, can be designed to undergo conformational changes such as volume phase transition or gel-sol phase transition. They can degrade in response to various physical stimuli, including temperature, electric and magnetic fields, solvent composition, light intensity, and pressure. Additionally, they can also respond to chemical or biochemical stimuli, such as hydrolysis mediated by enzymes or changes in pH, ions, and metabolites. This versatility in responding to specific stimuli makes these carriers highly versatile and adaptable for controlled drug delivery applications (Carolina de las Heras Alarcón, 2005).

The volume phase transition of polyelectrolytes can be managed by choosing an appropriate linker agent based on the desired activity of drug delivery carriers. The more linkers that need to be broken, the longer the volume phase transition time and the slower the drug delivery process will be. In simpler terms, if the volume phase transition is fast, the drug will be released quickly and spread before reaching the intended target. Conversely, if the transition is slow, biological processes may eliminate the drug before it reaches the target. Fast drug release can negatively affect surrounding tissue and even impair cell function. To address these concerns, our research focuses on using pH as the trigger for volume phase transition, coupled with polarity for cancer cell membrane targeting (Bryant Garret D., 2008).

The use of polymers for cancer drug delivery is widespread, with many of these polymers being sensitive to pH, temperature, and glucose levels. By adding different functional groups to the backbone or using different crosslinking agents, the volume phase transition and degree of swelling of pH-sensitive polymers can be controlled (Hongliang Du, 2015; Pokharkar, 2006). Polymers that are pH-sensitive contain

structurally acidic (such as carboxylic and sulfonic acids) or basic (such as ammonium salts) groups that respond to changes in the pH of the environment by gaining or losing protons. Anionic polyelectrolytes (basic polymers) are deprotonated at high pH levels, leading to a strong electrostatic repulsion between chains and significant swelling of the polymer as water molecules penetrate it (Daijiro Shno, 2015).

In low pH media, the charge density of acidic polymers (cationic polyelectrolytes) decreases due to protonation, causing a collapse in polymer volume. Conversely, cationic polyelectrolytes become ionized and swell at low pH. The degree of swelling is influenced by various factors that affect electrostatic repulsion, such as pH, ionic strength, and the type of counterions present (Morteza Bahram, 2016).

Chitosan is a polycationic polymer widely used in drug delivery carriers due to its pH responsiveness, as it can undergo protonation or deprotonation with slight pH changes. Chitosan-based nanoparticles have been extensively studied as pH-sensitive carriers (Rajasree Shanmuganathan, 2019). The lower pH of tumoral tissues, caused by active tumor cell metabolism, has inspired the development of pH-sensitive nanoparticles that can store drugs under physiological conditions and precisely release them in the acidic tumor microenvironment (Hongliang Du, 2015). This approach aims to increase drug concentration at the target site and enhance therapeutic effectiveness.

Additionally, the negative charge of mammalian cell membranes, attributed to phospholipids with negative head groups, facilitates the binding of cationic polysaccharides like chitosan to the membrane surface through electrostatic interactions, leading to improved cellular uptake (Yu Zhang, 2008; Xingzhen Zhanga, 2016). Previous studies have demonstrated that chitosan, particularly with low acetylation and high molecular weight enhances permeability in epithelial cells. Chitosan hydrochloride has shown promise in reducing transepithelial electrical activity, enabling the transport of peptides across cell monolayers. Ongoing

research focuses on exploring the mechanisms underlying chitosan's impact on cellular uptake.

1.2 CHITOSAN AS pH RESPONSIVE

1.2.1 Chitin and chitosan

Chitosan (CS) has emerged as a focal point of considerable attention in recent studies owing to its interesting physicochemical properties. Chitosan is a natural polymer, biodegradable, biocompatible, pH-sensible derived from chitin, which is a complex that is alkaline-insoluble and crystalline in aqueous and organic solvents. Chitin is found in arthropod exoskeletons, crustaceans, yeasts, fungi, and algae, and its composition varies depending on the season and type of organism (Mohammed Eddya, 2020). Chitin (**Figure 1-2a**) consists of a polymer of glucose units linked to β-1,3-glucans and N-acetylglucosamine units. (Mitchell Jones M. K., 2020; F. Di Mario P. R., 2008; Christophe Roca, 2012).

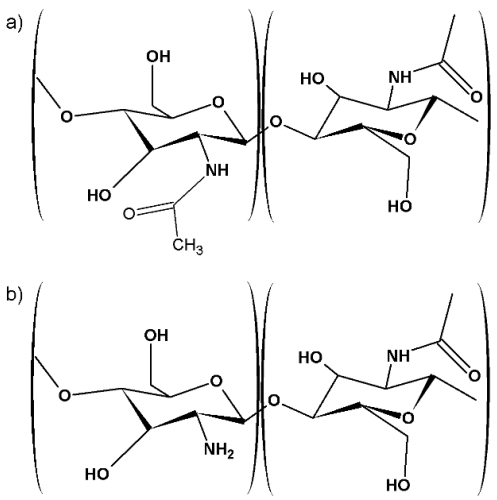

Figure 1-2. Chemical structure of a) chitin and b) chitosan.

Chitosan is a cationic polymer that is readily soluble. Chitin can be converted to chitosan through either homogeneous or heterogeneous alkaline N-deacetylation or enzymatic deacetylation. N-deacetylated chitin produces chitosan by cleaving the acetyl groups from chitin molecules into primary amino groups. Chitosan (**Figure 1-2b**) consists of randomly distributed deacetylated units (b-(1-4)-linked D-

glucosamine) and acetylated units (N-acetyl-D-glucosamine), (Mitchell Jones M. K., 2020; S. Islam, 2017).

The degree of deacetylation (DD) related to the free amine group ($–NH_2$) of chitosan, which is derived from chitin, is directly proportional to its degree of conversion. The DD of chitosan depends on several deacetylation parameters, such as the concentration of NaOH, temperature, and duration of treatment. The range of DD for chitosan is presented in **Table 1-1**. Water absorption is also affected by the degree of deacetylation, which limits its swelling ability during the volume phase transition at pKa (~6.5) (Piotr Owczarz P. Z., 2018; Rinaudo, 2006).

Table 1-1. Degree of deacetylation (DD) and degree of acetylation (DA) of chitosan found in market.

% DD	Solubility	% DA
70-95	Chitin, water insoluble	15-20.7
55-70	Water insoluble	45-30
70-85	Partially dissolved	30-15
85-95	Good solubility	15-5
95-100	Difficult to achieve	5-0

1.2.2 Chitosan as pH responsive polymer

The reactivity of chitosan is determined by the degree of deacetylation (DD), but also by its molecular weight (Mw), degree of crystallinity, and environmental factors such as pH, temperature, solvent, and ionic strength, the osmotic pressure of the counterions that neutralize the network charges, which affect its solubility (Rinaudo, 2006; Kumar, 2000). Chitosan contains ionizable basic groups (amine groups) that are sensitive to changes in pH, and their ionization and protonation are influenced by neighboring groups and electrostatic effects (**Figure 1-3**) (Hongliang Du, 2015). pH is related to pKa at which half of the ionizable groups are ionized, is determined by the presence of acidic or basic groups in the CS structure (Eun Seok Gil, 2004).

The acid-base properties of chitosan with respect to its dissociation degree has been demonstrated that pKa values are close to the pKa of the primary amine (ionizable groups) between 6.3 and 7.2 at complete dissociation, depending on the degree of N-deacetylation. Notably, pKa values increase significantly when the dissociation degree decreases. In a recent study (Qi Zhao Wang, 2006), chitosan with different degrees of deacetylation (DD) and molecular weight (MW) were examined to investigate their protonation constants (pKa). The results showed that changing the MM from 1370 to 60 kDa had a minimal effect on pKa, with a decrease from 6.51 to 6.39, while changing the DD from 94.6 to 73.3% the pKa values increases from 6.17 to 6.51. Hence, the balance of hydrophobic interactions and hydrogen bonding in chitosan is primarily dependent on the DD (Morteza Bahram, 2016; Qi Zhao Wang, 2006).

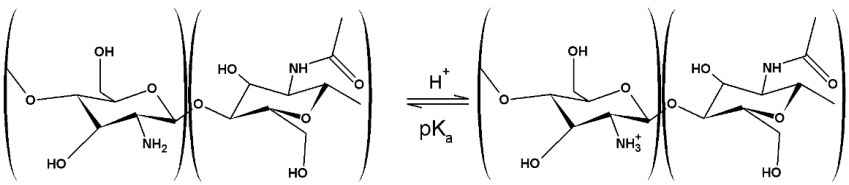

Figure 1-3. Protonation of the chitosan

Chitosan holds great promise for drug delivery due to its ability to control phase transition in response to the pH environment (Eun Seok Gil, 2004; Rajasree Shanmuganathan, 2019). The reversible phase transition, which involves conformational changes from a collapsed state to an expanded state, can be modulated by various means. One approach involves incorporating an ionizable or hydrophobic functional group with a pKa that corresponds to the desired pH range, into the chitosan backbone. Alternatively, a crosslinking agent can be used to reduce the solubility of chitosan in aqueous media over a wide pH range, which helps overcome chemical and biological degradation (Hongliang Du, 2015).

During the initial phase of the transition from the collapsed state to the swollen state, there is a change in the hydrodynamic volume, which is the result of interactions between the chitosan and the solvent. At acidic pH below 6.5, solid chitosan gains protons and swells, causing electrostatic repulsions among the same charges within the chitosan network. This results in a significant increase in hydrophilicity, leading to a drastic swelling, which occurs close to the dissociation constant pKa of chitosan (Qi Zhao Wang, 2006).

The second phase of the chitosan transition occurs when chitosan is in its swollen state and interactions between chitosan molecules become predominant. This transition is facilitated by mobile counterions, which apply osmotic pressure that neutralizes the amines in the chitosan backbone. When the protonation of the amines is complete, the swelling process and the pH solution increment stop, but the ionic strength increases. The increase in ionic strength results in an increase in hydrophobicity and contraction of the chitosan. At low pH, amine groups gain protons, and at higher pH (around 6.5), they release them. This causes chitosan to precipitate due to the deprotonation of amino groups, followed by hydrophobic molecular interactions (Mandeep Kaloti, 2010; Piotr Owczarz P. Z., 2018).

1.2.3 Complex CS/TPP formation mechanism

Introduction of hydrophobic groups to chitosan increases the electrostatic repulsion due to the increase in ionizable groups in the polymer. This leads to a shift of the hydrophobic groups from lower (pH 6.5) to higher pH ranges for phase transition. The transition is governed by the interplay between electrostatic repulsion and hydrophobic interactions. The degree of hydrophobicity in chitosan is directly proportional to the shift in pH transition (Eun Seok Gil, 2004).

The presence of hydrophobic groups in chitosan results in a delicate balance between ionic repulsion and hydrophobic interactions. Once chitosan is fully protonated, the electrostatic repulsion is eliminated, and the hydrophobic

properties take over, causing aggregation in the aqueous solution. The degree of aggregation is also affected by the hydrogen bonding between the hydrogen atoms in the protonated amine and electron-donating atoms, such as oxygen or nitrogen, in other functional groups present in the chitosan backbone, as the ionizable groups become deprotonated (Kleine-Brueggeney, 2015).

Chitosan's ionic groups can form both intermolecular and intramolecular linkages. In chitosan, the ionic interactions between positively charged amino groups and negatively charged counterions produce a crosslinking effect (Fwu-Long Mi S.-S. S.-B.-F.-T.-T., 1999). Glutaric dialdehyde, ethylene glycol diglyceryl ether, and TPP are some of the counterions used for this purpose. However, glutaric dialdehyde and ethylene glycol diglyceryl ether are crosslinking agents with physiological toxicity. (Qi Zhao Wang, 2006).

Chitosan's cationic nature provides significant benefits for ionic interactions. In acidic media (pKa 6.5), chitosan is polycationic and can interact with negatively charged species such as TPP and sodium sulfate (Pokharkar, 2006; Mandeep Kaloti, 2010). This characteristic makes it possible to create cross-linked chitosan nanoparticles. The interaction between chitosan and TPP leads to the formation of biocompatible cross-linked chitosan nanoparticles. CS/TPP particles have a positive charge over a wider pH range due to the electrostatic interaction between chitosan and TPP, whereas the surface charge of chitosan particles depends on the pH of the solution (Fwu-Long Mi S.-S. S.-B.-F.-T.-T., 1999; Kleine-Brueggeney, 2015). The crosslinking density, crystallinity, and hydrophilicity of crosslinked chitosan enable modulation of drug release and expand its potential applications in drug delivery (Pokharkar, 2006; Rajasree Shanmuganathan, 2019).

Sodium tripolyphosphate is a harmless crosslinking agent that is used to crosslink chitosan in aqueous solutions. TPP undergoes an equilibrium that produces several

chemical species shown in **Figure 1-4**, which depends on the pH of the solution as shown in equations **(**1-1 to (1-6**)**.

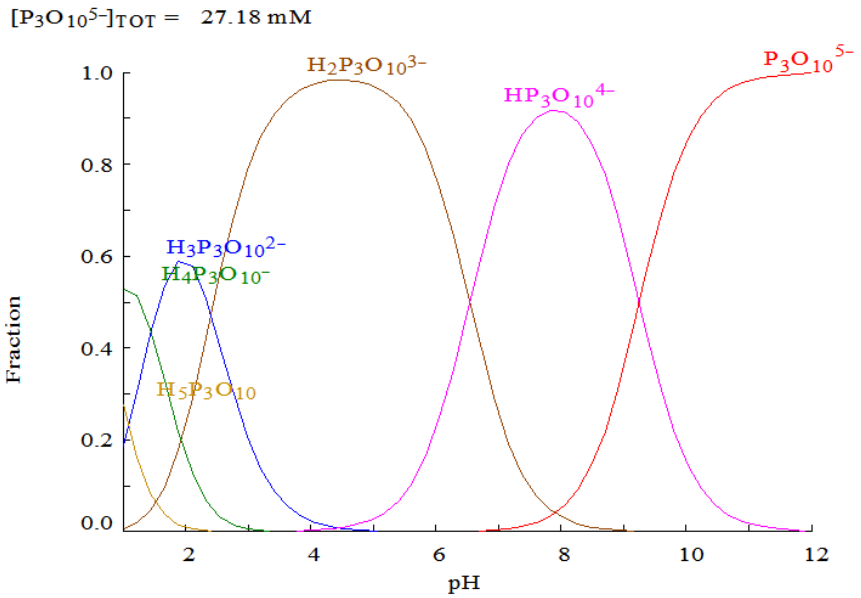

Figure 1-4. Diagram of species distribution of TPP at different pH (software medusa® pro_2.2.4.7).

Each equilibrium is defined by pKa_1 = 1.0, pKa_2 = 2.2, pKa_3 = 2.3, pKa_4 = 5.7, and pKa_5 = 8.5. This means that the species $P_3O_{10}^{5-}$, $HP_3O_{10}^{4-}$, and $H_2P_3O_{10}^{3-}$ can coexist in the tripolyphosphate solution in all pH ranges because Ka_1 is about 7.45 x 10^{-4} and $Ka_3 < Ka_2 < 10^{-7}$, Ka_1. In the original TPP solution (when pH is not adjusted), the concentration of $P_3O_{10}^{5-}$ and $HP_3O_{10}^{4-}$ is high, but the concentration of OH^- is also present. At pH>7, OH^- and TPP ions ($P_3O_{10}^{5-}$ and $HP_3O_{10}^{4-}$) can competitively react ionically by binding to the $-NH_3^+$ site in chitosan via deprotonation or ionic crosslinking, respectively (Devika R. Bhumkar, 2006; Juan D. Giraldo, 2019).

$$Na_5P_3 \xrightarrow{K_D \ \ Na^+} P_3O_{10}^{5-} \quad (1\text{-}1)$$

$$P_3O_{10}^{5-}H_3O^+ \overset{K_{a5}}{\longleftrightarrow} HP_3O_{10}^{4-}H_2O \quad (1\text{-}2)$$

$$HP_3O_{10}^{4-}H_3O^+ \overset{K_{a4}}{\longleftrightarrow} H_2P_3O_{10}^{3-}H_2 \quad (1\text{-}3)$$

$$H_2P_3O_{10}^{3-}H_3O^+ \overset{K_{a3}}{\longleftrightarrow} H_3P_3O_{10}^{2-}H_2 \quad (1\text{-}4)$$

$$H_3P_3O_{10}^{2-}H_3O^+ \overset{K_{a2}}{\longleftrightarrow} H_4P_3O_{10}^{-}H_2 \quad (1\text{-}5)$$

$$H_2P_3O_{10}^{-}H_3O^+ \overset{K_{a1}}{\longleftrightarrow} H_5P_3O_{10}H_2 \quad (1\text{-}6)$$

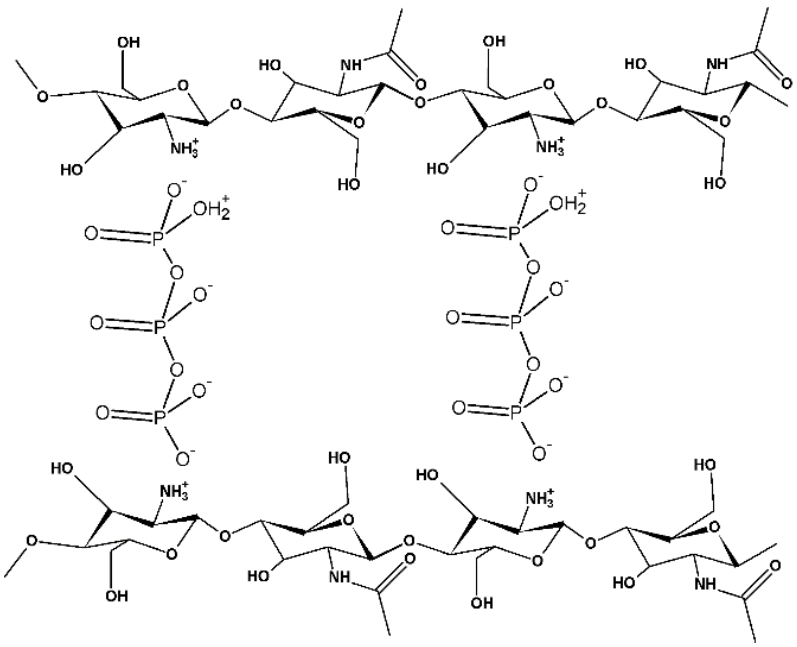

Figure 1-5. CS/TPP crosslinking diagram.

The interaction between chitosan, with its protonated amino groups ($-NH_3^+$), and tripolyphosphate ($-O^-$) results in the formation of a complex between a polycation and a multivalent anion as shown in **Figure 1-5**. The formation of this ionic complex is influenced by factors such as the molecular weight, degree of deacetylation, unit molar ratio, and the charge density of both chitosan and TPP. These factors contribute to the production of various CS/TPP complexes (Fwu-Long Mi S.-S. S.-Y.-T.-T.-F., 1999). The binding of protonated amino groups on the chitosan chain with hydroxyl ions leads to the reduction of chain stiffness, followed by TPP ions forming intramolecular linkages that fold the chains to create tailored aggregates (Mandeep Kaloti, 2010; Fwu-Long Mi S.-S. S.-T.-B., 1999).

1.2.4 Dispersions and dissociation of CS/TPP complexes in solution

The protonated amino groups on the chitosan chain can bind to TPP ions to form intermolecular linkages with other CS/TPP complexes, making them soluble and dispersible. This leads to the formation of aggregates that increase in size until they produce coacervates as shown in **Figure 1-6** (Pokharkar, 2006; Juan D. Giraldo, 2019). The stability of the colloidal dispersion depends on various factors, such as preparation conditions, pH, ions, and CS/TPP ratio (Fwu-Long Mi S.-S. S.-B.-F.-T.-T., 1999). The repulsive forces among particles play a crucial role in determining whether the solution is stable or not. If the repulsive forces are strong, the aggregation or flocculation is delayed, and the solution remains stable. However, if the particles' repulsive forces are weak, aggregation, flocculation, or coagulation can occur, leading to precipitation of the particles (Helene Jonassen, 2012; Leonardo M.B. Ferreira, 2020).

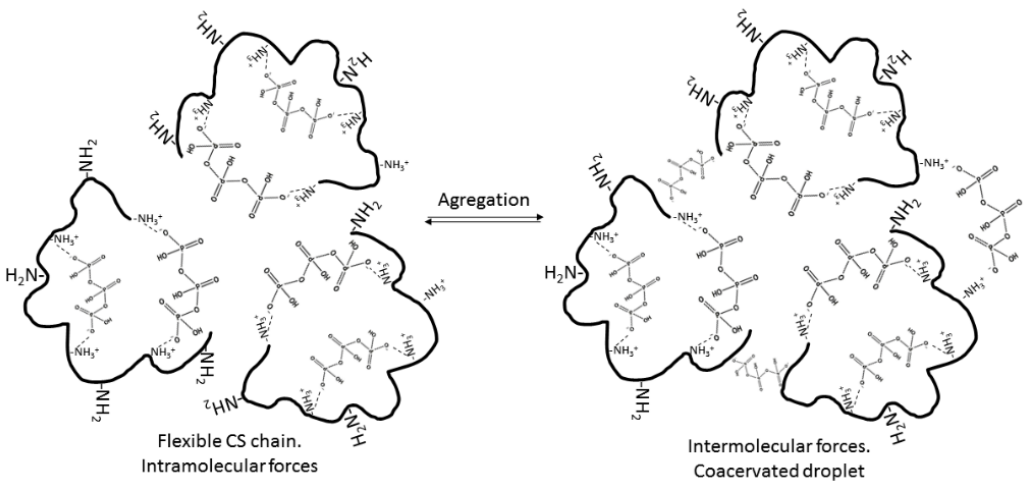

Figure 1-6. CS/TPP crosslinking to form particles and coacervates.

The stability of colloidal dispersions should also be evaluated regarding morphological changes in the particles, such as contraction and swelling. The degree of aggregation and contraction of nanoparticles is expected to be influenced

by the degree of crosslinking in the system (Fwu-Long Mi S.-S. S.-T.-B., 1999). In this study, we focus on investigating the physical stability of CS/TPP microcapsules that have been prepared and suspended in solvents with varying ionic strengths by analyzing morphology changes. We investigated the stability of the microcapsules over a period of 48 hours in order to study the average hydrodynamic radius, the stability of the solution, and particle compactness. Only a few quantitative studies have been performed on the stability of CS/TPP nanoparticles and any changes in particle compactness over time.

Our study aims to fill this gap in the literature and provide a comprehensive understanding of the stability of CS/TPP micro and nanocapsules under different aqueous solutions conditions. By analyzing the morphological changes in the particles, we can gain a better understanding of the underlying physical processes that govern the stability of colloidal dispersions.

Particle stability is related to the pH during the production of CS/TPP complexes as it is summarized in **Table 1-2** (Yuhang Cai, 2014). Since CS/TPP particles are typically prepared under low pH conditions, their application in physiological environments must be studied (M.N. Khalid, 2002; Helene Jonassen, 2012).

Most CS/TPP complexes that are prepared under low pH conditions dissociate at physiological pH, which produces precipitated chitosan chains with residual TPP (Petra Mazancová, 2018). The dissociation of CS/TPP complexes in an aqueous medium depends on the ionic strength of the solution. The higher the ionic strength, the greater the charge of the ionic atmosphere. In such a condition, any ion has a less net charge, which reduces the attraction between any cation-anion pair, and ion competition for the protonated $-NH_3^+$ of chitosan occurs. Therefore, dispersion pH and the ionic strength of the solution is important for dissolving the CS/TPP complexes (M.N. Khalid, 2002).

In general, the crosslinking reaction between chitosan and TPP has been widely studied and used in various applications. However, there are still knowledge gaps surrounding this reaction. The specific mechanism of the crosslinking process remains unclear as the molecular interactions and sequence of events, although it is known that electrostatic interactions and ionotropic gelation are involved.

Table 1-2. CS/TPP crosslinking depending on pH (Pokharkar, 2006).

CS/TPP complex	$3.5 < pH_{TPP} < 6.5$	$3.5 > pH_{TPP} > 7$
Degree of cleavage of the phosphorus chain from Cs	Lower	Higher
Structural stability of CS-TPP complexes	Higher	Lower
Degree of crosslink between CS-TPP.	Higher	Lower
Crosslinking density	Higher	Lower
Formation mechanism	1. Crosslinking by electrostatic interactions. 2. Coacervation- phase inversion	1. Intra-intermolecular bond formation Cs/TPP. 2. Diffusion competition -OH and phosphate groups

Additionally, the optimal reaction conditions, such as pH, temperature, and concentration, vary depending on the desired properties of the resulting material and its application. Factors like the degree of crosslinking, molecular weight, and the ratio of chitosan to TPP affect mechanical strength, swelling, and degradation properties of the complex. Long-term stability of CS/TPP crosslinked materials requires evaluation in terms of mechanical integrity, degradation, and release of encapsulated substances. While chitosan is generally biocompatible and biodegradable, the addition of TPP may modify these properties, necessitating further investigation into cytotoxicity, tissue compatibility, and biodegradation behavior. This knowledge is essential for biomedical applications like drug delivery systems and tissue engineering. Advancing the understanding of CS/TPP crosslinking

will enable improved material design, optimization of processing parameters, and expanded applications in general.

1.3 CHITOSAN CAPSULES AS DRUG DELIVERY SYSTEMS

CS/TPP complexes have demonstrated potential for drug delivery and cancer targeting, but there are several gaps in understanding of their drug loading and release mechanisms. Achieving controlled drug release from CS/TPP complexes is crucial for designing effective drug delivery systems. Further investigations are needed to explore the effects of crosslinking on the stability and degradation of many drug molecules, as well as to develop precise control over release profiles for different drugs. Understanding the relationship between crosslinking parameters and drug release kinetics will enable tailored delivery of specific drugs with desired release profiles. Although chitosan is generally considered biocompatible, the introduction of TPP during the crosslinking process may affect the biocompatibility and potential toxicity of the resulting drug delivery system (F. Di Mario P. R., 2008). Therefore, it is important to conduct further research to assess the biocompatibility and potential toxicity of CS/TPP complexes, considering the introduction of TPP during the crosslinking process.

Living cells are sensitive to their surroundings. The presence of external bodies like polymeric hydrogels, nano, and microparticles in a biological medium can be potentially harmful, reducing cellular viability. Tissue inflammatory and immune responses can lead to cell dysfunction and destruction due to adhesion, toxic degradation fragments, size, and hydrophobicity surface. The biological activity shown by polymers used for drug delivery depends on cell viability. The enzymatic activity may cause degradation of the polymeric carrier (Anna Lesniak, 2013).

The interaction between particles and cells is facilitated by the biomolecular corona formed by the surrounding biological environment, the pristine surface of the nanoparticles depending on the surface chemistry, charge, roughness, and size (Ashraf Abdelkhaliq, 2018; Peppino Mirabelli, 2019). Previous studies have shown that the uptake of nanoparticles by living cells depends on properties such as their

size and surface. However, in a biological fluid for in vivo experiments, nanoparticles are quickly covered by biomolecules like proteins and lipids, forming a biomolecular corona that effectively wraps the bare nanoparticle surface. In realistic circumstances, cells are typically exposed to the nanoparticle−biomolecular corona complex rather than the bare nanoparticle surface. Therefore, it becomes interesting to correlate nanoparticle uptake to the properties of the nanoparticle−biomolecular corona complex (Anna Lesniak, 2013).

The surface chemistry of polymer particles affects their interaction with cell membranes. Hydrophilic surfaces promote better cell adhesion compared to hydrophobic surfaces (Ashraf Abdelkhaliq, 2018). Folic acid (FA) is widely used to target specific cell membranes and enhance nanoparticle endocytosis through the folate receptor (Agnes Aruna John, 2017). Folate receptors are often overexpressed in various cancer cells, including ovarian, endometrial, colorectal, breast, and lung cancer cells. FA has a strong affinity for the folate receptor, and it is stable, inexpensive, and easy to conjugate therefore in this research using the targeting properties of CS/TPP together with FA will have a synergic effect. The cellular uptake mechanism for FA conjugates is highly effective, like that of free FA (Hamid Reza Naghibi Beidokhti, 2016). These conjugates enter cells through folate receptor-mediated endocytosis and undergo vesicular trafficking within organelles, facilitating the release of materials into the cell cytoplasm (Nathan D. Donahue, 2019). The folate receptor can recycle to the cell surface, allowing for the transport of more FA conjugates. Chitosan-based nanoparticles in combination with FA conjugates have been extensively studied.

The surface charge of the polymer particle can also affect cell adhesion. Cells generally have a negatively charged membrane, so positively charged polymer particles tend to have better cell adhesion. The size of the polymer particle can affect the interaction with the cell. Generally, smaller particles tend to have better cell adhesion than larger particles. The roughness of the polymer particle surface

can also influence cell adhesion. A smoother surface generally results in better cell adhesion due to regular composition on the surface. The adsorption of proteins to the polymer particle surface can also affect cell adhesion. For example, if proteins that promote cell adhesion adsorb to the surface, the cell is more likely to adhere to the particle (Nathan D. Donahue, 2019; Francisca Villanueva-Flores A. C.-L., 2019).

As explained previously, chitosan is a biocompatible natural product that contains basic groups (F. Di Mario P. R., 2008). Cells usually have a predominantly negative charge on their surfaces, so they adhere more strongly to substrates with basic groups like chitosan. However, the strongly positive charge of chitosan can cause cell metamorphosis and inhibit cell growth. Previous studies have reported that epithelial cells grew on a chitosan film, while fibroblast cells could grow on mixed films of collagen and chitosan. The addition of chitosan to collagen increases cell attachment but decreases cell growth (Hang Thu Ta, 2008).

Chitosan nanocapsules have been investigated for their potential effects on cancer cells and normal cells in various studies. The specific effects can depend on several factors such as the type of cancer, the type and concentration of chitosan used, and the size and surface properties of the nanocapsules (Rolim, 2016).

In summary, the effects of chitosan nanocapsules on cancer cells and normal cells can vary depending on several factors. While some studies have suggested that chitosan nanocapsules may have potential for delivering anticancer drugs while minimizing toxicity to normal cells, further research is needed to fully understand the effects of chitosan nanocapsules on different types of cancer cells and normal cells.

1.4 CHITOSAN-TPP CAPSULES PRODUCTION TECHNIQUES

There are many techniques available for producing micro- and nanoparticles that enhance properties such as high surface area, stability, and low interfacial tension, for various applications. In this classification, I have roughly categorized particle production techniques into two main categories based on well-known methods:

- **Solution-based techniques**, which include ionic gelation, microemulsification, and complex coacervation.
- **Spray-based techniques** namely spray drier and electrospray, with the latter still being actively explored.

It should be noted that the formation of the CS/TPP complex is approached similarly in each of these techniques as explained in explained in **Section 1.2.3**. The following subchapters will provide a detailed description of the fundamental concept behind particle production for each of these techniques.

1.4.1 Solution-based production of particles

Several authors have proposed various methodologies to produce CS/TPP capsules using the techniques discussed in this section (Xavier Montané, 2020). These techniques have been extensively explored, and their principles, advantages, and disadvantages have been elucidated. While these techniques are well-established for CS/TPP capsule production, they have not yet fully met the requirements set forth by the hypothesis of this research. Nonetheless, understanding the fundamentals of these techniques is crucial as it enhances our knowledge of CS/TPP complexes during particle formation. By building upon this foundation, we can continue to advance our understanding and strive to develop more effective strategies to achieve the objectives of this research.

a. Ionic gelation technique

The ionic gelation technique is used to create three-dimensional networks of cross-linked chitosan by forming ionic bonds between oppositely charged chitosan and TPP (Pasquale Sacco, 2016). It involves three major steps: (i) dissolving chitosan in a solvent to form a solution, (ii) adding the ionic solution of TPP, and (iii) crosslinking the chitosan chains through the addition of an ionic crosslinking agent (TPP). The resulting ionic gel can be shaped into various three-dimensional structures (R. Harris, 2011; Andréia Lange de Pinho Neves, 2014).

Compared to other techniques for creating nanoparticles, ionic gelation has several advantages. It is a relatively simple. Moreover, it produces particles and hydrogels with controlled size and shape. By adjusting the concentrations of the chitosan and ionic crosslinker (TPP), the pH and temperature of the solution, the properties of the resulting particles and hydrogels can be tailored (Pasquale Sacco, 2016; Kleine-Brueggeney, 2015). Additionally, the technique can create core-shell structures and microparticles (Tiyaboonchai, 2003).

Ionic gelation technique can be easily scaled up for industrial production. However, ionic gelation may face challenges related to batch-to-batch variability due to the dependence on electrostatic interactions, leading to potential variations in encapsulation efficiency. It is also necessary to carefully select and optimize the concentration and ratio of polymers to achieve desired encapsulation properties (Andréia Lange de Pinho Neves, 2014). Despite these limitations, ionic gelation remains a valuable method for the encapsulation of bioactive compounds with applications in drug delivery and tissue engineering.

b. Micro emulsification technique

The microemulsification technique is used to form stable emulsions comprising droplets of one liquid dispersed in another. The stability of the emulsion relies on

the properties of the solvent, surfactant, co-surfactant, and the ratio of the components. In general, a microemulsion is created when the energy required to form the interfacial tension between the two liquids is reduced to the point where the droplets become thermodynamically stable.

For example, in the microemulsification technique, chitosan is first dissolved in a solvent. Then, the TPP in water/benzyl alcohol solution is added to this chitosan solution, along with a surfactant and co-surfactant (Alessandro F. Martins, 2012). Finally, the mixture is stirred or sonicated to form a stable emulsion. Nanoparticles can be produced by using the microemulsification technique through various methods, such as the reverse microemulsion method, the spontaneous emulsification method, and the high-energy emulsification method.

The reverse microemulsion method involves the use of a water-in-oil microemulsion, in which the polymer is dissolved in the water phase and the surfactant and co-surfactant are dissolved in the oil phase. The two phases are then mixed to form the nanoparticles. The spontaneous emulsification method involves mixing the polymer solution with the oil phase and surfactant and co-surfactant at room temperature, resulting in the formation of nanoparticles. The high-energy emulsification method involves using high-speed mixing or sonication to create a stable microemulsion (Tiyaboonchai, 2003).

The selection of appropriate surfactants and co-surfactants is critical for microemulsion formation, which can be challenging due to their complex interactions and potential toxicity concerns (Alessandro F. Martins, 2012). The optimization of formulation parameters, such as the surfactant-to-oil ratio and water content, requires careful consideration. Moreover, the stability of microemulsions over extended periods can be a concern, and their tendency to undergo phase separation may limit their long-term storage potential. Despite

these limitations, the microemulsification technique remains a valuable approach for efficient encapsulation and controlled delivery of hydrophobic substances.

c. Simple and complex coacervation technique

Complex coacervation produces microcapsules by the electrostatic association of oppositely charged polyelectrolytes in a solution, resulting in the formation of a dense, polymer-rich phase named coacervate. The formation of the coacervate phase is dependent on several factors, including the pH, salt concentration, and polymer concentration of the solution (Bo Wang, 2008).

Simple coacervation involves the addition of a solution containing the oppositely charged polyelectrolytes to a solution containing a salt or buffer, which leads to the formation of the coacervate phase. Another method involves the use of microfluidic devices to control the formation and properties of the coacervate droplets (Mandeep Kaloti, 2010). The choice of method depends on the characteristics of the polyelectrolytes being used, the desired properties of the coacervate.

Complex coacervation is a technique used for encapsulating bioactive compounds, offering advantages such as high load capacity, exceptional encapsulation efficiency (up to 99%), controlled release characteristics, protection against degradation, and enhanced stability and bioavailability. However, it has certain disadvantages, including being a time-consuming process that involves multiple steps, being relatively expensive due to specialized equipment and materials, being a complex process that requires a deep understanding of polymer and colloid chemistry, and the potential for size distribution variation of coacervate droplets. Overall, complex coacervation provides significant benefits but also requires careful consideration of its drawbacks in terms of complexity, time, cost, and size control (Tiyaboonchai, 2003; Mandeep Kaloti, 2010).

1.4.2 Spray-based production of particles

While only a limited number of authors have proposed methodologies for producing CS/TPP capsules using the techniques discussed in this section, there is still a relative lack of comprehensive information regarding precise control over the production of CS/TPP particles by this technique (Park, 2005; Jelena Filipović-Grčïć, 2003; Zeng-liang Zhan, 2020). Although spray drier produces many CS/TPP microcapsules for physicochemical evaluation it has not fully met the requirements set forth by the hypothesis of this research. On the other hand, electrospray technique shows potential for producing crosslinked CS/TPP particles and fulfilling the requirements of the research hypothesis. However, the available information on electrospray is limited and requires further description. Therefore, additional investigation is necessary to address these knowledge gaps and enhance our understanding of CS/TPP capsule production using the electrospray technique. This section aims to provide an elucidation of the principles, advantages, and disadvantages of spray-based particle production, emphasizing the significance of this research area to the reader.

a. Spray dryer technique

The spray drier technique offers several benefits for particle production. One of its key advantages is the ability to control particle size, which is crucial for optimizing drug delivery and enhancing bioavailability. Furthermore, spray drier can improve drug solubility by creating particles with a high surface area and enhanced dissolution rates. The process itself is fast and efficient, making it well-suited for large-scale pharmaceutical manufacturing (Berta Nogueiro Estevinho, 2013).

The spray dryer operates by atomizing a liquid into small droplets, which are then introduced into a stream of hot air or nitrogen (Bo Wang, 2008). Rapid heating causes the liquid to evaporate, leaving behind a dry powder that is collected after the hot gas is removed through a cyclone (Berta Nogueiro Estevinho, 2013).

The concentration of the solution used in spray drier affects the porosity and water content of the resulting products (Dan-Lei Yang, 2024). Concentrated solutions yield products with higher porosity and lower water content, leading to the formation of amorphous polymeric products. While spray drier is an efficient and rapid particle formation process, it does have some limitations. Elevated temperatures are required, which may not be suitable for compounds with high melting points or limited thermal stability. Additionally, substances with poor solubility or volatile solvents can present challenges. Size distribution can also vary, ranging from nanometer to micrometer sizes (Berta Nogueiro Estevinho, 2013).

b. Electrospray technique

Electrospray technique produces nanoparticles by atomization of a liquid into fine, charged aerosol by applying an electrical potential to the capillary tube where the liquid is ejected. In general, the atomization of the liquid uses electrical forces to overcome the surface tension force, which forms a meniscus and a jet (Loscertales, 1994). The electrostatic repulsion fragments the expelled liquid from the meniscus and when the jet is formed, it can disrupt into the aerosol (Jaworek, 2008; Taylor G. , 1964).The size and charge of the aerosol droplets depend on several factors, including the electrical potential applied, the flow rate of the liquid, the properties of the liquid, and the distance between the capillary tip and the collector (Jaworek, 2008; Chul Ho Park, 2009).

The methods used in electrospray depend on the application and the properties of the liquid being sprayed. One method uses a coaxial needle, which produces a core-shell structure of the sprayed droplets [ ]. Another method uses single needle, which produces uniform, spherical particles. The choice of method depends on the characteristics of the liquid being sprayed, the desired properties of the particles.

On the other hand, the electrospray process depends on the characteristics of aqueous solutions used to produce capsules like viscosity (A. J. Hijano, 2015),

surface tension, conductivity (A. J. Hijano, 2015), dielectric constant, vapor pressure, and chemical properties, and miscibility related to coaxial electrospray as explained in **Table 1-3** .

Table 1-3. Characteristics of aqueous solution for electrospray

Solution properties	challenges	Droplet size
Viscosity	Size of droplets (	Larger droplet size.
Surface tension	Formation of a stable Taylor cone and formation of droplets without corona.	High surface tension form larger droplets. Scaling laws
Conductivity	The magnitude of the charge that accumulates at the surface of the liquid.	Higher the conductivity, the higher the charge density higher current, which leads to a less flow rate and smaller droplet sizes.
Dielectric constant	The strength of the electric field around the droplets.	Higher dielectric constant liquids require higher electric fields to overcome surface tension and form a stable Taylor cone.
Vapor pressure Particle formation	The evaporation rate of the solvent from the droplets	Liquids with lower vapor pressure produce smaller droplets.

Instabilities presents in the electrostatic field created between a charged droplet and its surroundings during the electrospray process are Coulombic instabilities (Bodnár, 2018). This instability causes the droplet to deform, leading to a non-uniform distribution of charges on its surface, and ultimately leading to the formation of multiple smaller droplets or a mist (Taylor G. , 1964). Coulombic instabilities can be influenced by several factors, including the surface tension of the liquid, the conductivity of the liquid, the applied electric field, and the surrounding gas or vacuum environment. Understanding and controlling Coulombic instabilities is crucial in optimizing the performance and reliability of electrospray-based applications, such as mass spectrometry and drug delivery (Muñoz, 2021).

The scaling laws describe the relationship between the physical parameters of the electrospray process, such as the flow rate, applied voltage, and droplet size. These laws provide a framework for understanding and predicting the behavior of the electrospray process under different conditions. One of the most well-known scaling laws is the Taylor cone-jet mode, which describes the formation of a conical droplet shape at the tip of the electrospray emitter under high electric fields (Taylor G. , 1964). This mode is characterized by a linear relationship between the flow rate and the applied voltage, as well as a power law relationship between the droplet size and the flow rate. Other scaling laws in electrospray include the Rayleigh limit, which describes the minimum droplet size that can be produced under a given set of conditions, and the electrospray stability limit, which describes the maximum flow rate at which stable droplet formation can be maintained (Joan Rosell-Llompart, 2018).

Electrospray provides precise control over size and shape, operates under mild conditions, and produces homogeneous nanoparticles of nanometric sizes. It allows for the generation of particles with varying surface charges and hydrophobicity, facilitating high drug loading capacity and enabling controlled release profiles. However, one drawback is the relatively low production rate. Additionally, the performance of electrospray is influenced by liquid properties such as viscosity and conductivity, making it sensitive to these factors. Despite these limitations, the advantages of electrospray make it a valuable technique in various applications, particularly in the field of nanomedicine and drug delivery systems. (Jaworek, 2008; Joan Rosell-Llompart, 2018).

1.5 HYPOTHESIS AND OBJECTIVES

This section presents the hypothesis proposed for the development of this research.

It is feasible to produce functional CS/TPP nanocapsules for use in anticancer treatments in the pharmaceutical industry, with low size dispersion and predetermined crosslinking degree of CS/TPP. Understanding these factors can provide insights into the potential for encapsulating cancer cells by the regulation of the dissolution pH for adherence to cancer cell membranes in in-vitro models.

Considering the previous hypothesis, the general objectives of this research were:

- To evaluate the performance of CS/TPP microcapsules in aqueous solutions prepared via spray drier by assessing their stability, morphology, and drug release characteristics.

- To develop a robust and efficient method based on electrospray to produce crosslinked CS/TPP nanocapsules suitable for pharmaceutical applications. The pharmaceutical suitability of the capsules in this work will be determined initially by requirements of size and morphology, and later by in vitro testing on cell cultures. The actual pharmaceutical development is outside the scope of this thesis.

- To evaluate CS/TPP capsules interaction with normal and cancer cell lines with the use of *in vitro* experiments.

The achievement of the general objectives was addressed and elaborated upon in the subsequent chapters, where specific objectives were intentionally delineated.

2 CS/TPP MICROCAPSULES BY SPRAY DRIER

Nothing in life is to be feared,
it is only to be understood.
Now is the time to understand more,
so that we may fear less.
_ Marie Salomea Skłodowska-Curie

2.1 INTRODUCTION

In this chapter, our primary focus is on the production of CS/TPP microcapsules using the spray drier technique. Spray drier involves the atomization of an emulsion containing CS, TPP, AcOH, and FA into fine droplets, which are then subjected to a high-temperature and low-pressure gas flow. This process leads to the evaporation of the solvent and the formation of solid particles within the drying chamber as shown in **Figure 2-1**.

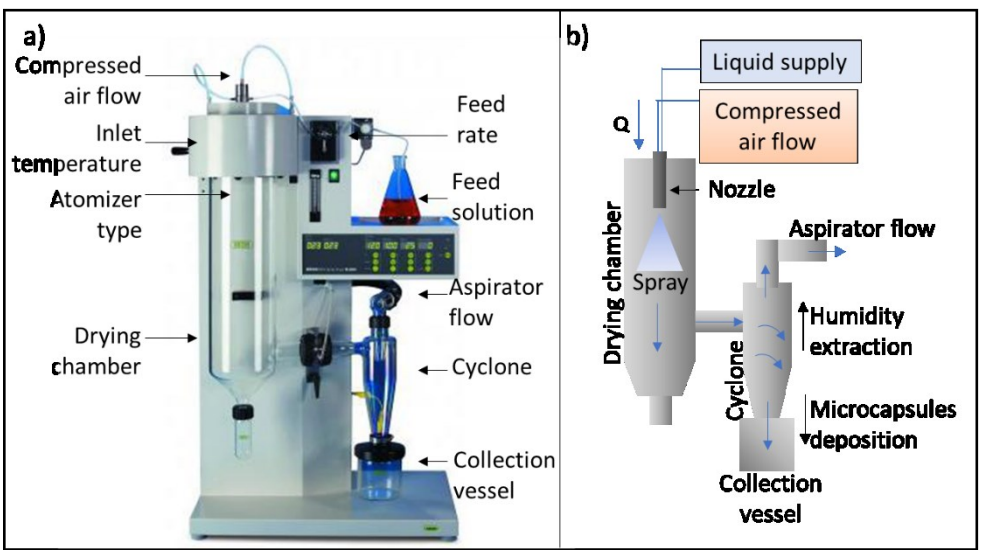

Figure 2-1. Model of a B-290 Mini Spray Dryer 093004|Q es Meierseggstrasse 40. a) manual and b) diagram.

During the spray drying operation, the heat and low humidity of the drying gas cause the droplets to shrink and solidify, resulting in the production of microcapsules (Julklang, 2015). The drying gas within the chamber follows a cyclonic pattern, facilitating the separation of solid particles from the remaining droplets and drying gas. The solid particles are collected in a cyclone or other separation device, while the drying gas is vented out of the system.

Spray drier is a valuable technique for producing solid CS/TPP microcapsules. By carefully selecting the equipment configuration parameters, such as the inlet temperature and gas flow rate, we can control the properties of the microcapsules generated. This versatility allows us to tailor the CS/TPP microcapsules to meet specific requirements for this research. Therefore, we investigate the influence of the production method on the morphology, size, and residual moisture of the CS/TPP microcapsules by modifying the spray drier configuration parameters, such as inlet temperature and pressure (aspirator), we also deeply studied the emulsion composition for CS/TPP microcapsule production. By examining these aspects, our aim was to deepen our understanding of CS/TPP microcapsule behavior in solution according to its production conditions and its potential to achieve the hypothesis of this thesis.

In chitosan delivery systems, various approaches can be employed to encapsulate drug agents like folic acid, an analogues molecule to methotrexate, used for cancer treatment. These agents can be added to the chitosan solution before the addition of crosslinking-inducing agents, incorporated into the gelation-inducing agents before mixing with the chitosan solution, or added to the crosslinking mixture solution consisting of both chitosan and gelation-inducing agents. The selection of the method depends on the properties of the chitosan delivery system and the specific drug agent to be encapsulated. Additionally, we conducted experiments to explore the behavior of CS/TPP microcapsules in solution when they encapsulated agents like folic acid. We measured the release profile to gain insights into their

drug delivery capabilities and evaluate their potential as effective carriers for controlled release applications.

2.2 OBJECTIVES

2.2.1 General objective

- To evaluate the performance of CS/TPP microcapsules in aqueous solutions prepared via spray drier by assessing their stability, morphology, and drug release characteristics.

2.2.2 Specific objectives

- To study the morphology, size, and size distribution of CS/TPP microcapsules produced through different emulsion compositions and spray drier parameters.
- To analyze the release profile of a folic acid analogue in simulated physiological media using CS/TPP microcapsules.
- To determine the crosslinking degree of CS/TPP microcapsules and compare it with the raw CS and TPP components.
- To investigate the pH-dependent behavior and stability of chitosan and CS/TPP microcapsules.
- To measure the zeta potential of CS/TPP microcapsules at different pH values and evaluate its impact on dispersion stability.

2.3 METHODOLOGY

2.3.1 Materials

Chitosan was purchased from Across Organics and Sigma-Aldrich, derived from yeast and animal sources, respectively. Chemical reagents such as hydrochloric acid, acetic anhydride, oxalic acid, potassium hydroxide, sodium hydroxide, Sodium tripolyphosphate, and glacial acetic acid were purchased from Sigma Aldrich Co. in St Louis, USA. Folic acid (FA) was obtained from BDH Chemicals in England. All chemical reagents were used as purchased without any further purification. Synthetic dry air with 99.5% purity was purchased from Carburos Metálicos in Spain. Ultrapure water from Millipore in the USA was used throughout the experiment.

A series of preliminary experiments were undertaken to explore a range of chitosan composition from the available market options. The concentration of the solutions was fine-tuned by analyzing the viscosity qualitatively, as outlined in **Table 2-1**. It was observed that reducing the pH of the solution resulted in a decrease in viscosity. However, caution must be exercised when opting for pH reduction, as it may not always be the most suitable approach due to the potential solution of the TPP to crosslink. Chitosan from animal source tend to be more viscous at the same concentration than chitosan from yeast source.

Table 2-1. Sources of chitosan at 75 % degree of deacetylation.

Source	Cod	Mw, KDa	Lotte	Viscosity in 1%AcOH, cP
Yeast	C87	100-300	A0406187	100
	C56	100-300	A0437756	100
	C58	100-300	A0426358	100
	C33	>300	A0422933	1000
Animal	C03	<100	BCCC0403	20-300
	C81	100-300	STBJ3281	200-800
	C04	>300	BCCD0404	800-2000
	C83	>300	BCCC6283	800-2000

The morphology of pure chitosan from fungi source exhibited a granular, nonporous, smooth membranous phase as observed in **Figure 2-2**. The morphology may be due to conformation of low degree of branches on the backbone (Mitchell Jones M. K., 2020).

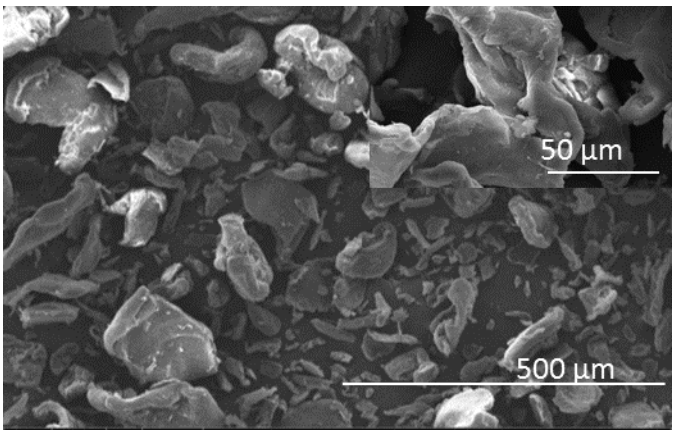

Figure 2-2. SEM images of chitosan from fungi source.

2.3.2 Preparation of CS/TPP emulsions and characterization

To prepare chitosan and TPP solutions, chitosan was first dissolved in an acetic acid (AcOH) solvent until the final pH of this solution reached 6.2. This pH value guarantees completely dissolution of chitosan (Chitosan pKa 6.5), while TPP was dissolved in water (pH above 8 dues to TPP speciation). Both solutions were kept under magnetic stirring until complete dissolution. The emulsions were mixed by slowly adding the TPP solution to the CS solution under constant magnetic stirring (500 rpm, Yellow line MAG HS7, IKA, Germany) at room temperature for 30 minutes prior to spraying.

Around 100 formulations were meticulously prepared, involving a variety of CS/TPP emulsions, for the purpose of generating microcapsules using spray-drying techniques. The primary objective of this study was to investigate the impact of these formulations on crucial factors, including morphology, size, size dispersion, and crosslinking degree of CS/TPP. Additionally, the capacity of the microcapsules in

encapsulating compounds, specifically demonstrated by folic acid, was evaluated. This assessment aimed to understand the behavior of the microcapsules when releasing their contents into the aqueous environment. The most relevant emulsion compositions are listed in **Table 2-2**.

Table 2-2. Emulsions for microcapsule production by spray drier.

Batch code	Emulsion composition				Study
	AcOH, %v/v	CS, %w/v	TPP, %w/v	FA, %w/v	
Cap13C	0.342	0.4	0	0	Effect on morphology and size
Cap14C	0.513	0.6	0	0	
Cap15C	0.684	0.8	0	0	
Cap9	0.342	0.4	0.15	0	
Cap10	0.513	0.6	0.15	0	
Cap11	0.684	0.8	0.15	0	
C15	0.171	0.2	0.16	0	Exploration of crosslinking degree due to stoichiometric mass ratios (CS:TPP) of 1:0.8, 1:0.4, and 1:0.2
C20	0.171	0.2	0.080	0	
C25	0.171	0.2	0.053	0	
C18	0.684	0.8	0.64	0	
C23	0.684	0.8	0.32	0	
C28	0.684	0.8	0.21	0	
CapAF1	0.342	0.4	0	0.015	Effect on morphology and size
CapAF2	0.513	0.6	0	0.015	
CapAF3	0.684	0.8	0	0.015	
Cap AFTPP1	0.342	0.4	0.15	0.015	
Cap AFTPP2	0.513	0.6	0.15	0.015	
Cap AFTPP3	0.684	0.8	0.15	0.015	Drug release profile

2.3.3 Spray dryer equipment and microcapsule production

CS/TPP microcapsules were produced using a Spray Dryer (B-290 Mini BÜCHI®). To evaluate the effects of different technical conditions on microcapsule production, 100 mL of the emulsions were used. As explained in the general introduction

chapter the more relevant technical conditions to manipulate morphology and size are inlet temperature (150, 160, 170, and 180 °C), aspirator pump flow rate (20, 24, 28, 32 x10^3 L/h), and feed flow rate (0.42 L/h). The air flow in the spray chamber was maintained at 357 L/h and 0.23 bar, while the nozzle had an inner diameter of 2 mm and an outer diameter of 4mm. The best technical conditions of the spray dryer were used in other experiments to produce microcapsules for comparison of compositions, the technical conditions of the spray dryer were set to an inlet temperature of 170 °C, an aspirator pump flow rate of 28x10^3 L/h, and a feed flow rate of 0.42 L/h. The resulting microcapsules were stored in amber glass at room temperature.

2.3.4 Characterization of the microcapsules

a. Morphology, size, and size distribution

The morphology, size, and composition of the microcapsules were analyzed using an environmental scanning electron microscope (ESEM) FEI Quanta 600. The microcapsules were transferred onto a carbon tape and coated with a ~27 nm Au layer (30 mA, 90 s) in a sputter coater (Quorum Q150T S plus). The diameter of the microcapsules was manually measured in the SEM images using ImageJ software (version 1.53e) to determine their size distribution.

b. FTIR analysis

The crosslinking degree of the microcapsules was analyzed using infrared spectroscopy with a Jasco FT/IR-6700 Infrared Spectrometer equipped with an attenuated total reflection (ATR) PRO ONE accessory and a diamond crystal kit or a Ge crystal kit. The microcapsule samples were directly placed on the surface of the optic lenses without any prior treatment. The FTIR spectra were recorded in transmittance mode with a resolution of 4 cm^{-1} by accumulating 32 scans from 4000 to 400 cm^{-1}.

2.3.5 Microcapsule performance at different pH solutions

To investigate the behavior of microcapsules in different environments, we dispersed them in solutions with varying pH levels (4.5, 5.5, 6.5, 7.5, and 8.5) without buffer effect. These pH values were chosen to mimic the pH range typically found in solid tumors originating from different tissues and stages (Peter Vaupel, 1989). We regulated the pH by adding 0.001M HCl or 0.001M NaOH. We also tested the microcapsules in buffer solutions such as sodium phosphate buffer, used as a physiological simulated solution, and lactic/lactate buffer, used as a cancer extracellular simulated solution (**Table 2-3**).

Table 2-3. Simulated physiological media.

Buffer solution	Concentration, M	pH	μ, M
$HC_3H_5O_3/C_3H_5NaO_3$	0.1	4.5	0.20
Na_2HPO_4/NaH_2PO_4	0.004	7.4	0.016

a. pH analysis

We evaluated the morphology of the microcapsules in solution at 0 and 60 minutes (time enough for most of drugs to distribute in the body with high efficiently) using an optical microscope, and we measured the change in pH of the solution by adding 100 mg of microcapsules to 10 mL of solution. We used a Thermo Scientific™ Orion™ 3-Star Benchtop pH Meter to take pH measurements every 30 seconds.

b. Zeta potential measurements

The size and zeta potential (ZP) of the microcapsules were measured using a Malvern Zetasizer Ultra instrument (Malvern Panalytica) at a temperature of 25.0 ± 0.5 °C. The size measurement was performed using a dynamic light scattering (DLS) technique, and the ZP measurement was conducted using Laser Doppler Anemometry (LDA). The microcapsules were analyzed in suspension immediately after preparation to avoid any changes in their size or charges due to Ostwald

ripening or particle growth. For each experiment, the mean of three measurements was calculated.

c. Folic acid profile release from the microcapsules.

To determine the folic acid release profile, 100 mg of microcapsules were added to 10 mL of buffer solutions and stirred at 300 rpm at room temperature. Aliquots were taken every 10 minutes for 30 minutes, without substantially modifying the 5% v/v of the total volume of the solution. The filtered matrix (using a 200 nm pore size filter) was then analyzed by HPLC-DAD Shimadzu LC-40C with a C18 column (Kromasil 100-5 phenyl®, 300X4.6 mm, 5 µm) purchased from Agilent Technology. The mobile phase composition is shown in **Table 2-4**.

Table 2-4. Mobil phase composition for HPLC-DAD analysis.

Mobil phase		Ratio, %w/v	
Buffer solution at pH 6.0	0.2 M K_2HPO_4	63	90
	0.1 M Citric acid	37	
Acetonitrile (ACN)		10	

The HPLC analyses were carried out at an isocratic elution of 1.5 mL/min at room temperature, and the detection was monitored at a wavelength of 290 nm. Two calibration curves were generated for low (0.2-1 ppm, R^2 = 0.9991, y = 77.622x + 7198.9) and high concentrations (1-5 ppm, R^2 = 0.9993, y = 104031x + 12488). The retention time of folic acid was found to be 3.23 minutes. The mean of three measurements was calculated for each experiment.

2.4 RESULTS AND DISCUSION

Initially, we tried to produce CS/TPP microcapsules by using the ionic gelation method. However, this method resulted in low quantities of globular microcapsules that were difficult to filter from amorphous aggregates (Pacheco, 2019). Therefore, we found spray drier to be a proper method to produce larger number of microcapsules for analysis. However, spray drier produces particles with heterogeneous size distribution.

We formulated different CS/TPP emulsions to produce microcapsules and to investigate the effect of the inlet temperature, aspirator pump flow rate, and a feed flow rate parameter of the spray-drying. Our objective was to examine the resulting morphology, size, and distribution of the microcapsules. The technique allowed us to generate many microcapsules that were useful for evaluating their behavior in aqueous media, including simulated physiological media for both normal and cancer extracellular environments. We examined the release profile of folic acid analogue to methotrexate (highly toxic) in simulated physiological media using HPLC-DAD and studied the behavior of the CS/TPP microcapsules in the presence of the drug.

2.4.1 Characterization of the CS/TPP microcapsules

a. Microcapsule morphology dependent on composition

Some preliminary microcapsules were produced by using emulsion with 0.4, 0.6 and 0.8 %w/v CS mixed with and without TPP and FA, in order to observe morphology and size dependency on composition, microcapsules are shown in **Figure 2-3**. The parameters of the spray drier were the same in all experiments, inlet temperature 170 °C, aspirator 29.75 m^3/h and feeding rate 6 mL/min. The microcapsules are mostly collapsed. In general microcapsules look more collapsed with lower content on CS, what might be due to the drying process.

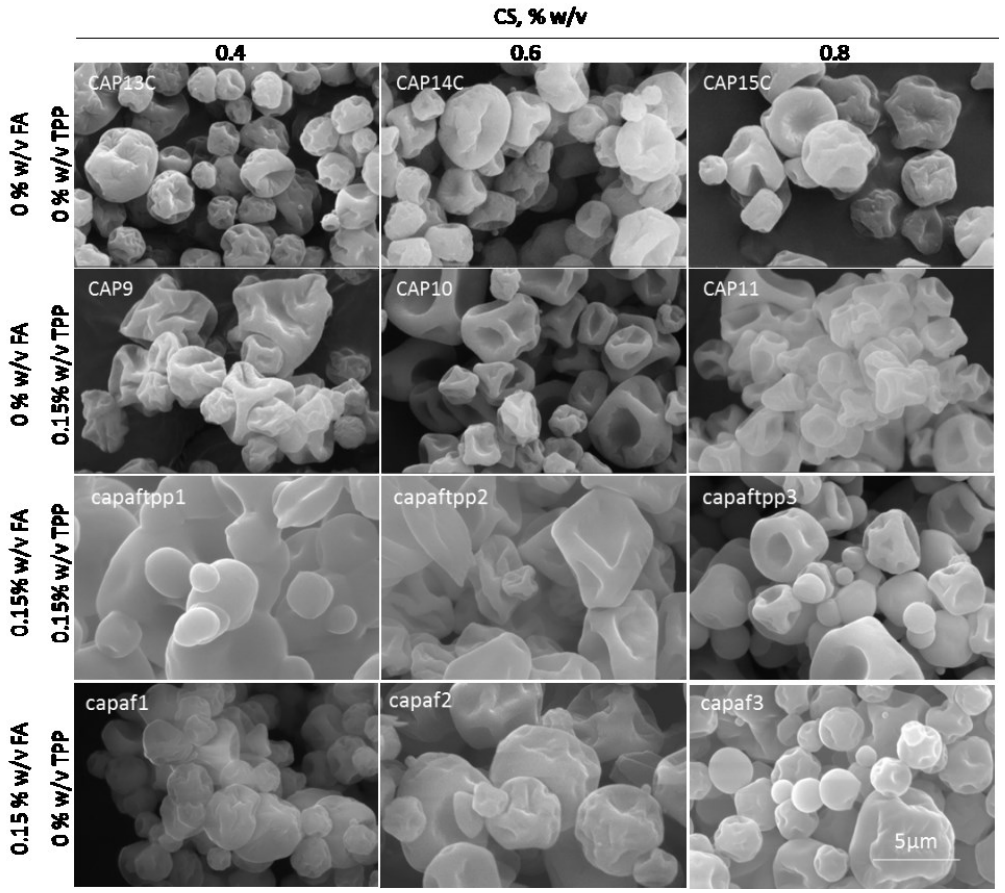

Figure 2-3. Microcapsules produced by SD at different CS and TPP composition.

During spray-drying processes, each droplet typically forms a single microcapsule, which means that the final microcapsule size is determined by the initial droplet size and solid content. It is important to note that spray drier typically results in a low level of control over droplet formation, leading to microcapsules with a broad size distribution. The wide size distribution might be due to droplet explosions into smaller pieces during the drying and the low solution concentration. We can say that during the formation of microcapsule shells, the moisture rapidly moves from the droplet interior to maintain surface saturation and minimize surface energy. As the water, and later, AcOH (acetic acid) evaporates at the droplet surface, so the droplet surface is fully wetted. The droplet diameter decreases, and the maximum

drying rate is achieved. As the evaporation rate increases, the surface reaches its critical supersaturation faster, leading to early shell formation. This stage results in the formation of a corrugated shell on the droplet surface.

Later, the droplet surface cannot maintain saturation by moisture migration. The vapor produced inside the shell diffuses out to the surface through the shell's pores or molecular gaps. The drying rate decreases as the thickness of the shell increases. This diffusion time is the same in all experiments due to the aspiration rate 29.75 m^3/h. So, the drying process of the droplets depends on the interactions of compounds in the emulsion drop. The shell's thickness is influenced by the solid content and the feed rate of raw materials (Philipp Seydel, 2006; Dan-Lei Yang, 2024).

b. Microcapsule morphology as a function of on spray drier parameters

We used different configurations of the spray-drying process to explore the effects of the inlet temperature and aspirator gas flow rate on the morphology, size and size distribution of the microcapsules by choosing the emulsion composition that produced more globular microcapsules, as shown in **Figure 2-4**. The emulsion used in the experiments contained 0.80 %w/v CS and 0.64 %w/v TPP, and the flow rate was kept constant at 6 mL/min.

The inlet temperature of the drying gas is one of the most critical parameters in spray drier. It determines the drying capacity of the humid droplets and the solvent evaporation rate. The inlet temperature significantly affects the crystallization degree, porosity rate, and drug loading of the particles. High gas flow rates increase microcapsule movements, reducing the air-droplet interaction time. A low drying gas flow rate ensures complete particle moisture removal. Microcapsules produced at higher inlet temperatures result in faster drying rates, leading to higher porosity rates and uniform morphology. Lower inlet temperatures and high aspirator gas flow rates caused higher moisture retention and longer residence time inside the

drying chamber, this increase extraction of humidity to guarantee dried microcapsules (Nienke M. Eijkelboom, 2023; Dan-Lei Yang, 2024).

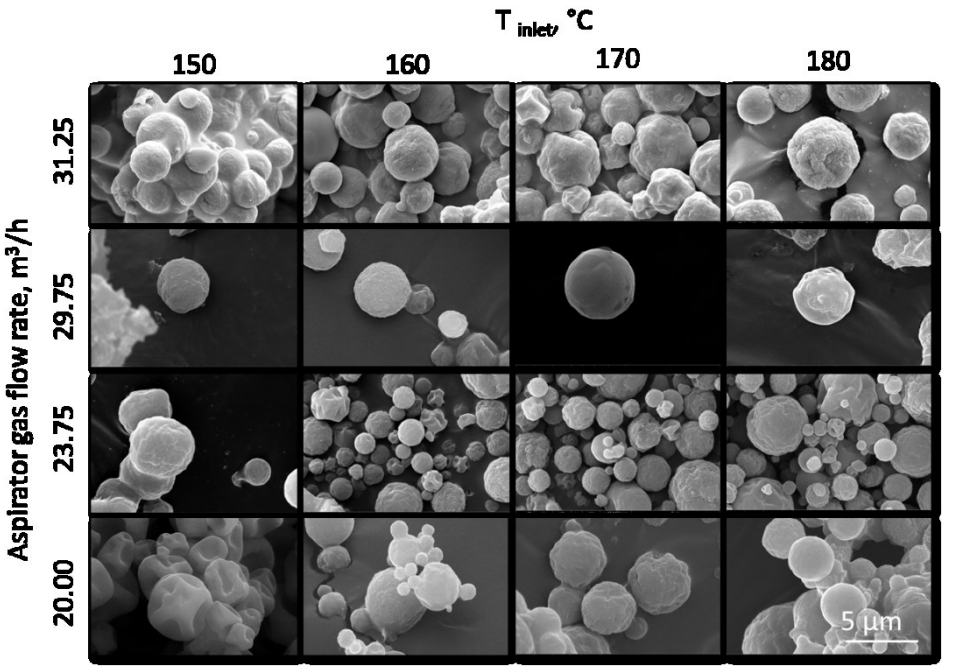

Figure 2-4. SEM images of CS/TPP microcapsules C18 (0.80 %w/v CS/0.64 %w/v TPP) at different aspirator gas flow rates and inlet temperatures.

c. Microcapsule morphology depending on crosslinking degree

We produced microcapsules at various stoichiometric ratios of CS and TPP to evaluate the crosslinking degree. Specifically, we selected the CS concentration that resulted in the formation of more globular microcapsules. Additionally, we aimed to compare these microcapsules with emulsions featuring the same stoichiometric ratios but lower mass content. The spray drier conditions used were 180°C, flow rate 6mL/min, aspirator gas flow rate 31.25 m^3/h. The morphology is showed in **Figure 2-5.**

The microcapsules produced with higher TPP content than CS exhibit a globular morphology with a regularly rough surface; TPP enhances rougher, while more CS

becomes smoother. The spherical is achieved with the maximum structural stability of microdroplets. In contrast, microcapsules produced with higher CS content than TPP collapsed, with both rough and flat surfaces. The compacted and spherical microcapsules had enough time for the CS, TPP, and solvent (water and AcOH) to diffuse homogeneously into the droplet.

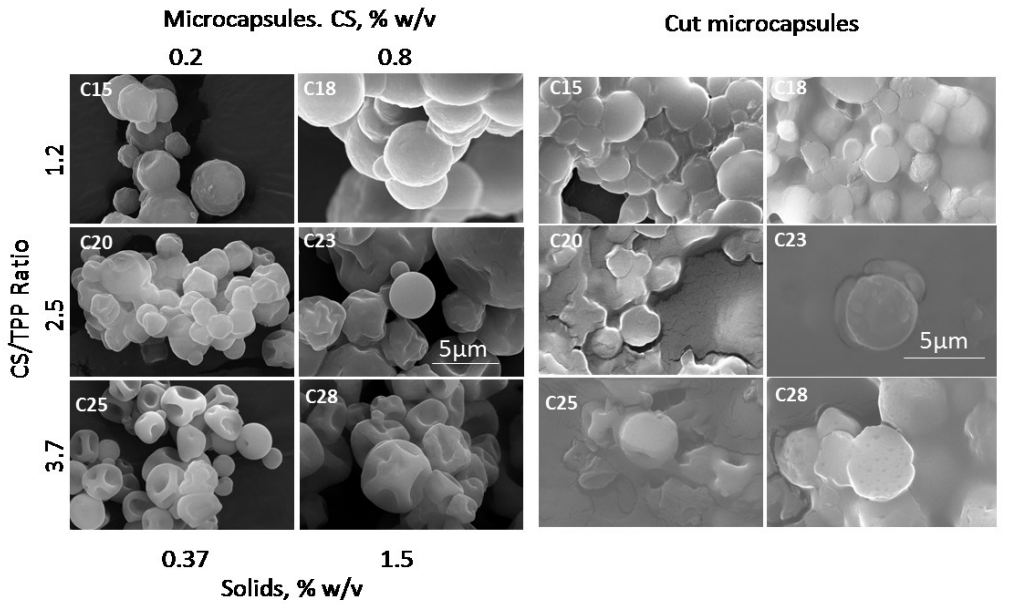

Figure 2-5. SEM images of CS/TPP microcapsules obtained by SD at 1.2, 2.5 and 3.7 CS/TPP ratio.

The collapsed microcapsules morphology might be attributed to the faster diffusion of the CS and TPP solids to the shell and the lowest migration of liquids outside of the microcapsule. However, if the drying process is too fast, and there is no chance for CS and TPP to diffuse, a hollow structure of the microcapsules will be formed as in C28 microcapsule (Philipp Seydel, 2006; Dan-Lei Yang, 2024).

d. Microcapsules' size and size distribution

The size distribution of microcapsules, produced from emulsions with different ratios of CS to TPP, but under the same spray-drying conditions (inlet temperature:

170°C, aspirator gas flow rate: 29.75 m^3/h, pump rate: 6 mL/min) is shown in **Figure 2-6a**. As expected, the microcapsules' size is directly proportional to the CS concentration. However, at low CS concentrations (0.2% w/v), the size is drastically affected by the TPP concentration. This may be due to the lower compactness of the net and crosslinking degree at higher TPP concentrations, resulting in a higher size distribution.

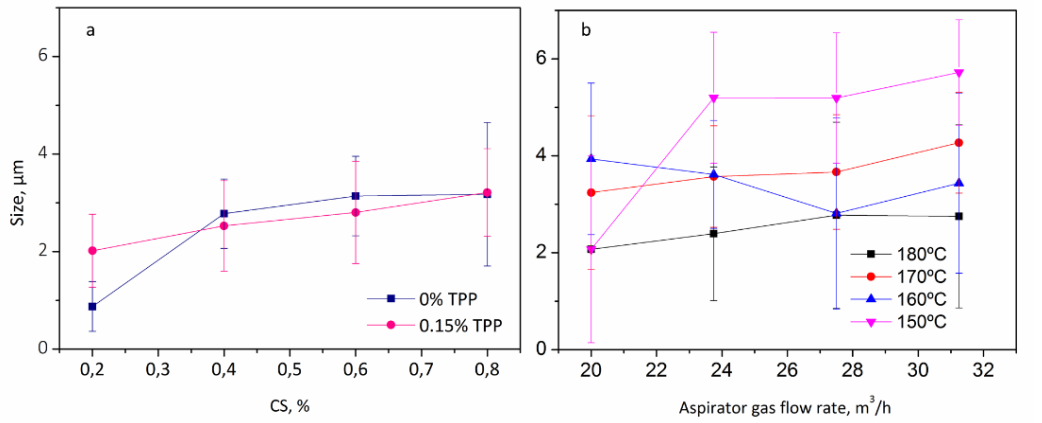

Figure 2-6. Comparison of the size diameter momentum (average of standard deviation of 100 microcapsules SD) of CS/TPP and CS microcapsules obtained by spray drier at different a) CS concentration of the solutions and b) SD conditions.

Microcapsules produced at different spray drier conditions but same composition (**Figure 2-6b**), as expected, are larger at lower inlet temperatures due to the higher moisture content during the drying process. Additionally, microcapsules produced at lower aspirator gas flow rates remain in the spray drier chamber for a longer period, hindering the evaporation process. However, despite our efforts to study the composition and spray drier parameters, it was not possible to obtain microcapsules with a narrower size distribution. The mean size of the microcapsules remains consistent in both plots in **Figure 2-6**, regardless of the emulsion concentration and spray drier conditions.

e. Evaluation of microcapsule crosslinking degree

The crosslinking degree is a crucial factor in microcapsules to be used for drug delivery applications as it determines the point at which the resulting structure is dissolved into the solution to release the load. In order to analyze this parameter, we compared the FTIR spectra of raw CS and TPP, CS/TPP coacervated, and C18 microcapsules, as shown in **Figure 2-7**. To obtain the FTIR spectra of the emulsion, we subtracted the background signal from the water.

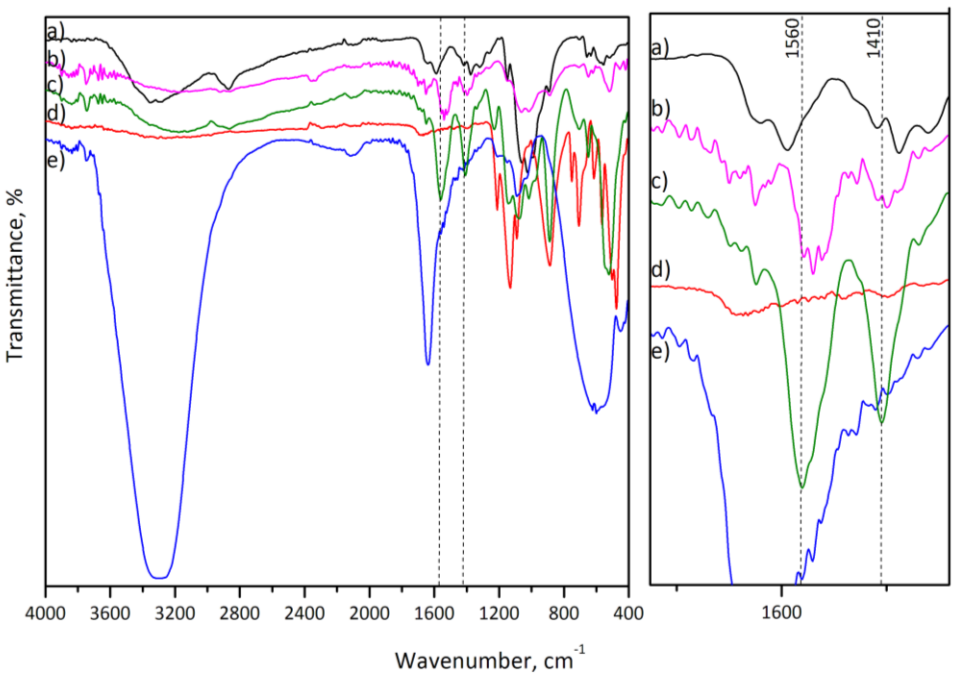

Figure 2-7. FTIR spectra of different components involved in the production of CS/TPP microcapsules. The spectra of a) CS, b) coacervated with composition C18 without water background, c) microcapsule with composition C18, d) TPP, and e) coacervated with composition C18 with water background.

Typically, the FTIR bands of CS and TPP overlap when the compounds were mixed, but new bands or elongations appear when a new bond is formed, as seen at 1410 and 1560 cm^{-1}, which elongate due to electrostatic interaction between CS and TPP. This elongation is caused by the stretching movement between the -C-N- and -N-H

of the chitosan, due to the presence of the electrostatic interaction of the phosphorus compound from TPP. This electrostatic interaction promotes crosslinking between the CS chains' (-NH_3^+ group) and TPP molecules' (-OH group) to form a net. The net's density depends on the quantity of TPP per CS chain (Ilaria Silvestro, 2020).

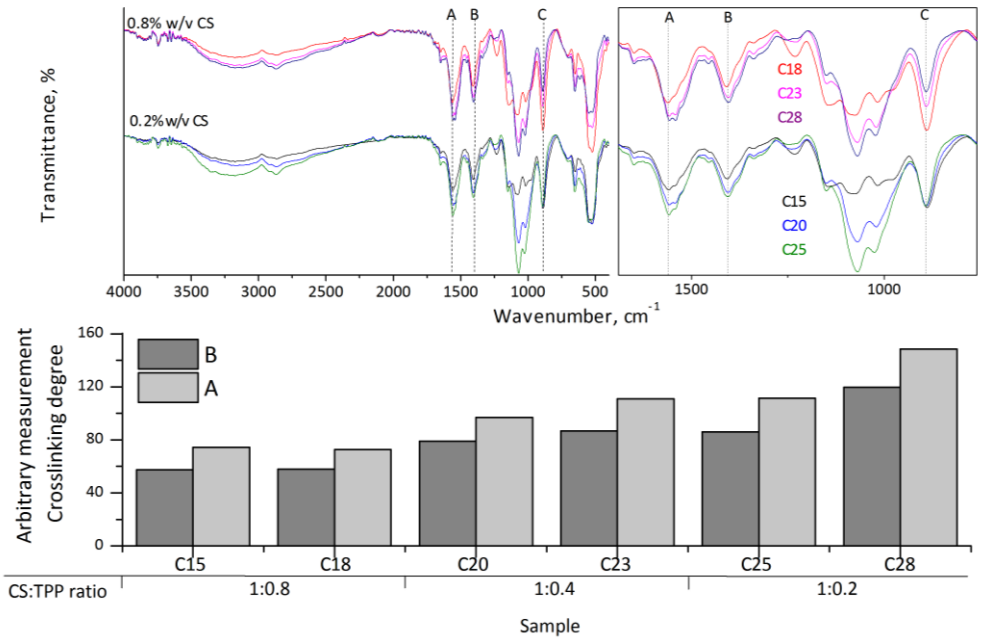

Figure 2-8. Qualitative evaluation of crosslinking degree of CS/TPP microcapsules through FTIR analysis, CS/TPP mol ratio: C15 and C18 (1:0.8), C20 and C23 (1:0.4), and C25 and C28 (1:0.2).

The crosslinking degree of the microcapsules was investigated on the microcapsules with CS/TPP stoichiometrically prepared, as shown in **Figure 2-8**. The degree of crosslinking was determined by analyzing the length of the bands that belong to the stretching and vibrational infrared bands at 1410 and 1560 cm^{-1}, respectively, and comparing them to the length of the band that belong to the vibrational mode of TPP at 890 cm^{-1}. In **Figure 2-8**, it can be observed that at high TPP concentrations, the crosslinking degree is lower. This can be attributed to the steric effects caused

by the spatial arrangement of atoms, which lead to high electrostatic repulsions and hinder the movement of TPP structures through the CS chains.

2.4.2 Microcapsules performance in solution

a. Microcapsule morphology in simulated physiological media

Chitosan is a weakly basic polymer with amino groups that can protonate under acidic conditions, resulting in a positive charge on the polymer. At low pH values, chitosan becomes more soluble due to the protonation of the amino groups, which increases the electrostatic repulsion between the polymer chains and reduces their aggregation. As a result, CS microcapsules are more stable and less prone to aggregation at low pH values.

In contrast, CS/TPP microcapsules are less pH-sensitive than chitosan capsules due to the presence of the TPP as crosslinker. TPP is a negatively charged molecule that can react with the positively charged amino groups on chitosan to form a network of crosslinked polymer chains. This crosslinking process can make the CS/TPP capsules more stable and less prone to aggregation at a wide range of pH values.

In summary, the behavior of chitosan and CS/TPP microcapsules at different pH solutions is different due to the presence of TPP crosslinker in CS/TPP microcapsules. Chitosan capsules are more pH-sensitive and prone to aggregation at low pH values, while CS/TPP microcapsules are less pH-sensitive and more stable due to the presence of the crosslinked network of polymer chains.

Crosslinked microcapsules containing folic acid (FA) were produced to investigate their release profile and integrity behavior. Microcapsules produced from a sample solution named (capaftpp3), consisting of 0.80 %w/v CS, 0.15 %w/v TPP, and 0.015 %w/v FA and a blank (cap11) without FA, were submerged at pH 4.5, 6.5 and 7.5 and observed under an optical microscope (40X) at 0 and 24 h. In **Figure 2-9**, microcapsules obtained from sample cap11 remain unswollen compared to those

obtained by capaftpp3. The microcapsules obtained by capatpp3 after 24h immersion swelled. This swelling is caused by the ionization of the ionic pendant groups (-OH) in the presence of protons over time, leading to the development of charges on the polymeric networks and resulting in electrostatic repulsion forces among them.

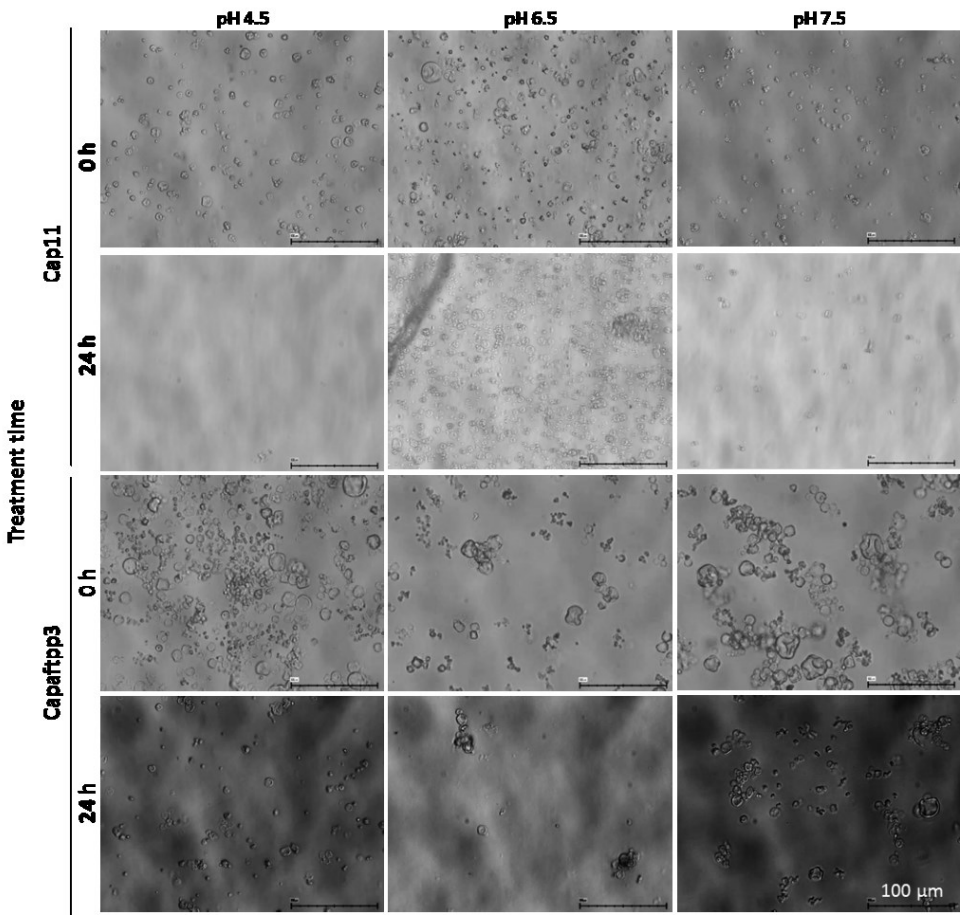

Figure 2-9. Optical images of microcapsules captured at different exposure times and pH values.

The swelling behavior of the microcapsules is directly related to the applied external stimulus, which in this case is pH. As a result, the microcapsules undergo a significant volume phase transition or gel-sol phase transition in response to

changes in pH. This ability to maintain structure in response to pH is due to the physical cross-linking of individual CS chains related to its capacity to be protonated as shown in **Table 2-1**.

b. Zeta potential measurement dependent on the pH of the solution

The surface charge of nanoparticles plays a crucial role in targeted drug delivery (Bingdi Chen, 2016). When conventional nanoparticles lacking surface modifications or negatively charged particles are introduced into the bloodstream, they experience rapid opsonization and significant clearance by fixed macrophages. Hence, it is important to explore the behavior of microcapsule surface charge (Zahir., 2013).

The behavior of microcapsules in solution is influenced by factors such as pH and surface charge (Kleine-Brueggeney, 2015). In our study, it was observed that microcapsules tended to aggregate and precipitate, indicating poor stability in dispersions below 30 mV. Zeta potential (**Figure 2-10a**) and pH measurements (**Figure 2-10b**) were performed with sample capaftpp3 (**A**) and cap11 (**B**) which composition are described in **Table 2-2**. As can be seen in **Figure 2-10a,** the reference microcapsules in **Figure 2-10a**(**B**) exhibited a lower value of zeta potential, indicating an increase in electrostatic attraction and sedimentation tendency. Conversely, microcapsules containing FA in **Figure 2-10a**(**A**) showed a higher zeta potential value, indicating a greater surface charge due to FA and enhanced electrostatic repulsion. This suggests improved dispersion stability.

In other words, the surface charge of CS/TPP microcapsules is pH dependent as shown in **Figure 2-10a**(**A-B**)**.** At low pH values, the chitosan molecules on the microcapsule surface remain partially protonated, resulting in a net positive charge, leading to greater electrostatic repulsion and higher zeta potential. This increased stability can be attributed to the continued protonation of the CS chain. Therefore, FA distribution on the microcapsule surface was evident through the increased

surface charge at low pH. The zeta potential was directly correlated with CS concentration, indicating that higher CS concentration resulted in an increased zeta potential.

At neutral pH, the surface charge of CS/TPP microcapsules is close to zero due to the balance between the positive charge from chitosan and the negative charge from TPP phosphate groups.

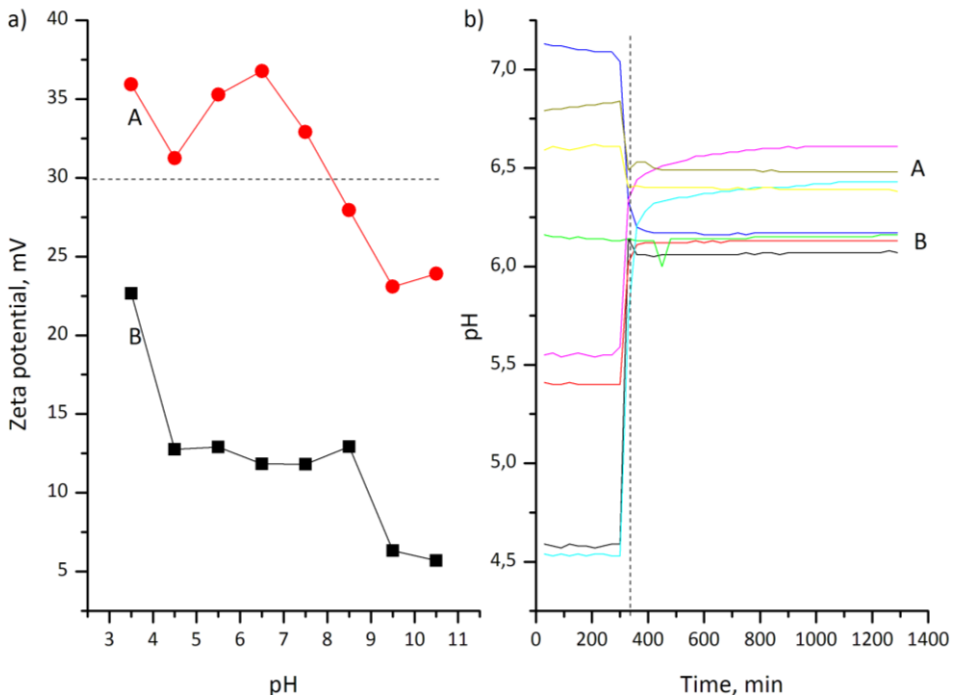

Figure 2-10. Estimation of CS/TPP microcapsules stability in various pH solutions and the proton exchange compared to reference and FA microcapsules. a) zeta potential analysis and b) pH measurement of samples in contact with different pH solutions where A: sample capaftpp3 and B: sample 11.

Above neutral pH, the surface charge of CS/TPP microcapsules becomes increasingly negative due to the deprotonation of TPP hydroxyl groups, leading to a decrease in the positive charge. This shift towards a negative surface charge enhances the

stability and dispersion of the microcapsules, reducing aggregation tendencies and improving colloidal stability.

Controlling the surface charge through pH adjustment is a crucial feature for the targeted delivery of microcapsules to specific tissues or cells, enhancing efficacy and minimizing unwanted side effects (Kleine-Brueggeney, 2015). This pH-dependent surface charge has significant implications for microcapsule behavior in different environments and their potential applications in drug delivery (Bingdi Chen, 2016). Microcapsules with FA were found to have a higher tendency to attach to proteins for medical purposes while remaining dispersed. (Mandeep Kaloti, 2010).

As shown in **Figure 2-10b**, the microcapsules containing FA in **Figure 2-10b**(**A**) are able to release more protons to the medium than the reference microcapsules in **Figure 2-10b**(**B**)**.**

DLS measurements were conducted using various pH and salt solutions in order to increase microcapsule dispersion. However, the results were not satisfactory and there was not any change with respect the previous results, as microcapsules were not dispersed efficiently. The size measurement was inconsistent with SEM images, likely due to the presence of large aggregates beyond the detection limit of the equipment. The electrostatic interactions on the microcapsules were too significant to achieve dispersion across different solution compositions.

c. Release profile of folic acid

The representative microcapsules sample containing folic acid (FA) was subjected to testing in various buffer solutions, specifically phosphate and lactate buffers. These buffer solutions were chosen to mimic the concentrations found in both physiological healthy environments and tumoral environments.

The release profile of FA shown in **Figure 2-11**, from crosslinked microcapsules in phosphate buffer solution, shows that over 20 %w/v FA is released from the

microcapsules at 0 min, indicating that FA is not fully incorporated into the microcapsules. However, over 60 min, there is an increasing tendency to donate protons to the media, suggesting that the cationic FA is becoming more susceptible to being released into the phosphate buffer solution. In contrast, when the microcapsule is exposed to buffer lactate for 60 min, the microcapsules show a tendency to trap protons from the media and remain swollen, while FA remains attached to the CS/TPP crosslinked chains. This indicates that FA is more effectively attached on the microcapsules in presence of the buffer lactate, resulting in a lower release rate compared to phosphate buffer solution.

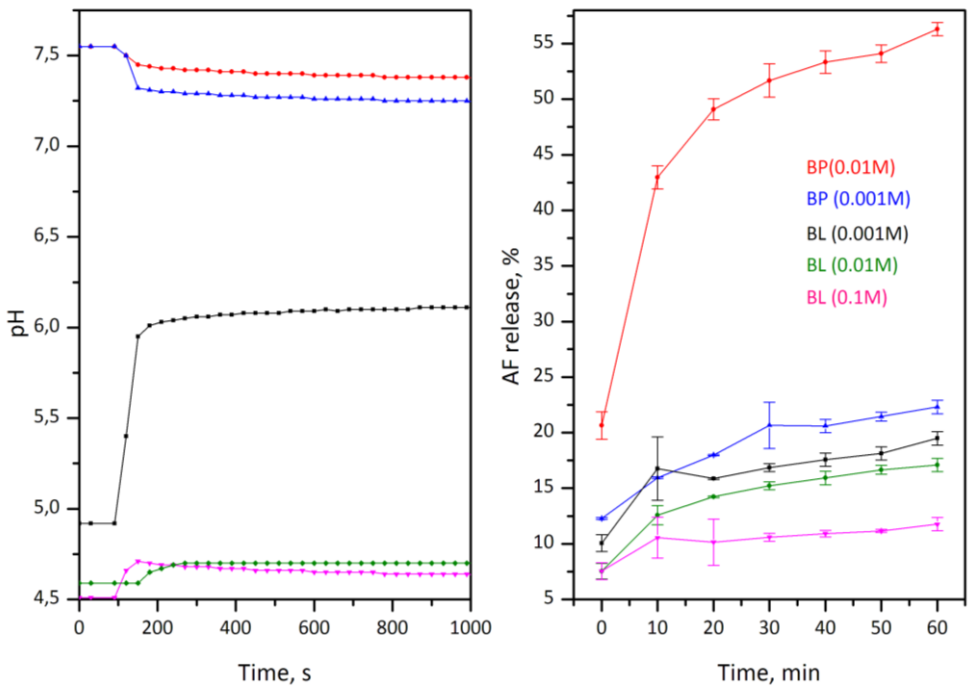

Figure 2-11. a) Buffer effect on microcapsule (CapAFTPP3) containing FA, and b) release profile of folic acid (FA) in phosphate buffer (PB) and lactate buffer (LB).

These results are interesting as they reveal the potential of CS/TPP microcapsules containing folic acid. Chitosan effectively retains folic acid under low pH conditions, which are typically found in aggressive tumor environments (Natarajan Raghunand R. J., 2000). This property makes the microcapsules suitable for efficiently targeting

cancer cells (Agnes Aruna John, 2017). Additionally, the microcapsules in the proximity of cancer cells can release other anticancer drugs without experiencing chemical deactivation, making them promising candidates for pharmaceutical applications.

2.5 CONCLUSIONS

In the study of production and physicochemical evaluation on simulated physiological environment of CS/TPP microcapsules, several important findings emerged:

Microcapsules produced by spray drier: This method provided a broad size distribution from 0.8 µm to 50 µm. Other spray drier parameters like nozzle size, atmospheric gas and pressure might be optimized in order to obtain reduce size distribution. The low air inlet temperature results in a low evaporation rate, which leads to microcapsules with high-density membranes, high moisture content, low fluidity, and ease of agglomeration. Upper 170 °C of inlet temperature results in extreme vaporization, and membrane cracks may occur, and subsequently premature degradation of the integrity of the microcapsule.

Behavior of CS/TPP microcapsules in different pH solutions: The presence of the TPP crosslinker in CS/TPP microcapsules provides stability across a wide range of pH values upper pH 4.5. Chitosan capsules, on the other hand, are more pH-sensitive and prone to dissolution at low pH values. The protonation of chitosan's amino groups under acidic conditions increases the electrostatic repulsion between polymer chains, making them more soluble and less prone to dissolution. The physical cross-linking of CS chains contributes to the microcapsules' ability to maintain their structure in response to pH changes below 6.5.

The surface charge and release behavior of CS/TPP microcapsules containing folic acid (FA): The surface charge of microcapsules is pH-dependent, with higher zeta potential at low pH values, indicating increased surface charge and enhanced dispersion stability. The presence of FA on the microcapsule surface further increases the surface charge due to its cationic nature, improving dispersion stability. The pH-dependent surface charge of CS/TPP microcapsules has significant

implications for their behavior in different environments and their potential applications in targeted drug delivery.

In terms of FA release, the experiments conducted in phosphate and lactate buffer solutions showed different outcomes. In phosphate buffer solution, FA exhibited a higher release rate, with over 20% released at 0 minutes and an increasing tendency to donate protons to the media over 60 minutes. This suggests that cationic FA becomes more susceptible to be released in phosphate buffer solution. However, in lactate buffer solution, the microcapsules retained their swollen state, trapping protons from the media, and exhibited a lower release rate of FA. This indicated that FA was more effectively attached to the CS/TPP crosslinked chains in the presence of lactate buffer.

Overall, the experiments demonstrated that CS/TPP microcapsules exhibit pH-dependent behavior, with enhanced stability, reduced aggregation, and improved dispersion stability due to the presence of the TPP crosslinker. The surface charge of the microcapsules was influenced by pH, and the attachment of FA further modified the surface charge, affecting dispersion and stability. The release profile of FA was also pH-dependent, with higher release rates in phosphate buffer solution compared to lactate buffer solution. These findings highlight the potential of CS/TPP microcapsules for targeted drug delivery applications (Agnes Aruna John, 2017), where pH adjustment can be utilized to control their behavior and release profiles.

3 CS/TPP NANOCAPSULES BY ELECTROSPRAY

"A thing of beauty is a joy for ever
Its loveliness increases; it will never
Pass into nothingness; but still will keep…"
— John Keats

3.1 INTRODUCTION

The spray drier technique is associated with several limitations concerning the production of microcapsules with several materials due to the use of high temperatures and degradation of thermolabile compounds, difficult to control morphology and size distribution (Jelena Filipović-Grčlić, 2003). Although we can generate large quantities of chitosan crosslinked sodium tripolyphosphate (CS/TPP) microcapsules for physicochemical characterization using spray drier, they are micron scale size, which implies lower interaction in biological systems. This limitation has prompted us to explore other alternative techniques as ionotropic gelation and electrospray.

Contrary to spray drier in electrospray there are just a few commercially available and some handmade setups. However, these setups don't allow control over the size distribution, which represent challenges and opportunities for improvement. In our research, we needed to create our own setup and method for making cross-linked CS/TPP nanoparticles (rods, capsules, spheres, starts among others) using electrospray. This was a challenge because there aren't many documented procedures or evidence of successful cross-linking using electrospray for CS/TPP materials.

To develop methodology and "lack of" literature, we have collaborated with the respected research group DEW "Droplets, intErfaces and floWs" from Universitat Rovira I Virgili. Together, we are undertaking the development of the electrospray technique from scratch, leveraging the expertise and resources of this research

group. Our ultimate objective is to produce CS/TPP nanocapsules with precise control over size and distribution through the utilization of the electrospray method.

The principle of electrospray technique is explained in section **1.4.2**. Electrospray (**Figure 3-1a**) is an electrohydrodynamic method, widely used to fabricate nanofibers or nanoparticles based on the use of electrostatic forces, offers control over the size and morphology of the particles (Bodnár, 2018), and it produces all the feed material in nanocapsules being highly efficient and scalable (Joan Rosell-Llompart, 2018). The electrospray process involves the use of a high voltage power supply to create an electric field between the nozzle, usually a capillary tube, and a downstream electrically-grounded electrode, resulting in an electrical force that focuses the liquid into a thin jet, whose width is much smaller than the size of the capillary tube (Joan Rosell-Llompart, 2018).

However, (Chen, 2017; Esmaeili, 2021; Xu, 2007; Naghibi Beidokhti, 2017; Kultida Songsurang, 2011), the available data on producing crosslinked CS/TPP nanoparticles by electrospray is insufficient due of a lack of characterization of the particles, and previous attempts in crosslinking chitosan with TPP have not probe crosslinked CS/TPP. The process proposed in the literature involves electrospray chitosan particles into TPP-containing baths (Yixiang Xu, 2008). Unfortunately, there is a lack of robust control over these methodologies, and the evidence supporting successful crosslinking between CS and TPP remains limited.

Given these limitations, we embarked on reproducing these methodologies given in literature (Chen, 2017; Esmaeili, 2021; Xu, 2007; Naghibi Beidokhti, 2017; Kultida Songsurang, 2011), but soon we realized the need to develop a novel approach for crosslinking CS/TPP during electrospray. This required a thorough understanding of important concepts, leading us to use and further design a coaxial experimental setup.

.

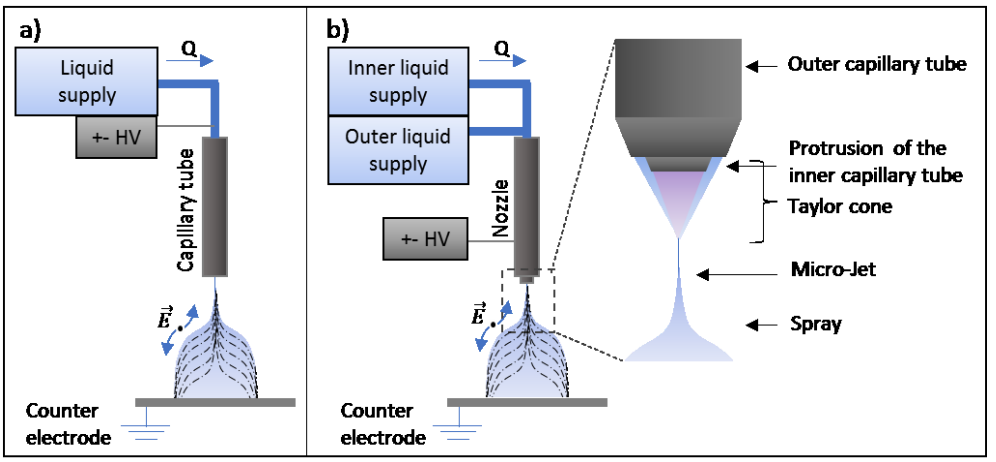

Figure 3-1. Electrospray diagram a) one liquid supply in a single capillary tube and b) two liquids mixed in coaxial capillary tubes (nozzle).

The electric field deforms the interface of the liquid leaving the capillary tube or nozzle (coaxial capillary tubes); the liquid meniscus is deformed to produce a steady Taylor cone that focuses the liquid into a steady micro-jet (Taylor G. , 1964). The fluid dynamic structure is named a cone-jet, and this fluid dynamic mode called the cone-jet mode. The charged droplets, produced by the spontaneous breakup of the jet, drift downfield through the air towards the counter electrode. Meanwhile, the drying leads to the formation of solid nanocapsules (Jaworek, 2008).

The coaxial method shown in **Figure 3-1b**, is a derivative method of electrospray, usually used to from layered structures from immiscible liquid (Jung, 2013) to encapsulate molecules under mild conditions with high efficiency but we used for mixing two aqueous solutions during this research. In this method, two capillary tubes are placed concentrically (nozzle), and two liquids, immiscible or not, flow separately through the nozzle (Brynn N. Sundberg, 2018).

In order to have stable electrospray in a coaxial mode, the protrusion, diameters of the capillary tubes and concentricity need to be studied. The inner capillary

protruding from the outer capillary depends on the feeding rates of the inner and outer liquids as the liquids properties (Meghdad Kamali Moghaddam S. M., 2015).

The concentricity of the capillary tubes (Dazhi Wang, 2022) and the nozzle tip shape can be also important factors in producing a stable electrospray in our ES system. The nozzle shape influences the electric field strength, which in turn determines the shape of the Taylor cone, the size of the droplets, and the velocity of the charged particles (López-Herrera J. M., 2023). We have empirically learned of the importance of keeping good concentricity, indicating that keeping the symmetry of the flows is important.

The tip shape of the nozzle also affects the formation of the electric field and the concentration of the electrical charge. A nozzle with a sharp or pointed tip can create a more intense electric field for a given applied voltage. The rounded tip facilitates wetting, leaving the drop's anchoring point undefined; and that doesn't help maintain a constant flow or a drop with a repeatable shape whose size will affect the required voltage value. Therefore, the shape of the nozzle is critical in controlling stability of the nanocapsules produced by electrospray. The optimization of the nozzle shape can improve the efficiency and reproducibility of the electrospray process and enhance the quality of the final product.

The liquids properties used for coaxial electrospray affect the formation of the coaxial jet and the resulting nanoparticles or fibers (Dazhi Wang, 2022). The coaxial configuration is frequently used in electrospinning producing fibers. In the electrospinning literature there are examples of use of partial miscible liquids to from encapsulations or mixed compounds in the fibers (Shameek Vats, 2021). When the liquids are miscible, they tend to mix at the interface, and the resulting coaxial jet may have a more uniform composition and morphology. On the other hand, if the liquids are immiscible (water is less used in ES; ethanol, acetone are more typical in ES are organic solvents like dichloromethane, butanone) they tend to form

a core-shell structure, where the inner and outer fluids are separated by an interface, which can affect the encapsulation efficiency and the release properties of the resulting particles or fibers.

Electrosprays using organic solvents have been extensively studied (Bodnár, 2018; Faezeh Bagheri-Tar, 2007), but there are still significant knowledge gaps in electrospray regarding aqueous solutions. Understanding the dynamics of droplet evaporation and solidification is crucial for controlling particle size and morphology. Achieving control over the size and size distribution of the particles produced by electrospray is essential for applications such as drug delivery and materials synthesis. Aqueous solutions are technically more challenging to use in electrospray, which are prone to degradation and changes in electrical conductivity over time, which can impact the spraying process and resulting particle properties. Additionally, the main challenge faced in this project is the combined use of coaxial electrospray with an in-situ crosslinking reaction, specifically CS/TPP crosslinking, which provide extra complexity. Such a complex situation has not been studied much and is not yet fully understood due to the complex mechanisms involved.

3.2 OBJECTIVES

3.2.1 General objective

- To develop a robust and efficient method based on electrospray to produce crosslinked CS/TPP nanocapsules suitable for pharmaceutical applications. The pharmaceutical suitability of the capsules in this work will be determined initially by requirements of size and morphology, and later by in vitro testing on cell cultures. The actual pharmaceutical development is outside the scope of this thesis.

3.2.2 Specific objectives

- To determine the morphology and size distribution of CS nanocapsules produced by electrospray using a single needle and a specific solution sample batch, aiming for suitable characteristics for pharmaceutical applications.
- To compare different experimental methods for achieving crosslinking of CS nanocapsules with TPP, such as the process of depositing wet CS nanocapsules onto TPP solutions.
- To characterize the morphology and crosslinking of CS nanocapsules collected onto a TPP solution bath with different concentrations and under different experimental approaches, with the aim to achieve stable and crosslinked nanocapsules suitable for pharmaceutical use.
- To characterize produced nanocapsules from solutions containing CS and TPP by electrospray, focusing on optimizing the electrospray conditions and studying the particle size range.
- To design and evaluate the performance of a coaxial electrospray-microfluidic nozzle to achieve homogeneous mixing of CS and TPP solutions during the electrospray process, aiming to enhance the crosslinking degree of CS/TPP nanoparticles and improve the stability and structural integrity of the resulting nanocapsules.

3.3 METHODOLOGY

3.3.1 Materials

The chemicals and reagents used in this study were obtained as commercial products and used without further modification. Chitosan (CS) with a molecular weight average from 100 to 300 kDa (CAS Number 9012-76-4) was purchased from Across Organics (Spain). Sodium tripolyphosphate (TPP) was purchased from Sigma Aldrich Co. Acetic acid glacial extra pure (AcOH) was obtained from Scharlab (Spain). Ultrapure water from Millipore (USA) was used throughout the experiments. Ethanol absolute (EtOH) (ACS reagent grade, CAS Number 64-17-5) was obtained from Scharlab (Spain). The experiments were performed with in three different gases atmospheres: 1) Synthetic dry air with 99,998% purity (20.9 ±1% O_2 with 3 ppm of H_2O, 0.2 ppm of THC and 1 ppm of CO and CO_2, the rest being N_2); 2) Nitrogen 99,98% purity; and 3) CO_2 99,998% purity, which were purchased from Carburos Metálicos (Spain).

3.3.2 Production of nanocapsules by electrospray

Various methodologies were employed to produce crosslinked CS/TPP nanocapsules using electrospray. These included:

• Producing CS nanocapsules first, and then crosslinking TPP in a subsequent step. In this approach, TPP solutions with different compositions were added on top of the CS nanocapsules (described in **section 3.3.2.1**).

• The CS nanocapsules were produced via electrospray and collected in a bath containing TPP solutions at different compositions including ethanol (described in **section 3.3.2.2**).

• Using stable CS/TPP microemulsions to produce nanocapsules through electrospray (described in **section 3.3.2.3**).

• Designing a novel methodology for coaxial electrospray that involved mixing the CS and TPP solutions right before the electrospray process to produce crosslinked CS/TPP nanocapsules (described in **section 3.3.2.4**).

• Production of nanoparticles by two systems, 1- and 4-nozzle systems (described in **section 4.3.1.2**).

3.3.2.1 Production of chitosan nanocapsules by electrospray

The electrospray experiment was performed by loading the solution batch code 2C10A50E that contained 2% w/v CS, 10% v/v AcOH, 50% v/v EtOH, 40% v/v H_2O solution into a Terumo syringe (500 µL). The solution was transparent, with a conductivity of 1053 µS/cm; the electrical conductivity was measured with a conductivity meter (CRISON 35) using a glass-body probe (CRISON 50 61). The flow rate was controlled using a Harvard Apparatus PHD 2000 infusion syringe pump, and a high voltage of 15 kV was applied to the liquid. The nanocapsules were collected on a silicon wafer substrate located 2.9 cm away from the needle silica + metal capillary (OD: 375 µm, ID:100 µm) acting as the ground electrode. The humidity was maintained at 60% to 70%, and the temperature was kept at room temperature. The flow rate during the electrospray process was 3 µL/min. A digital camera (Panasonic M2050) was used to detect the formation of spraying modes, and a nanoamperimeter was connected to a PC and monitored by software.

3.3.2.2 Two steps preparation of CS/TPP nanocapsules

Nanocapsules composed of chitosan were fabricated using the electrospray technique, as detailed in Section **3.3.2.1**. Subsequently, these CS nanocapsules were employed in two separate experiments for the purpose of crosslinking them with TPP.

In the first experiment, the collected CS nanocapsules were impregnated with 0.1% and 1% w/v TPP solutions and dried at room temperature.

In the second experiment, CS solution was electrosprayed to produce nanocapsules and nanodroplets, which were then collected on a TPP bath to facilitate the formation of crosslinked CS/TPP nanocapsules.

The TPP solutions used in the experiments contained water, either isopropanol or EtOH. The resulting microcapsules were centrifuged at 10,000 rpm, rinsed with water thrice, and an aliquot from the bottom was placed on a silicon wafer and dried at room temperature. Finally, the nanocapsules were characterized using FESEM.

3.3.2.3 Microemulsions in electrospray

The CS/TPP microemulsions were prepared by mixing aqueous stock solutions from CS and TPP. The first solution contained 6.0 %w/v CS with 0.6 %v/v AcOH, while the second solution had 0.2 %w/v TPP. To ensure the elimination of bubbles, the resulting emulsions were sonicated for 5 minutes.

A total of 60 emulsions were prepared by stoichiometrically mixing different proportions of CS and TPP, ranging from 0.01 to 0.80 %w/v CS and 0.008 to 0.07 %w/v TPP. The objective was to observe the stability of the emulsions. Unfortunately, most of the emulsions precipitated within 10 minutes, indicating the formation of aggregates. These unstable emulsions were discarded. However, a small number of emulsions showed stability for over one hour, as shown in **Table 3-1**. Therefore, achieving high stability in the emulsion is essential to ensure uniformity and consistency throughout the electrospray process.

Electrospray process for these compositions requires a low flow rate (less than 1 µL/min), therefore the production of nanocapsules takes a long time. When the solution used in electrospray is very diluted, the nanocapsules production time increases significantly.

In order to maintain the chemical conditions of the crosslinking process, the same stoichiometric ratio of CS and TPP as used in the spray drier method was employed to prepare the emulsions for the electrospray (ES) experiments. The emulsions with longer stability times, as identified in **Table 3-1** (C29, C30, C31), were chosen for the ES experiments.

Table 3-1. Evaluation of particle concentration and stability of the emulsions.

Batch code	Solute, % w/v		Solvent, %w/v	Size, nm	Concentration, x10^8 Particle/mL	Concentration, w/v w/v, x10^{-6} mg/mL	Stability time, min
	CS	TPP	AcOH				
C29	0.5	0.07	33.3	197	3.3	1.3	>60
C30	0.6	0.05	37.5	593	0.90	9.8	>60
C31	0.8	0.09	33.3	637	0.80	0.11	>60
C32	0.6	0.05	0.0100	591	1.1	0.12	30
C33	0.6	0.05	12.3	712	1.4	0.26	40
C34	0.6	0.05	24.7	424	1.8	7.2	40

Equation **(3-1**) describes the concentration of material per mL in the emulsion.

$$Concentration\ w/v = \frac{Particle\ concentration * 10^8 * \pi * Size * 10^5 * 10^8}{6} \quad \textbf{(3-1)}$$

The electrospray experiments in cone-jet stability were conducted under different conditions, including negative: Q_{liq}= 0.1-0.4 µL/min, V_{HVPS} -7.7 to -8.8 KV and positive voltage: Q_{liq}= 0.1-0.5 µL/min, V_{HVPS} 7.16-10 KV, I_{ES} -200 to 250 nA, and with variations in the relative humidity (<10 and ~50 %) inside the chamber and the presence of CO_2.

3.3.2.4 In situ mixing system at the Taylor-cone during electrospray

An alternative method for producing crosslinked CS/TPP nanocapsules involved mixing both solutions in situ prior to electrospray atomization-jetting process. In order to determine the crosslinking reaction time, a qualitative kinetics experiment was conducted using a microfluidic system. The experiment employed two concentric capillary tubes, with the CS solution flowing through the outer tube (ID:

530 µm, OD: 660 µm) and TPP through the inner tube (ID: 75 µm, OD: 220 µm) at a flow rate of 10 µL/min. The peristaltic pump was used to move the solutions. The concentrated 1.6 w/v% CS and 1.3 w/v% TPP solutions were placed in separate 1mL syringes. The reaction progress was monitored by optical observation using a photographic camera, observing the change in color of the solution from a transparent to an opalescent liquid which is produce by the crosslink reaction.

a. Designs of the electrospray nozzle

The electrospray experiments were conducted using a newly designed nozzle that allowed in situ mixing of both CS and TPP solutions. The design of the nozzle includes the possibility to use capillary tubes with different diameters, as outlined in **Table 3-2**. To ensure proper alignment, some of the capillary tubes were centered using a copper wire in a coil shape with a diameter of 60 µm, which was placed between both capillary tubes as shown in **Figure 3-2**.

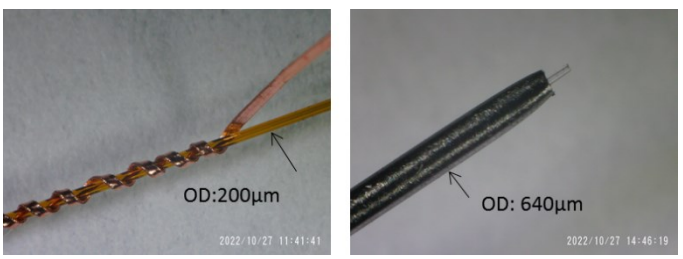

Figure 3-2. Image of the copper coil that center the inner tube of the nozzle.

The stability of the electrospray is dependent not only on the technical conditions but also on the shape of the nozzle. Parameters such as the shape of the ended capillary tubes (whether they are flat or conical), concentricity, and protrusions play a crucial role in stabilizing the Taylor-cone over time.

In order to examine the morphology of the Taylor cone produced by the nozzle, three different protrusions (201 µm, 264 µm, and 284 µm) were evaluated using a nozzle N1 formed by silica inner capillary tube and a stainless steel 23G capillary tube according to **Table 3-2**. The diameter of the silica capillary tube was reduced

by pulling it out, while the metallic tube was polished to create a conical end. As a result, the OD of the metallic capillary tube was 433.6 µm, while the silica capillary tube had an OD of 126.9 µm. The shape and concentricity of the ended capillary tubes, as well as the size of the protrusions, were all important factors for stabilizing the Taylor cone during the electrospray. Other nozzle configurations were evaluated but the Taylor cone jet was absent during the electrospray experiments due to fast dryness of the CS and TPP solutions on the tip.

Table 3-2. Nozzle diameters proposals.

Nozzle code	Inner tube, µm		Outer tube, µm			
	OD	ID	Gauge	OD	ID	Cross section
N1	200	75	23	640	320	120
N2	200	75	21	820	510	310
N3	400	160	21	820	510	110
N4	400	160	17	1473	1067	907

The solutions were prepared as previously described and loaded into the electrospray setup. The nozzle was connected to the power supply, and the downstream TPP solution was also connected. The collector, a silicon wafer, was positioned 2.9 cm away from the nozzle. The general electrospray process was monitored as described in **section 3.3.2.1**.

3.3.2.5 Production of nanocapsules by coaxial electrospray

Several concentrations of CS and TPP solutions were tested to determine the best electrospray mode for producing stable Taylor cone jets, as well as dripping mode. The solutions were tested according to the recipes listed in **Table 3-3** and **Table 3-4**, they were randomly tested by trial and error. The CS solutions were prepared every three weeks and mixed overnight prior to use (the solutions presented black precipitations after three weeks of preparation). The electrospray experiments were also performed at different gas atmospheres like synthetic air, nitrogen and CO_2. For biological experiments it was required to label nanocapsules, therefore,

fluorescein isothiocyanate (FITC) was chemically attached to the CS and incorporated into the solution.

Table 3-3. Composition of the CS solutions for coaxial electrospray.

CS solution	CS, % w/w	FITC, % w/w	AcOH, % v/v	K, µs/cm	pH
CS1	1.7	0	0.64	3560	4.4
CS2	2.0	0	90	446	1.1
CS3	2.0	0	10	3640	3.1
CS4	3.0	0	10	5300	3.2
CS5	2.0	0	60	1478	2.2
CS6	2.0	0	1.7	5110	3.5
CS7	2.0	0.003	90	381	1.1

Table 3-4. Composition of the TPP solutions for coaxial electrospray.

TPP solution	TPP, % w/v	AcOH, %v/v	EtOH, %v/v	K, µs/cm	pH
TPP1	0.050	0	0	617	9.2
TPP2	0.100	0	0	1135	9.1
TPP3	0.120	0	0	1295	9.5
TPP4	0.140	0	0	1465	9.2
TPP5	0.160	0	0	1657	9.3
TPP6	0.180	0	0	1831	9.5
TPP7	1.000	HCl	0	9200	6.5
TPP8	1.000	0	0	10500	7.5
TPP9	1.600	10	0	11530	3.3
TPP10	1.100	10	0	8220	3.3
TPP11	0.500	10	0	4510	2.8
TPP12	0.006	10	0	116	2.2
TPP13	0.006	0.120	10	234	3.5
TPP14	0.025	0.030	10	555	3.6
TPP15	0.050	0.050	10	960	3.5

a. Synthesis of CS-fluorescein isothiocyanate (FITC) to produce fluorescent nanocapsules

Fluorescein isothiocyanate (CAS 3326-32-7) was purchased from Abcr Labs. To synthesize CS-FITC, FITC was dissolved in EtOH, and a 2 %w/v CS solution was prepared. The FITC solution was then added to the CS solution and mixed at 400

rpm overnight in darkness. The resulting solution was precipitated with 1M NaOH, and the gel was washed and rinsed with MilliQ water to remove any excess FITC. The gel was freeze-dried and pulverized for further use. (Hun Min Lee, 2017; Min Huang, 2002).

3.3.3 Characterization of the nanocapsules

a. Morphology, size and size distribution

The morphology and size of the nanocapsules were analyzed using a Field Emission Scanning Electron Microscope (FESEM) (Hitachi, SU3500) after coating them with a ~27 nm Au layer (30 mA, 90 s) in a sputter coater (either a Quorum Q150R ES or a Quorum Q150T S plus). The size distribution of the nanocapsules was determined from the FESEM images using ImageJ software (version 1.53e).

b. FTIR analysis

The crosslinking degree of the nanocapsules was evaluated using FTIR analysis, following the same methodology as described in **section 2.3.4b**. The collected particles on silica wafer substrate were placed on the sampler of the FTIR instrument.

c. Nanocapsule performance in different solutions

The stability of the nanocapsules in solution was investigated by observing the morphology of the nanocapsules by performing high-resolution transmission electron microscopy (HR-TEM) (JEOL JEM-2100, Japan) with an acceleration voltage of 200 kV. To prepare the samples for TEM analysis, the nanocapsules were collected directly from the electrospray onto a TEM grid (formvar/carbon 200 mesh). The grid with collected nanocapsules was wet with a single drop of phosphate buffer or lactate buffer solutions. .

3.4 RESULTS ANS DISCUSIONS

3.4.1 Production of Chitosan nanocapsules by electrospray

The initial electrospray experiments were performed with a single capillary tube/needle. CS nanocapsules were produced using the solution sample batch code 2C10A50E. It is a transparent solution, with a conductivity of 1053 µS/cm at 21 ˚C. The electrospray conditions were as follows: Q_{liq} = 0.8 µL/min, I_{ES} = 375 nA, V_{HVPS} = 9.59 kV, and 31.8% RH. The morphology and size of the resulting nanocapsules were found to be nanometric size, as depicted in **Figure 3-3a**. The CS nanocapsules exhibited a globular shape, measuring approximately 200 nm in size (diameter), and displayed a narrow size distribution.

Two experiments were designed to facilitate the post crosslinking of the produced CS nanocapsules with TPP as follows in sections **3.4.1.1** and **3.4.1.2**.

3.4.1.1 Post treatment of chitosan capsules with TPP solution

To crosslink the CS nanocapsules with TPP, the supported nanocapsules on a silica wafer were wetted with 100 µL of 0.1% and 1% w/v TPP solution separately, and then rinsed with MilliQ water. The samples were stored at room temperature in a desiccator chamber overnight. The images of the nanocapsules after treatment are shown in **Figure 3-3**. Upon treating the nanocapsules with TPP solutions of 0.1 and 1% w/v, a loss of morphology was observed, accompanied by the formation of a distinct layer of material. To investigate whether this layer was caused by the TPP solution, the nanocapsules deposited on the silicon wafer substrate were also exposed to MilliQ water. However, the nanocapsules exposed to MilliQ water not only lost their morphology but also failed to exhibit any layer of material.

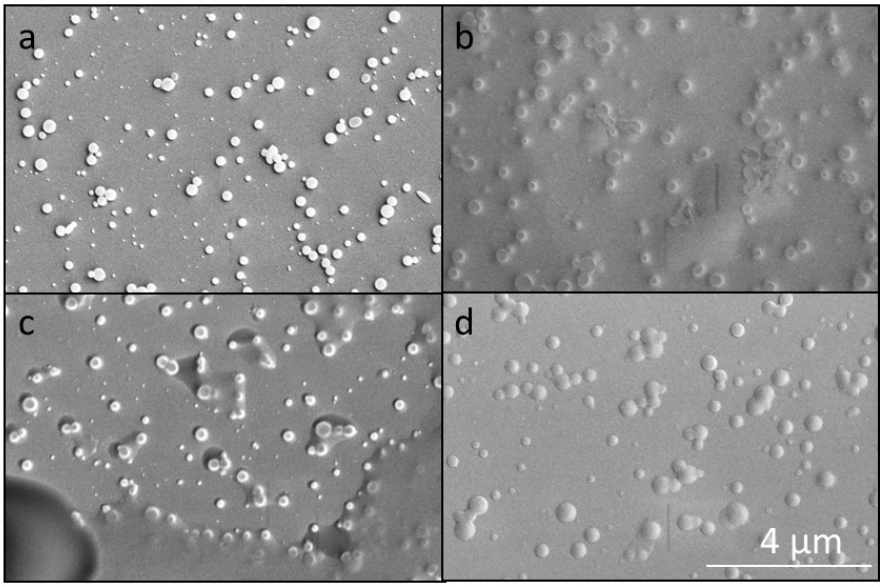

Figure 3-3. FESEM images (ETD detector, high vacuum, magnification 20.000X) of the nanocapsules produced with solution batch code 2C50E10A a) reference sample, b) exposed to 0.1 % w/v TPP solution, c) exposed to 1 % w/v TPP solution and d) exposed to MilliQ water.

It is well known that the protonated amino groups on the chitosan chain can bind to hydroxyl ions, which reduces the chain stiffness and enables TPP ions to increase contact and form intramolecular linkages. This allows the chitosan chains to fold and crosslink the nanoparticles, as described by (Pokharkar, 2006). However, it is important to note that chitosan loses its protonated amino groups once the CS nanocapsules have been produced, which affects its ability to crosslink with TPP (Fwu-Long Mi S.-S. S.-T.-B., 1999).

3.4.1.2 Chitosan nanocapsules collected onto TPP solution bath

The procedure for crosslinking CS to TPP was modified by collecting the electrospray solution from batch 2C50E10A into a bath containing different concentrations of TPP solution. Initially, the electrospray was collected in a 1 %w/v TPP solution, but the resulting spray formed a layer of CS on top of the collecting bath. A solution of 10 %v/v EtOH was added to TP solution to decrease the surface tension. However,

when the nanocapsules were centrifuged to precipitate the solids, the recovered solids were found to be amorphous, as shown in **Figure 3-4**.

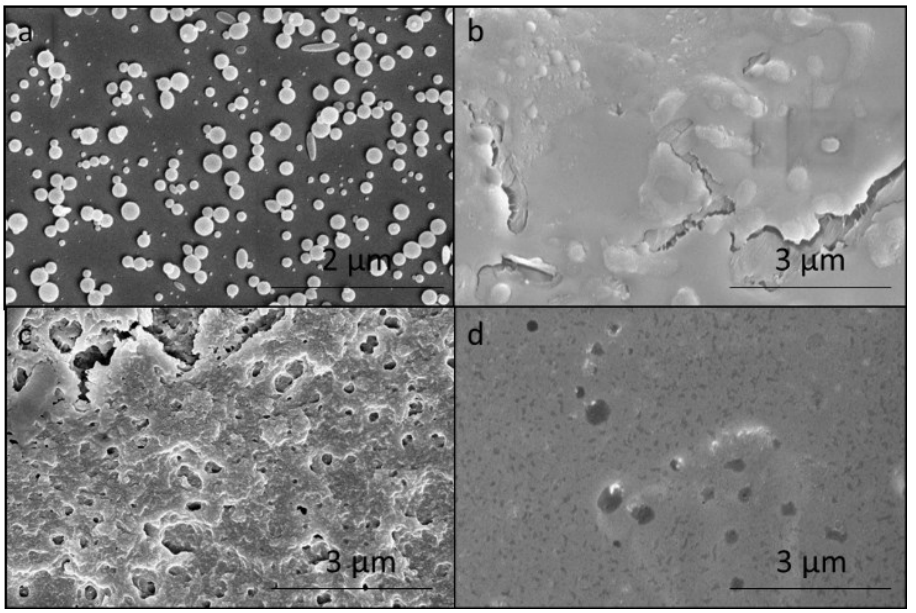

Figure 3-4. FESEM images of a) reference sample of the solution 2C50E10A. b) 1 %w/v TPP in 10 %v/v EtOH/H_2O. c) 1 %w/vTPP in 20 %v/v EtOH/H_2O d) 5 %w/v TPP in 10 %v/v EtOH/H_2O.

A follow-up experiment was conducted using a manual dripping method, in which 2C50E10A solution was dripped into the TPP solution bath. The droplet successfully penetrated the solution and formed a microcapsule. However, when the electrosprayed droplets or nanocapsules of 2C50E10A solution were introduced onto the collecting bath, they were unable to go deeper into the solution but remain on the surface. This prevented CS from coming into contact with TPP due to their inability to break through the surface tension of the TPP solution, thus forming a superficial barrier that hindered their penetration.

During the performance of these experiments, we were not successful to produce stable nanocapsules by the addition of TPP solutions, therefore we move on performing experiments discuss in section **3.4.2**.

3.4.2 Production of nanocapsules from the mixture of CS and TPP solutions.

Initial electrospray experiments using the microemulsion were not successful in producing crosslinked CS/TPP nanocapsules. The electrospray microemulsions should ideally be homogeneous and free of agglomeration of suspended particles in order to prevent clogging of the capillary tube.

The CS/TPP microemulsion C30 was used to produce nanoparticles described in **section 3.3.2.1**. The electrospray conditions are listed in **Table 3-5**. Synthetic air and CO_2 were used to study the stability of the Taylor cone due to some issues with dryness. Electrospray processes are typically performed with a flow of chamber air or other gaseous environments to facilitate the drying of the charged droplets and particles, but such gas flow also might affect the dryness of the Taylor cone. The gas-breakdown properties can also be useful to prevent the formation of corona discharges when using very high voltages, and therefore may impact the formation of the Taylor cone, and the overall efficiency of the process.

Table 3-5. ES conditions during the production of CS/TPP nanoparticles of the emulsion`s batch code C30.

Experiment code	Chamber atmosphere	RH, % (±5)	Coflow	Q_{liq}, µL/min	I_{ES}, nA	V_{HVPS}, kV
1	Synthetic air	40	EtOH	0.50	400	9.29
2		<10			450	9.59
3		40	0		320	8.48
4		<10			400	9.84
5	CO_2	40	EtOH	0.40	230	10.0
6		<10			200	10.3
7		40	0		300	10.5
8		<10			280	10.5

Carbon dioxide, nitrogen, and synthetic air can all be used as chamber environments for electrospray processes. The choice of gas used affects the evaporation rate of the solvent and the stability of the charged droplets (Paul Kebarle, 2009). Carbon dioxide contrary to nitrogen or synthetic air avoids electric discharges from the tip of the capillary tube/nozzle especially when the experiment is performed in low flow rates like less than 0.3 µL/min. (J. M. López-Herrera, 2004).

The size of the particles produced by electrospray from C30 emulsion are between 5 nm or less until 90 nm at any condition of the electrospray listed in **Table 3-5**.

3.4.2.1 Morphology of nanocapsules produced by emulsions

The nanocapsules morphology shown in **Figure 3-5** were produced using the electrospray conditions from experiment code 5 in **Table 3-5**, which is representative of all the electrospray conditions studied in **Table 3-5**. The morphologic analysis was performed by FESEM in the center, intermediate and periphery of the spot (nanoparticles collected in the silicon wafer substrate). Spider web-shaped materials were observed in the center of the spot with particles around 250nm and single particles of <100nm were observed in the other regions. The size of the particles decreases towards the periphery of the spot, which is likely due to the electrospray acting as a micro-spray-dryer for the suspended particles in the microemulsion. We believe crosslinked CS/TPP agglomerates were formed in the microemulsions prior to the electrospray process; those agglomerates were dried and deposited during the electrospray process.

Unfortunately, this spider web-shaped material is a problem if we decide to remove the particles from the silicon wafer substrate, as the bulk of the collected particles will contain amorphous material decreasing the quality of the single particles.

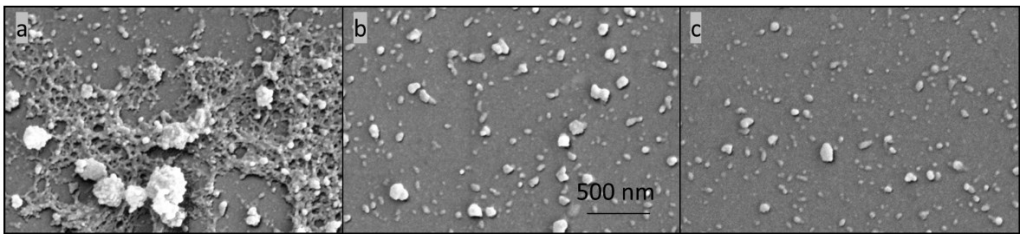

Figure 3-5. Representative FESEM image at 80.000X with ETD detector of sample C30 at any condition of the studied electrospray conditions, a) center, b) intermediate, c) periphery of the spot, during 30s collection onto silicon wafer substrate.

3.4.2.2 Evaluation of the crosslinked degree

The crosslinking degree of the particles produced by electrospray was analyzed using FTIR, as shown in **Figure 3-6**.

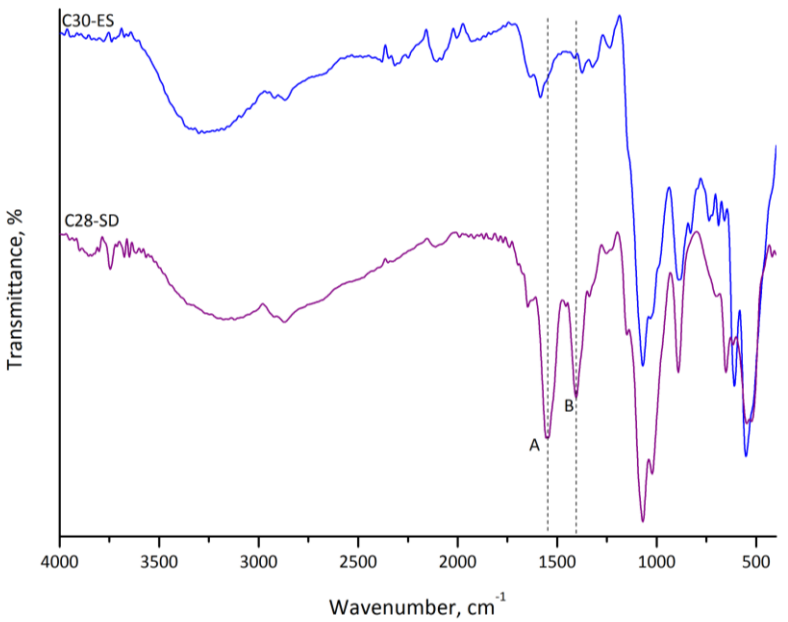

Figure 3-6. FTIR spectra of the of the particles obtained by electrospray (ES) to evaluate the extent of crosslinking, and comparison to a typical spectrum of CS/TPP microcapsules made by spray drier (SD) discussed in **section 2.4.1c**.

The crosslink bands A: 1547 and B: 1397 cm^{-1} where compared between those obtained from particles produces by electrospray and spray drier. It was observed

that the crosslinking between CS and TPP disappeared from the samples obtained by electrospray using the microemulsions, which can be attributed to the competition between OH- ions and $P_3O_{10}^{-4}$ or $P_3O_{10}^{-5}$ ions from TPP to react with the protonated amino group of CS chains. The presence of OH- ions in the TPP solution decreases the structural stability of the CS/TPP complexes, leading to a higher degree of cleavage of the phosphorus chain from CS. In the absence of ions to stabilize the CS/TPP interaction, the degree of cleavage is even higher. (Pokharkar, 2006).

3.4.3 Design of an electrospray-microfluidic nozzle by mixing solutions in-situ in-line

Based on previous findings, we concluded that the achievement of homogeneous and crosslinked nanocapsules required the in-situ mixing of CS and TPP solutions during the electrospray process. The rapid crosslinking of CS and TPP solutions posed a challenge in detecting its progression visually. To determine an approximate timeframe before crosslinking occurred, a microfluidic experiment was conducted, as depicted in **Figure 3-7**.

In this experiment, the TPP solution was pumped through the inner silica capillary tube (ID: 75 µm, OD: 220 µm) (the yellow tube shown in the figure), while the CS solution was passed through the outer silica capillary tube (ID: 530 µm, OD: 660 µm). As both solutions converged, turbidity became evident, indicating the onset of crosslinking, as shown in **Figure 3-7a**. Furthermore, the resulting crosslinked gel stuck to the outer tube walls as in **Figure 3-7b**. In **Figure 3-7c**, the capillary tube was shortened to avoid crosslinked gel that stuck the line and to allow a droplet to form for further electrospray process.

In further steps in the initiating electrospray process, the remaining liquid in the tip of the capillary tube was reduced, resulting in the formation of a cone-jet. This approach was undertaken to facilitate the in-situ in-line mixing of CS and TPP

solutions to produce cone-jets despite the challenges posed by the rapid crosslinking and the surface of the droplet.

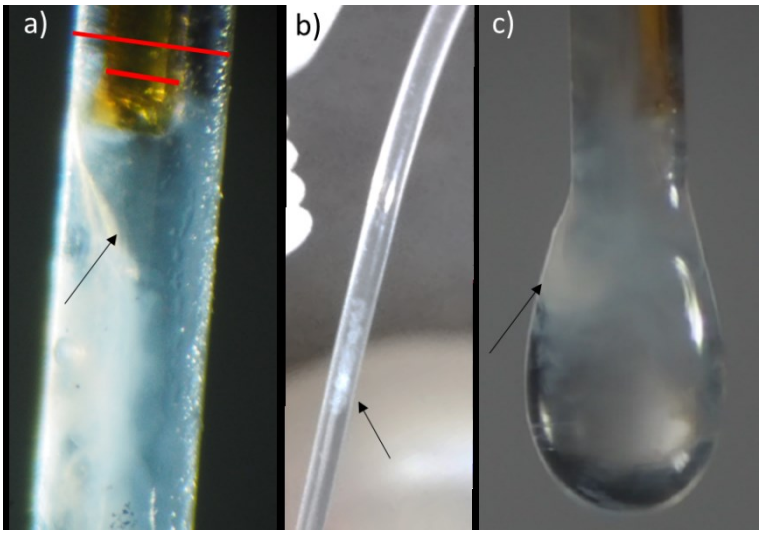

Figure 3-7. Microfluidic system designed to estimate the crosslinking reaction time.

Based on the qualitative evaluation of the crosslinking kinetics of CS and TPP, it was determined that the crosslinking process occurs at a similar rate to the filling of the Taylor cone. In order to address this challenge, a coaxial electrospray was developed as follows in the following section.

3.4.4 Coaxial design methodology

3.4.4.1 Evaluation of nozzle design on the shape of the Taylor cone and-stability

After designing different coaxial needles with metallic and silica materials according to **Table 3-2** and perform some experiments to observe the morphology of the Taylor cone. We found out that the shape of the Taylor cone was highly dependent on the concentricity of the inner tube, which affects the repulsion of both solutions during the electrospray process at the electrospray conditions were the experiments were found to be closer to form a Taylor cone-jet mode, as illustrated in **Figure 3-8**. The Taylor cone formed in **Figure 3-8 (1a)**, the resulting collection

spots on the silica wafer substrate had a higher concentration of particles on one side. On the other hand, when the Taylor cone took the shape shown in **Figure 3-8 (1b)**, it produced a centered homogeneous collecting spot. **Figure 3-8 (2)** represented an ideal Taylor cone able to produce nanocapsules.

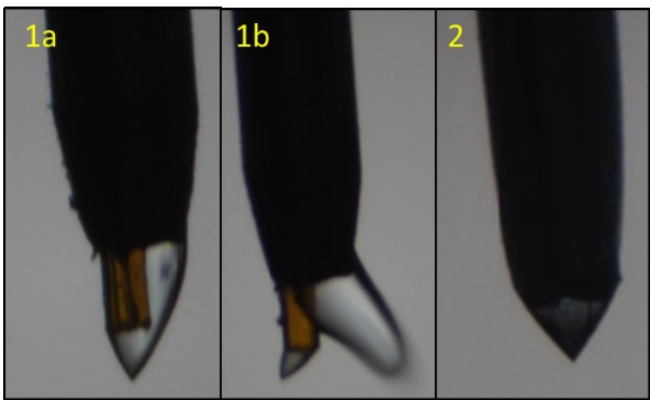

Figure 3-8. Relationship between concentricity and the formation of the Taylor cone shape based on nozzle dimensions 1a) N3, 1b) N2 and 2) N1.

a. Effect of Inner needle protrusion

In the previous experiments, we realized that the shape of the Taylor cone became shorter or cero as the protrusion of the inner tube beyond the end of the outer tube increased, leading to the volume of the CS and TPP solutions remaining in the cone for a longer period before arriving to the jet. This extended contact time can affect the stability of the electrospray process, leading to the formation of CS/TPP crosslinks in the Taylor cone and eventual solidification, as observed in **Figure 3-9**. The goal of this experiment was to increase stability of electrospray during the collection process to avoid size dispersion. Early crosslinking in the cone-jet was the principal factor that affects stability and we found out that the length of the protrusion help to avoid it. During experimentation, no protrusion produced faster crosslinking of the solution on the tip of the nozzle, however, when the protrusion was observed like in **Figure 3-9 (a-b),** the Taylor cone was stable but when the

protrusion was like in **Figure 3-9 (c)**, the CS and TPP solutions crosslinked after some minutes producing dryness.

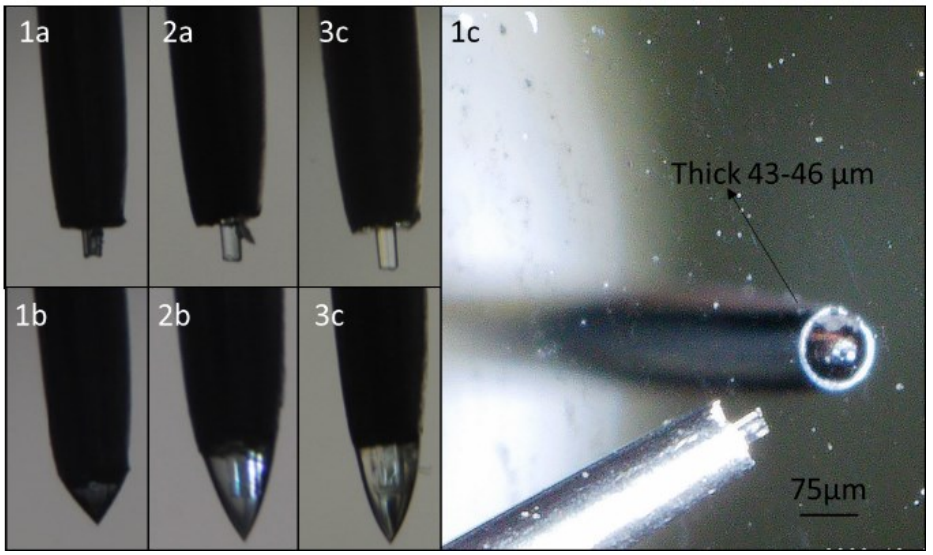

Figure 3-9. The relationship between protrusion and the formation of the Taylor cone shape. Length of protrusion in 1) 201, 2) 264 and 3) 284µm.

b. Effect of the nozzle shape exit

Effect of the nozzle shape exit played an important role in the electrospray process. It not only affected the electric field's penetration through the outer fluid but also influenced the shape of the inner interface into a Taylor cone-like meniscus. The geometry of the nozzle, whether flat or conical, can significantly impact the flow rate and the electric tangential stresses and velocities at the free surfaces. For instance, near a flat surface the liquid flow may decay, resulting in a recirculating region. This recirculation region can affect the size and shape of the droplets or particles produced but mainly the production of a gel within the Taylor cone might be more likely if recirculation zones of the two liquids exist in it, especially for the inner tube. Therefore, designing the nozzle carefully was crucial for controlling the electrospray process and the properties of the resulting particles or droplets (Jose M. López-Herrera, 2020; J.M. López-Herrera, 2023).

Through extensive testing of various configurations for the nozzle, including size, protrusion, tip shape, concentricity, and nozzle size, we have made a significant discovery. By implementing smaller needle sizes (with a protrusion <300 µm), incorporating conical ended tips on both tube ends, and achieving concentricity through a coil-shaped wire between them, we consistently achieved a stable Taylor cone shape that maintained its stability over time. Based on these findings, we confidently assert that these specific nozzle configurations were optimal to produce nanocapsules. Consequently, we employed these configurations to investigate different solution compositions, aiming to enhance the crosslinking degree of CS/TPP nanoparticles.

c. Stability of coaxial-electrospray process

For the production of sufficient amount of nanocapsules one criterion was the long-term stability of our electrospray process. We monitored the stability through periodic visual observation of the Taylor cone with a camera and a continuous ES current measurement. Time to time we observed some drying, which required occasional local nozzle tip cleaning and we also observed a little bit of fluctuation in the ES current (range), but stability often recover quickly. The reason for occasional instabilities could be due to bubbles or inhomogeneous flows from syringe pump (as tiny flows are more sensitive to any fluctuation). The stability of the electrospray process was observed for a period of 3 hours as depicted in **Figure 3-10.** The solutions were composed by 2% w/w CS with K of 446 µs/cm, pH of 1.3, and the solution 1.6% w/w TPP with a K of 3700 µs/cm and pH of 3.3. The electrospray conditions were as follows: Q_{liq} (TPP and CS solutions) of 0.9 µL/min, V_{HPSV} of 10.85 KV, I_{ES} of 404 nA in a CO_2 atmosphere within the chamber, the collected nanocapsules are shown in **Figure 3-11**. This prolonged stability was beneficial for obtaining stable morphologies of the nanocapsules, and it indicated that scaling up the process will be feasible by employing longer periods to collect nanocapsules.

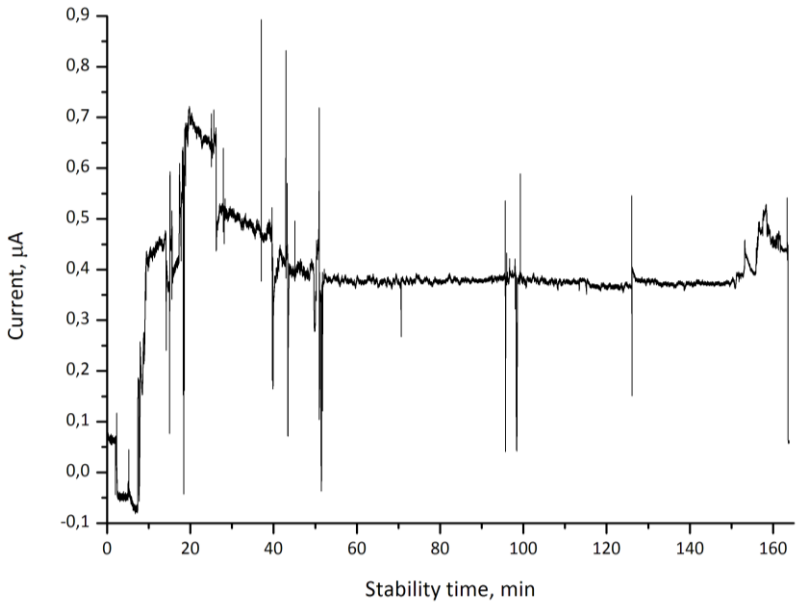

Figure 3-10. Electrospray current versus experiment time for a stable coaxial electrospray of the solutions: 2% w/w CS and 1.6% w/w TPP.

Generally to start any experiment, it took some time to stabilize. For example, the current increased at the start of the experiment as the beginning the voltage was adjusted at 5 KV until both solutions took place in the tip the nozzle, this voltage was applied in order to avoid a capillary effect on any of the tubes of the nozzle. The stability of the cone-jet was achieved after 26 minutes. However, the current decreased as a result of adjusting the flow rate from 0.4 to 0.3 µL/min. From 36 to 41 minutes, the same procedure was repeated with a flow rate of 0.25 µL/min. During this time, the current remained stable at 0.370 µA. Some current fluctuations in the experiment of **Figure 3-10** were observed outside the stable range due to stabilization of the process from 0 to 40 minutes and the fluctuations found in 46, 92 100 and 128 were due to the movement of the silicon wafer substrate during sampling collection process.

d. Preliminary morphology of the produced nanocapsules

The morphology of the nanocapsules was studied as a function of the shape, crosslinked CS/TPP, dry collection, individual particles. These requirements have

been fulfilled partially through all the tested compositions from **Table 3-3** and **Table 3-4**.

For example, the nanocapsules from **Figure 3-11**, were produced from the solutions 2% w/w CS with K of 446 µs/cm, pH of 1.3, and the solution 1.6% w/w TPP with a K of 3700 µs/cm and pH of 3.3. The electrospray conditions were as follows: Q_{liq} (TPP and CS solutions) of 0.3 µL/min, V_{HPSV} of 10.85 KV, I_{ES} of 404 nA in a CO_2 atmosphere within the chamber. However, when the nanocapsules from **Figure 3-11a**, which are spherical with sizes from 40 to 200 nm were exposed to a humid environment, the morphology of the nanocapsules dissolves as shown in **Figure 3-11b**, as observed by the change in the collected spot's appearance from white to transparent, this fact indicated that the nanocapsules were instable with the relativity humidity of the environment (>10% RH)

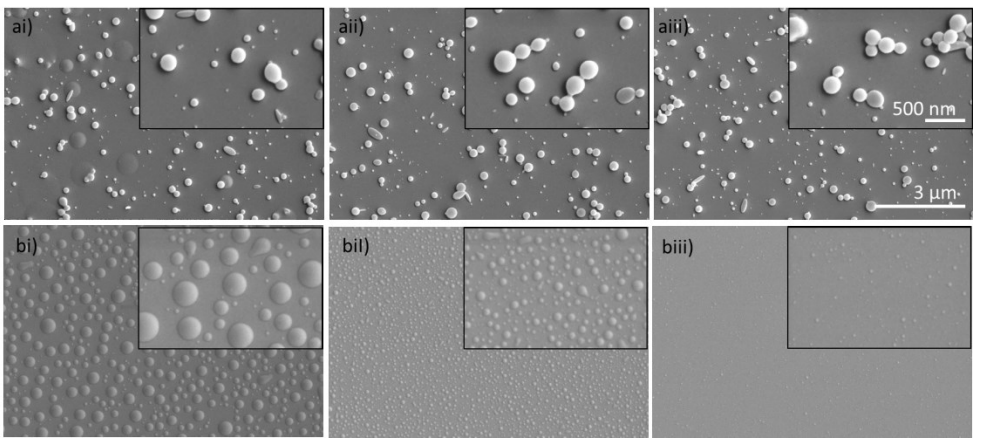

Figure 3-11. FESEM image of the CS/TPP nanocapsules produce by coaxial electrospray a) dry and b) after exposure to humid environment. The spot was observed from the i) center, ii) Intermediate and iii) periphery.

FTIR characterizations were performed but, it was not possible to identify crosslinking from the nanocapsules even though the electrospray process was stable. Further studies on the influence of the coaxial electrospray parameter during

the production of the nanocapsules was done in following sections as well as the study on composition of the solutions.

3.4.5 Parameters that influence the coaxial electrospray production of nanocapsules

After successfully establishing the method of electrospray, which involved mixing two CS and TPP aqueous solutions in the Taylor cone (coaxial configuration), we focused on mixing appropriate CS and TPP solutions that produced crosslinked, spherical nanocapsules that could be removed from the silicon wafer substrate. One of the objectives of this chapter was to identify a CS/TPP nanocapsules that could maintain its structural integrity without dissolving at pH levels ranging from 7.3 to 7.4. This attribute is vital for facilitating in vitro assays involving both normal and cancer cells.

In pursuit of this objective, a series of coaxial electrospray experiments with the solutions found in **Table 3-3** and **Table 3-4** were performed to generate nanoparticles with consistent size distribution and exceptional stability in buffer solutions. These experiments aimed to investigate the significant influences of various process factors on the production of nanocapsules, as described next.

3.4.5.1 Influence of solution composition on the morphology of the nanocapsules

The concentration of TPP in the formulation was expected to crosslinked efficiently the CS present during the mixture to produce nanocapsules for testing stability at different buffer solutions. It was found a significant impact in the size of CS/TPP nanocapsules. Generally, as the TPP concentration increases, the size of the formed capsules tended to decrease. This can be attributed to the higher availability of TPP crosslinking agents, which leads to stronger crosslinking interactions with chitosan molecules. As a result, the formed nanocapsules exhibit greater structural integrity, reduced coalescence, and smaller sizes. The relationship between TPP concentration and capsule size was not linear, however. At extremely high TPP

concentrations, there can be excessive crosslinking, resulting in the formation of rigid or agglomerated nanocapsules, which may lead to fragile and larger nanocapsule sizes.

In addition, the nanocapsules observed in **Figure 3-12** produced with the electrospray conditions Q_{liq} 0.33 µL/min each liquid, 10.95 KV and 753 nA approximately in both experiments, the size is governed by conductivity of the solution. In our coaxial electrospray there are two streams with different conductivities for the solutions of CS (5110 µS/cm) and TPP (230 and 960 µS/cm). The CS solution (**Table 3-3**) (external) is the most conductive than TPP solution (**Table 3-4**), then in the higher conductivity of the TPP (960 µS/cm)) decreased the size of the nanocapsules as shown in **Figure 3-12b**.

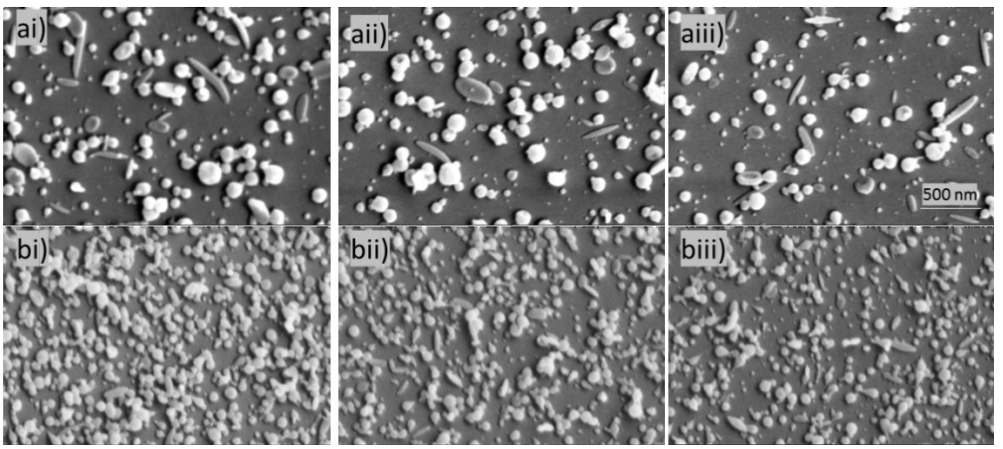

Figure 3-12. Effect of TPP concentration on the size of Cs/TPP nanocapsules. a) 0,006 %w/v TPP (K: 230 µS/cm) and b) 0,05 %w/v TPP (K: 960 µS/cm) at the i) center, ii) intermediate and iii) periphery of the spot.

3.4.5.2 Influence of the order of the fluids in the nozzle

During the experimentation, we also exchanged the feeding solution configuration. We observed that when the CS solution was directed through the inner capillary tube and the TPP solution through the outer capillary tube, the resulting nanocapsules were smaller from 60 nm to 3nm in average. This observation can be attributed to the difference in conductivity between the two liquids. The outer

liquid, the TPP solution, possesses higher conductivity compared to the chitosan solution. In general, the shift to smaller operates flow rates when the conductivity increased display a strong dependency of the nanocapsules size with the flow rate as shown in **Figure 3-13**.

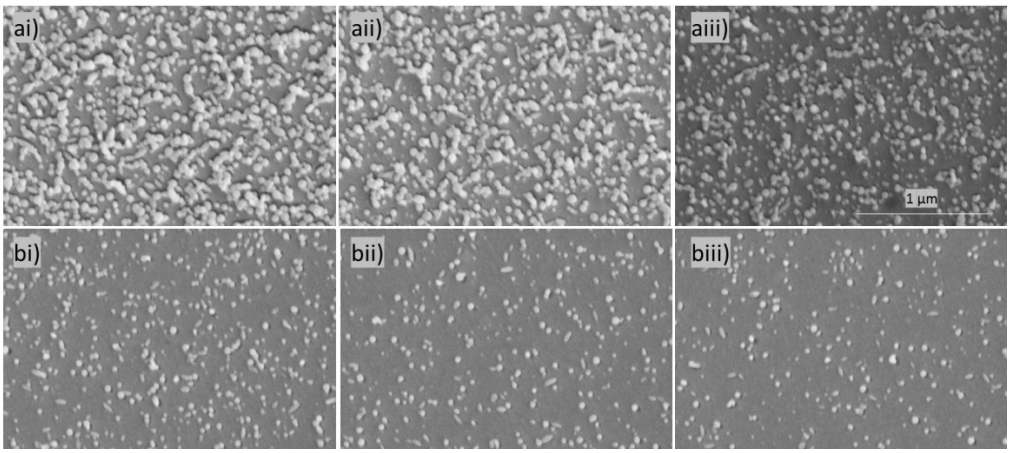

Figure 3-13. FESEM images of 2 %w/v CS and 0.05 %w/v TPP nanocapsules produce by a) TPP in the inner needle and b) TPP in the outer needle at the i) center, ii) intermediate and iii) periphery of the spot.

3.4.5.3 Influence of chamber humidity on capsule size

An experiment was conducted by using in the outer solution of the electrospray a composition of 2 %w/v CS, 0.17 %w/w AcOH, and in the inner solution 0.05 %w/v TPP 0.05 %w/w AcOH and 10 %w/w EtOH. The electrospray conditions were kept the same but modifying the chamber humidity levels in the CO_2 chamber atmosphere. It was observed that the influence of humidity on the electrospray process stems from its impact on solvent evaporation rate.

At humidity levels around 34% RH in the spraying environment, the humidity can slow down the water evaporation from the droplets by reducing the vapor pressure gradient between the droplets and the surrounding air. Voltages vary from 9.5 to 10.8 and the cone-shapes are shorter and elongated according to voltages that depend on flow rates, these flow rates are from 0.1 to 0.3 µL/min. Consequently,

larger flow rates leading to an increase in the size of the nanocapsules formed as showed in **Figure 3-14a**. Conversely, lower humidity levels less than 10 %RH need less flow rate resulting in the formation of smaller droplets and, consequently, smaller capsule sizes as showed in **Figure 3-14b**.

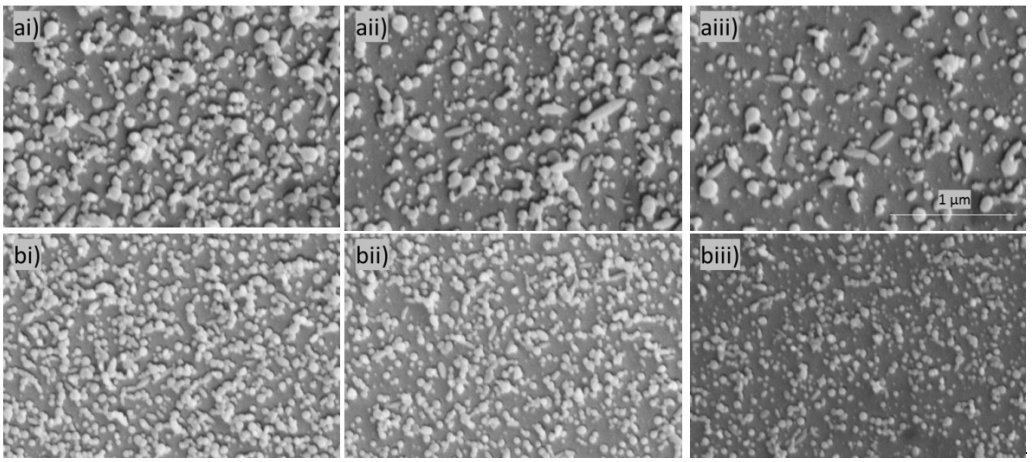

Figure 3-14. FESEM images of nanocapsules produce by comparing the effect of the humidity of the chamber. a) 34% HR and b) <10% HR at the i) center, ii) intermediate and iii) periphery of the collection spot on a Si wafer substrate.

3.4.5.4 Influence of flow rate on the capsule size

The electrospray experiments were primarily focused on achieving stability of the Taylor cone. Consequently, due to the specific characteristics of the solution arising from its high salinity, including high conductivity and high surface tension, it was challenging to modify the electrospray conditions over a three range of flow rates and voltages changed to stabilize the Taylor cone. Nanocapsules were successfully produced at flow rates of 0.1, 0.2, and 0.3 µL/min. However, it was not feasible to further increase the flow rate due to the increased demand for voltage, which eventually led to instability of the cone-jet (possibly due to the onset of gas discharges on or near the Taylor cone).

The flow rate played a significant role in determining the size of the resulting capsules for the given concentration of TPP and CS. As expected for the electrospray

process, an increase in flow rate led to greater size of the nanocapsules. Higher flow rates around 0.3 µL/min generally result in the formation of larger droplets than at lower flow rates, subsequently leading to the production of larger nanocapsules around 80nm.

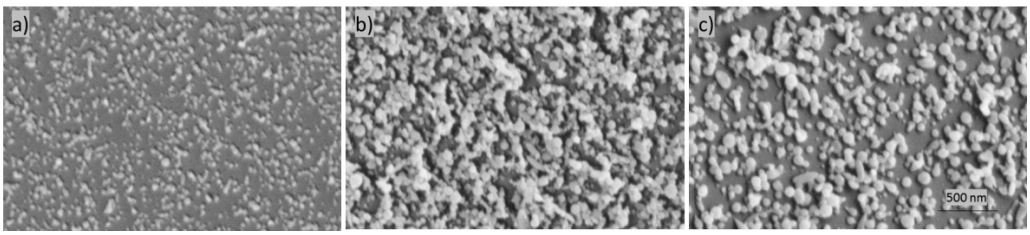

Figure 3-15. FESEM image of the center of the collecting spot. 2% w/v CS and 0.05 %w/v TPP nanocapsules produced at a flow rate of a) 0.1 µL/min, b) 0.2 µL/min and c) 0.3 µL/min. Collection times: 30, 45 and 35s.

The images of **Figure 3-15** show the produced nanocapsules obtained by varying amounts of mass due to differences in flow rates. It is important to note that the relationship between flow rate and nanocapsule size is not always linear.

3.4.5.5 Influence of the concentration of EtOH in the solution of CS

Early cross-linking within the Taylor cone was a challenge, making the process less stable. To prevent premature mixing and enhance stability, we needed to increase the immiscibility between the CS and TPP solutions. This was achieved by adjusting the concentrations of ethanol and acetic acid, as shown in **Table 3-4**. Through several iterations, we identified an optimal solution composition range.

However, the stability of the Taylor cone remained limited. In some cases, it would last only about 10 minutes before solid layers of crosslinked CS/TPP formed, leading to a dry Taylor cone. This issue was particularly evident in certain situations, where the stability duration was consistently short.

Our main objective was to extend the stability period for scaling up the process. To achieve this, we focused on the interaction between the inner and outer fluids in

coaxial capillary tubes, which previous research (Shameek Vats, 2021) had shown to be influenced by their miscibility.

When the fluids were entirely immiscible, they displayed a clear interface tension. However, this tension could potentially break the inner core, hindering its integration into the overall fluid stream. Conversely, when the liquids mixed completely, the distinct core-sheath structure disappeared, causing premature gelation within the Taylor cone.

To prevent the Taylor cone from drying out and to enhance stability, we increased the immiscibility between the CS and TPP solutions during their presence within the Taylor cone. We achieved this by varying the concentrations of ethanol, which helped create better separation between the two liquids without altering the nanocapsule morphology.

3.4.5.6 Performance of the nanocapsules in solution

The nanocapsules needed to be tested at different buffer a solution that simulates in vitro experiments around pH (7.3-7.4). The stability of the nanocapsules was tested in lactate and phosphate buffer solutions. The collected nanocapsules observed by TEM displayed some bubbles as shown in **Figure 3-16a**, indicating that the nanocapsules were wet and the bean heat them causing a detrimental effect on the integrity of the nanocapsules.

The nanocapsules were removed from the silicon wafer substrate and they were treated in MilliQ water (pH 6.9) for 1 minute, and sonicated for 3 minutes. The TEM sample preparation is described in section **3.3.3c** Samples were affected by the bean of the TEM as the nanocapsules shown bubbles in **Figure 3-16a.** In the other hand, some of the nanocapsules swelled, but a fraction of them remained intact as shown in **Figure 3-16a b**, they dissolved, and some material like chitosan around them was visible confirming low stability of the crosslinking nanocapsules at pH 6.9, taking into account that chitosan dissolve under pH 6.5. These observations suggest

that there is room for improvement in the CS and TPP composition to enhance the stability of the nanocapsules.

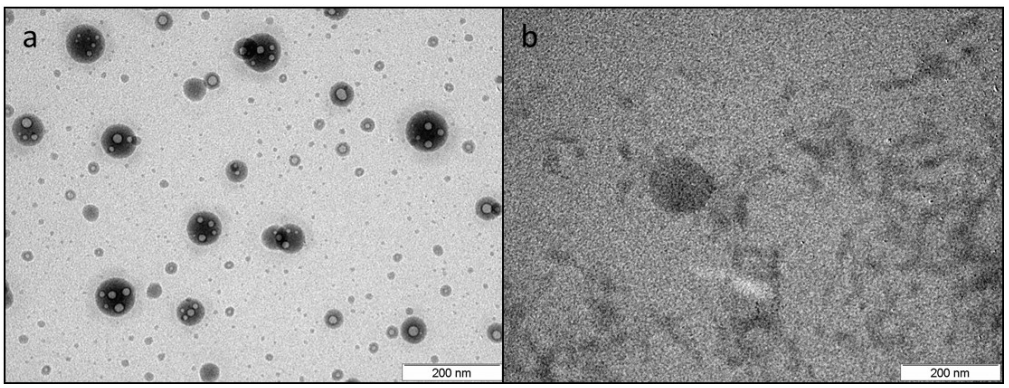

Figure 3-16. TEM images of the nanocapsules obtained at 120k. a) Reference and b) nanocapsules treated with MilliQ water.

3.4.5.7 Stability of the CS/TPP nanocapsules in buffer solution

The underlying hypothesis of this research was that CS/TPP nanocapsules dissolved in the vicinity of cancer cells due to the low pH generated by lactic acid, and that this dissolution enables the chitosan to form a net-like structure around the cancer cell. At the same time, it is necessary for the CS/TPP nanocapsules to remain stable in a neutral pH environment. Therefore, the previously produced nanocapsules were subjected to immersion in solutions with low pH (4.6) and neutral pH (7.3 to 7.4) to assess their mechanical stability for subsequent in vitro experiments.

CS solutions (**Table 3-3**) with lower acetic acid content yield stable nanocapsules when exposed to pH 7 solutions. The swelling behavior of the nanocapsules can be observed in **Figure 3-17**, where nanocapsules increase in size by approximately 50%.

The impact of different pH solutions on the morphology of the generated nanocapsules is illustrated in **Figure 3-18**. Comparing the blank sample with the other samples taken from the TEM grid, we observed smaller nanocapsules, consistent with the findings shown in **Figure 3-14**. Notably, when the grid was

immersed in a solution just for few seconds with a pH of 3.5, we observed larger dark spots (>500 nm), resembling the accumulation of CS/TPP material.

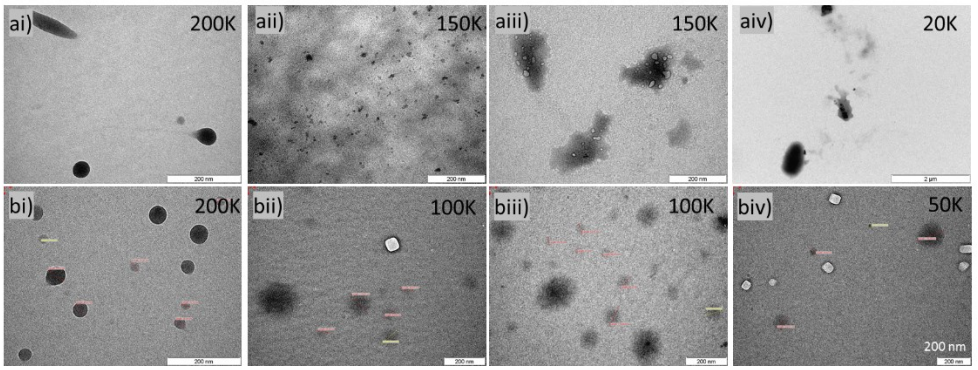

Figure 3-17. TEM images of nanocapsules obtained from 2 %w/v CS outer solution solution and a) 0.025 %w/v TPP and b) 0.006 %w/v TPP inner solution after being treated. i) blank, ii) treated with water, iii) treated with buffer phosphate and iv) treated with buffer lactate.

In buffers of low and high pH, the nanocapsules tend to dissolve. However, in high pH buffers with higher ionic strength than lactate buffer, the HPO_4^{2-}/H_2PO^{4-} ions tend to bind with the protonated $-NH_3^+$ of chitosan. In low cross-linked capsules formed at very low or high TPP pH solution, where $-NH_3^+$ sites are still available, the anions are exchanged at the protonated $-NH_3^+$ sites of chitosan in high ionic strength media.

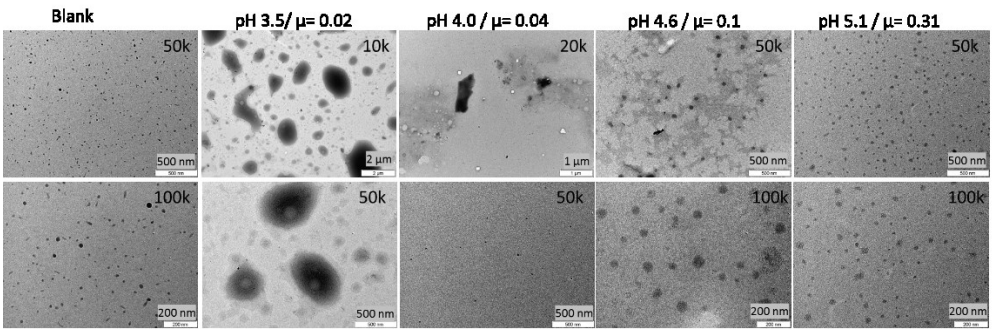

Figure 3-18. TEM images of nanocapsules produced with 2 %w/v CS through inner tube and 0.05 %w/v TPP solution through outer tube and treated with pH solutions produced at 0 min.

Furthermore, the nanocapsules dissolved in the pH 4 buffer solutions, while they remained intact but swelled at pH 4.6 and 5.1. These results suggest that the nanocapsules can withstand solutions with a pH below 5.1 and exhibit changes in size and morphology in response to varying pH conditions. After proving stability of the CS/TPP nanocapsules at low pH solution, we achieved one of the main objectives of this thesis. These compositions can be used for biological activities studies.

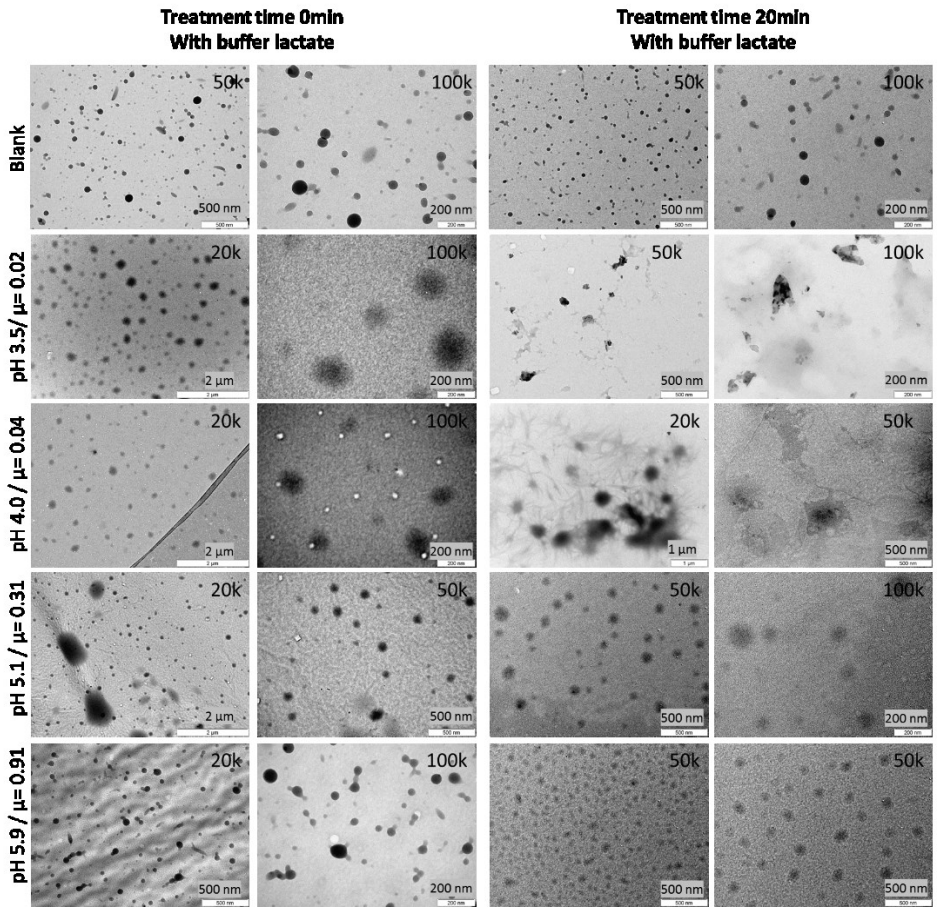

Figure 3-19. TEM images of stability of 2 %w/v CS and 0.05 %w/v TPP nanocapsules in buffer lactate at different pH with its respective ionic strength.

The nanocapsules observed in **Figure 3-14**, were from the same experiment and then immersed in solutions at different pH to study the stability by TEM as shown in **Figure 3-19**. The following observations were made:

The initial treatment (0 min) of the nanocapsules was when the TEM grid was wet with the buffers of pH 3.5, 4.1, and 5.1, the particles appeared to swell as they retained their round shape. The particles showed stability when treated at pH 5.9. However, at pH 4.6, the particles dissolved as they lost their shape. At 20 minutes treatment time: The particles dissolved when treated at pH 3.5 and 4.1, as they lost their shape. At pH 5.1 and 5.9, the particles seemed to swell as they maintained their round shape. These observations provide insights into the behavior and stability of the particles in different pH solutions over time.

Table 3-6. Size of nanocapsules after treatment with solutions at different pH

Exp	Sample	Treatment time, h	Water	pH 4.5	pH 5.9	pH 7.3
			Size of nanocapsules, nm			
1	2CS0.05TPP	1	47-75	49-161	29-67	24-76
	2CS0.05TPP	6	26-27	56-65	38-64	31-86
2	3CS0.075TPP	1	86-133	92-161	114-124	81-114
	3CS0.075TPP	6	50-96	208	190-198	118-282
3	3CS0.05TPP	1	41-117	56-84	67-257	80-178

Upon comparing several experiments involving nanocapsules produced using solutions of 2% and 3 %w/v CS and 0.05% and 0.075% w/v TPP, followed by treatment with solutions of varying pH to observe swelling on the TEM images, we noted distinct differences in the size of the nanocapsules. The **Table 3-6** shows the sizes of the Experiment after 1 and 6-hour immersion, it demonstrated a decrease in size. This reduction can be attributed to the dissolution of larger nanocapsules, while the smaller ones remained relatively unaffected.

Based on these observations, we can conclude that the dissolution behavior of the nanocapsules follows a specific pattern. Initially, there was swelling of the less dense nanocapsules, followed by their dissolution. Subsequently, the smallest nanocapsules undergo a slower swelling process, taking more than 1 hour to reach their fully swollen state.

3.4.6 Scaling laws

Scaling laws in electrospray are theoretical predictions that describe the relationship between different parameters and characteristics of the process. These predictions estimate the behavior of electrospray under several conditions. However, experimental data often deviates from these theoretical predictions due to the complex nature of the phenomenon (A. M. Gañan-Calvo, 1997).

The size and shape of the Taylor cone formed during electrospray were influenced by factors such as flow rate, electric field strength, and liquid surface tension. Theoretical predictions based on scaling laws can estimate cone dimensions, but experimental results may differ due to additional factors like solution conductivity, solvent properties, and electrochemical effects (Loscertales, 1994).

Scaling laws also predict the relationship between input parameters (e.g., flow rate, voltage) and the distribution of droplet sizes. Theoretical models provide insights into the expected sizes and statistical distribution of the droplets. However, experimental results may deviate due to factors like liquid properties, solvent evaporation, and coulombic repulsion effects. Furthermore, scaling laws describes how factors like voltage, capillary size, and liquid properties affect the spray angle. However, the actual spray angles may vary due to ambient conditions, solvent volatility, and the presence of additives (Loscertales, 1994; A. M. Gañan-Calvo, 1997).

Our system is complex and the nature of the solution and the crosslinking reaction during the spray increase complexity, however, we dare to at least find out the theoretical minimum flow rate (Q_{min}) ejected from the stable cone jet was computed according to the equations of (**3-2**(3-3) (A. M. Gañan-Calvo, 1997). To calculate the Q_{min} we assumed a single flow rate considering from previous observation that the main effect in the morphology and size of the nanocapsules was leading by CS solution.

$$Q_0 = \frac{\sigma \varepsilon_0}{\rho k} \quad (3\text{-}2)$$

$$\mathrm{Q_{min}} = \mathrm{Q_0}\beta \quad (3\text{-}3)$$

Where σ is the surface tension (72.8 mN/m), ρ is density (0.995 g/cm³), k is electric conductivity of the solution (5.11 and 9.11 mS/cm), and $\beta = \varepsilon_i/\varepsilon_0$ is the relative electrical permittivity (dielectric constant) (79 u.a.), ε_0 and ε_i are the electrical permittivity of vacuum and of the liquid, respectively.

Theoretical calculations indicated (Gamero-Castaño, 2019) that the Q_{min} should be approximately 3.3×10^{-3} to 6.0×10^{-3} µL/min for CS solution. However, experimental measurements showed a significantly higher Q_{min} of 0.1 to 0.2 µL/min. The large error percentage of up to 3000% between the theoretical and experimental values, this can be attributed to the specific physical conditions of the experiment. It was reasonable to assume that the stable conditions for electrospray occur at lower flow rates, as observed in the narrow working flow rate range of 0.1 to 0.2 µL/min, upper this flow rate the cone jet become unstable. The physical design of the syringe pump used in the experiment restricts the ability to achieve even lower flow rates

3.5 CONCLUSIONS

In the study of production of nanocapsules by using electrospray techniques and their evaluation on simulated physiological environment of CS/TPP nanocapsules, several important findings emerged:

Initial production experiments were conducted using a transparent CS solution sample, and the electrospray conditions were optimized. The resulting nanocapsules exhibited a globular shape with a narrow size distribution.

Two kinds of experiments were designed and conducted to facilitate the crosslinking of chitosan (CS) nanocapsules with tripolyphosphate (TPP). The addition of TPP solutions to the nanocapsules led to a loss of morphology and the formation of an undesired flat external layer of material. This layer was found to be a result of the crosslinking reaction between CS and TPP separately from the capsules. Nanocapsules exposed to MilliQ water did not show any layer formation, indicating the role of TPP in the crosslinking process.

The production of crosslinked CS/TPP particles from microemulsions was explored as an alternative approach. The electrospray conditions, and gas composition, were varied to optimize the process. The resulting particles showed agglomeration and the presence of spider web-shaped material. However, the particles collected from the periphery of the spot exhibited smaller sizes, suggesting the role of electrospray in drying the suspended particles.

The crosslinking degree of the particles produced by electrospray was analyzed by using FTIR. It was observed that the crosslinking degree between CS and TPP was smaller than the obtained by spray-drying. The presence of OH- ions in the TPP solution affected the stability of CS/TPP complexes, leading to a higher degree of cleavage. The findings highlighted the need to mix the CS and TPP solutions during the electrospray process to enhance crosslinking.

To achieve homogenous and crosslinked nanocapsules, a coaxial electrospray approach was developed. The shape of the Taylor cone, protrusion, and nozzle configuration were optimized to maintain stability and improve crosslinking. The resulting nanocapsules exhibited a spherical morphology and showed prolonged stability in solution. Further improvements were suggested to enhance the stability and performance of the nanocapsules for pharmaceutical applications.

Overall, the study explored the production of nanocapsules by electrospray and investigated different approaches to achieve crosslinking between CS and TPP. The findings highlighted the importance of solution composition, electrospray conditions, and nozzle configuration in controlling the morphology and stability of the nanocapsules. Further research is needed to optimize the CS/TPP formulation and improve the performance of the nanocapsules for pharmaceutical applications.

4 BIOLOGICAL ACTIVITY OF CS/TPP NANO AND MICRO CAPSULES

"Million-to-one chances happen nine times out of ten."

_Terry Pratchett

4.1 INTRODUCTION

In this chapter we dealt with the biological activity of the nanocapsules developed in the previous ones, the goals are to demonstrate that the capsules produced have the effects on healthy and cancer cells needed to develop a treatment. Two kinds of cells were used that are cancer cell line SCLII and normal cell line BJ. We investigate the interactions and adherence of the capsules to the cell membrane, aiming to validate the hypothesis put forth in this thesis.

To address these shortcomings, the in vitro experiments were conducted at the Laboratory of Tissue Engineering in the Department of Urology and Andrology, Ludwik Rydygier Collegium Medicum in Bydgoszcz, Nicolaus Copernicus University in Toruń, Poland.

Following an extensive search presented in chapters 2 and 3, a suitable CS/TPP crosslinked capsule was identified that could dissolve at the desired pH of the cancer cell surrounding environment. This pH varies according to the solid tumor and its stage, as reported by (Peter Vaupel, 1989). Additionally, these capsules were expected to exhibit electrostatic attachment specifically to the cancer cell membrane, based on research conducted by (Samah A Loutfy, 2016), while remaining unseen by normal cells. However, the level of this specific objective was not explored quantitatively, but qualitative observations were done in our current study. Nevertheless, we will dig deeper into this aspect in future investigations.

Four formulations for micro and nanocapsules were obtained, and sterilization was performed to prevent any potential infections during *in vitro* experiments. Viability

assays were conducted to assess the cytotoxic effects of the capsules on SCLII and BJ cell lines at 24 and 72 hours. Subsequently, experiments were conducted to determine the interaction of the capsules to the cell membrane by optical detection.

Various approaches were employed to evaluate the effectiveness of capsule interaction with the cell membrane, thereby ensuring accurate results and minimizing false positives.

4.2 OBJECTIVES

4.2.1 General objective

- To evaluate CS/TPP capsules interaction with normal and cancer cell lines with the use of *in vitro* experiments.

4.2.2 Specific objectives

- To evaluate the potential toxicity of CS/TPP capsules on normal and cancer cells.
- To evaluate the selective interaction of CS/TPP capsules with normal and cancer cells.

4.3 METHODOLOGY

4.3.1 Materials

4.3.1.1 Normal and cancer cell lines

Three cell lines were used for the in vitro experiments:

The BJ (CRL-2522^{TM}) human cell line is a fibroblast cell line derived from normal foreskin tissue purchased from the American Type Culture Collection (ATCC, USA). The human cell line SCLII was derived from an undifferentiated squamous cell carcinoma from facial tissue, and it was purchased from Cell Lines Service GmbH (CLS, Germany). In addition, we also used the BALB/3T3 fibroblast cell line (CCL-163TM, ATCC, USA) developed by S.A. Aaronson and G.T. Todaro in 1968 from BALB/c mouse embryos. 3T3 cells are easy to maintain in culture, allowing us to perform preliminary experiments.

All cell culture procedures were performed in a class II laminar flow cabinet (Bio II Advance-Telstar, Spain) to ensure sterility and safety. The cells were grown in an incubator with a humidified atmosphere of 5% CO_2 and 95% air at 37°C (Thermo Fisher Scientific).

4.3.1.2 Microcapsules and nanocapsules for in vitro analysis

The microcapsules and nanocapsules used for in vitro analysis were composed of CS/TPP and met specific requirements such as a crosslinked CS/TPP net, stability in neutral solutions, and controlled dissolution at a specific pH. Spray drier and electrospray methods were used to produce microcapsules and nanocapsules, respectively. Microcapsules were initially used to test the methodology and observe cell behavior due to the availability of quantity of samples. During spray drying experiments the nanocapsules were in low production capacity, therefore, electrospray technique was develop to get high reproducibility and low size dispersion.

a. Microcapsule production by spray drier

Microcapsules were successfully produced using the spray drier method, as detailed in **Section 2.3.3**. The composition of these microcapsules is outlined in **Table 4-1**. To ensure uninterrupted cell growth, solutions containing the 1 and 0.3 mg/mL capsules were employed in the cell culture, minimizing any potential interference caused by the presence of the capsules themselves. The technical conditions of the spray drier were the same as described in **Section 2.3.5**.

Table 4-1. Composition of microcapsules used for in vitro analysis.

Lot		A0426358	A0437756	A0406187		**TPP**
Sample		**1SD**	**2SD**	**3SD**	**CS**	
Dry microcapsules, % w/w	CS	97.4	97.5	97.5	100	0
	TPP	2.56	2.42	2.34	0	100
	FTIC	2.60×10^{-2}	2.40×10^{-2}	6.30×10^{-2}	0	0
Solution, mg/mL		**1**				
Weight, mg	CS	0.974	0.975	0.975	1	0
	TPP	2.56×10^{-2}	2.42×10^{-2}	2.34×10^{-2}	0	1
	FTIC	2.60×10^{-4}	2.40×10^{-4}	6.30×10^{-4}	0	0
Sample		**D1SD**	**D2SD**	**D3SD**	**DCS**	**DTPP**
Solution, mg/mL		**0.333**				
Weight, mg	CS	0.321	0.321	0.322	0.333	0
	TPP	8.44×10^{-3}	7.98×10^{-3}	7.72×10^{-3}	0	0.333
	FTIC	8.58×10^{-5}	7.92×10^{-5}	2.08×10^{-5}	0	0

The microcapsule morphology was examined using Field Emission Scanning Electron Microscopy (FESEM). **Figure 4-1** shows two distinct morphologies of the microcapsules: globular and corrugated shapes. The size distribution ranges from 2 to 50 µm, exhibiting a wide range of sizes. During imaging, the microcapsules were dispersed on carbon tape, resulting in agglomeration of some microcapsules while others remained separately.

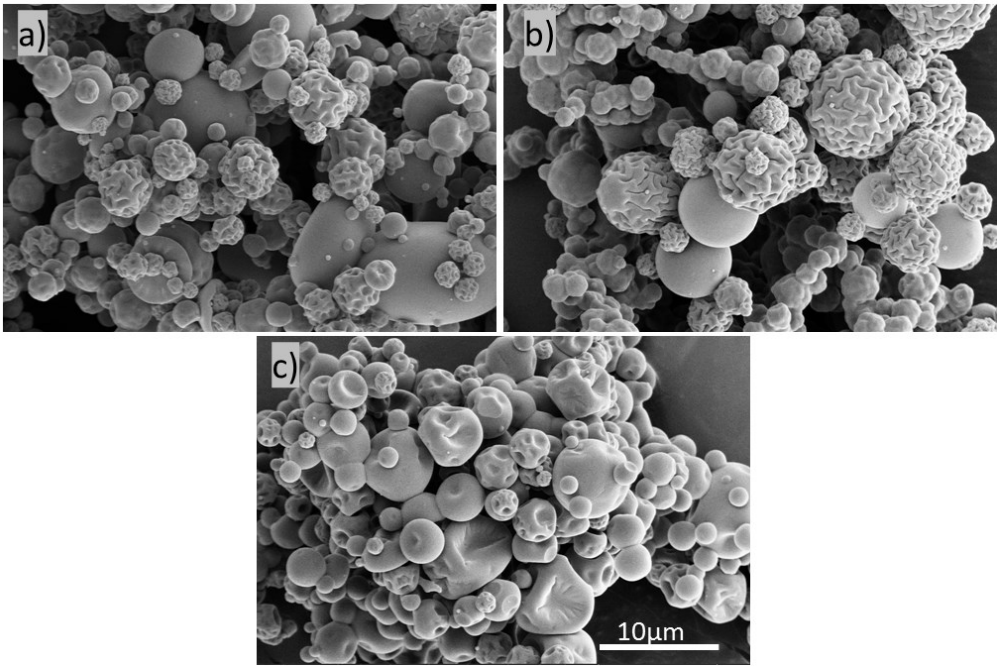

Figure 4-1. Morphology of the microcapsules a) 1SD, b) 2SD and c) 3SD.

b. Production of nanoparticles by 4-nozzle systems

CS/TPP nanocapsules were produced by an electrospray in a scale up set up system with 4 coaxial nozzles by using the CS solution as driving liquid composed by 3 %w/w CS, 10 %w/w EtOH, and 0.06 %w/w AcOH, and the TPP solution as core liquids composed by 0.075 %w/w TPP and 10 %w/v EtOH.

Table 4-2. Composition of nanocapsules used for in vitro analysis.

Sample		**ES**	**DES**
Solution, mg/mL		0.333	0.033
Dry nanocapsules, %w/w		**weight, x10^{-2}mg**	
CS	86.8	28.60	2.860
TPP	11.9	3.92	0.392
FTIC	1.28	0.42	0.042

The most suitable CS/TPP nanocapsule composition produced by coaxial-electrospray mode is described in **Section 3.3.2.5**. The composition of nanocapsules

is described in **Table 4-2**, it was used for the in-vitro experiments due to high stability in neutral solutions and dissolution at low pH solutions.

We found out that nanocapsules concentration of 0.33 and 0.033 mg/mL was enough to avoid any unoccupied spaces on the well surface and thus minimize cell growing.

Electrospray equipment

The single nozzle coaxial electrospray system was designed as explained in **Section 3.4.3** and scaled up (in order to increase productivity and explore future comercial production) with the support of the "***Prueba de Concepto, del Programa Estatal para Impulsar la Investigación Científico-Técnica y su Transferencia, del Plan Estatal de Investigación Científica y Técnica y de Innovación 2021-2023, en el marco del Plan de Recuperación, Transformación y Resiliencia,*** **founding by European union**" project funding in collaboration with Dr. Joan Rossell Llompard. The system utilized four coaxial nozzles. To ensure independent supply, each nozzle was equipped with two separate lines that delivered CS and TPP solutions, following the configuration explained in **Section** 3.3.2.5. Each solution was contained in a 1mL syringe and pumped using a syringe pump. The nanocapsules were collected on a silicon wafer, as illustrated in **Figure 4-2**.

During the electrospray process, the following conditions were maintained: a flow rate of 0.1 µL/min, voltage set at 9.0 kV, current at 400 nA, and a 40% relative humidity (RH) within the CO_2 atmosphere of the electrospray chamber. The rate of nanocapsules collection was 0.01 mg/h. After collection, the nanocapsules were carefully scraped off the silicon wafer and stored in Eppendorf tubes at room temperature, in a dark environment.

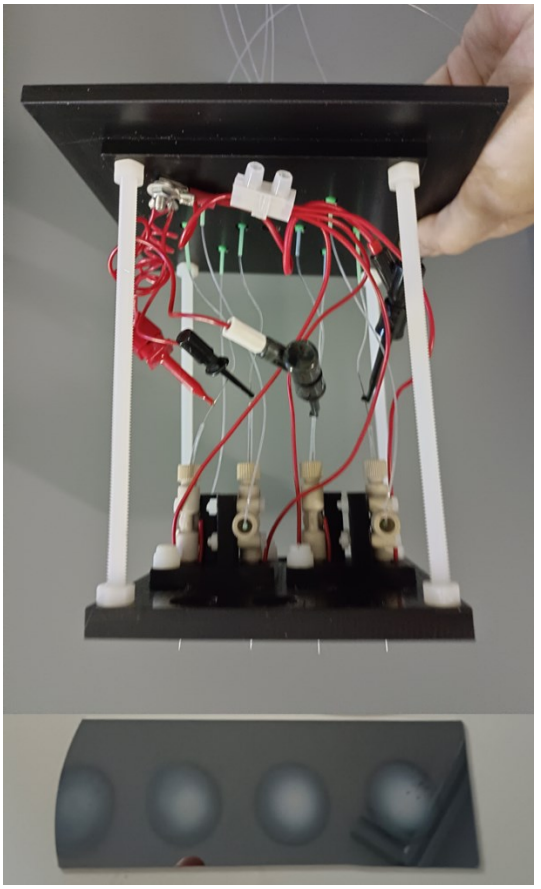

Figure 4-2. Illustration of the electrospray chamber with four electrospray coaxial nozzle and collecting spots on silicon wafer substrate.

Nanocapsules morphology

The CS/TPP nanocapsules were examined using FESEM to analyze their morphology, size, and size distribution as shown in **Figure 4-3**. On average, the nanocapsules measured 60 nm in size. Thanks to the highly stable electrospray system, the nanocapsules were continuously collected on the silicon wafer for over 4 hours without requiring cleaning. Interestingly, it was observed that the nanocapsules exhibited a preference for certain spots on the silicon wafer, resulting in the formation of agglomerates resembling a cauliflower-like shape. This phenomenon was anticipated due to the high electrical charge present in the initial deposition areas, which facilitated the accumulation of more nanocapsules as they fell onto the

collector. The nanocapsules collected from different spots were analyzed, revealing similar morphologies.

To retrieve the nanocapsules, a blade was used to scrape them off the silicon wafer, as depicted in images **Figure 4-3b** and **Figure 4-3c**. The nanocapsules that grew in a cauliflower-like shape remained agglomerated, while in other instances, nanocapsules displayed a more laminar shape, as shown in image **Figure 4-3c**.

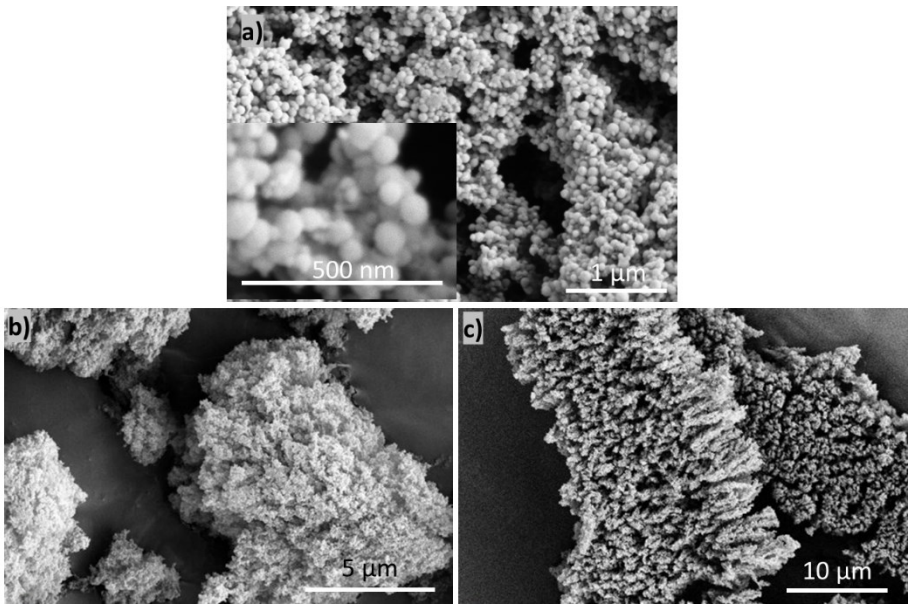

Figure 4-3. Morphology of the nanocapsules obtained by 4 coaxial electrospray nozzles.

In the FTIR spectra shown in **Figure 4-4**, it is possible to observe bands at 1565 and 1410 cm-1, which are indicative of the presence of crosslinked chitosan and TPP. These bands align with the findings reported in previous experiments in **Section 2.4.1e**. The FTIR characterization not only confirms the successful production of crosslinked CS/TPP using a coaxial electrospray technique but also represents the first reported achievement of this nature in the literature. This breakthrough opens exciting opportunities for further exploration beyond the scope of this thesis, including investigating different compositions and elucidating the crosslinking mechanism during the electrospray process. These findings also open exciting

opportunities for the development of in-situ reactions in aqueous media during electrospray and produce nanoparticles.

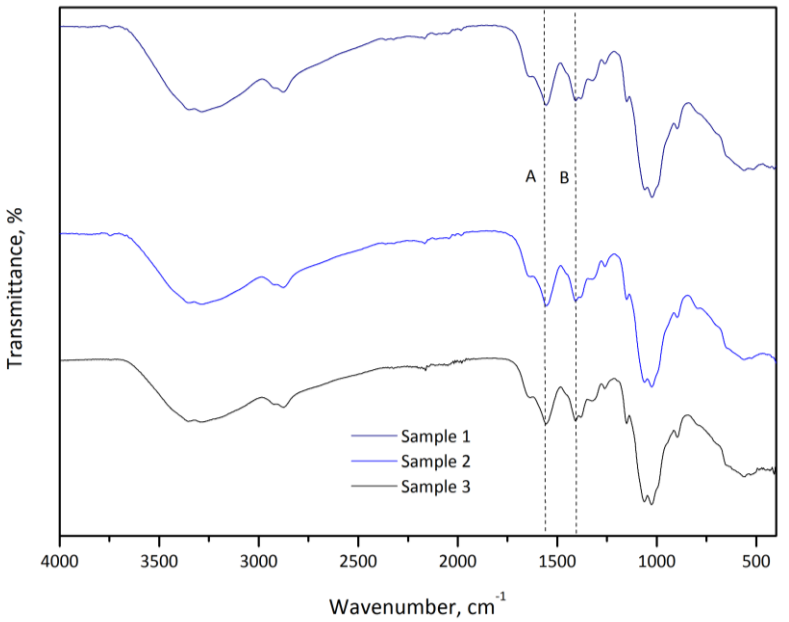

Figure 4-4. Comparison between the FTIR spectra of CS/TPP nanocapsules obtained from different electrospray collections.

c. Sterilization of capsules

The microcapsules and nanocapsules underwent sterilization by Aragogamma SL., using radiation within the range of 25 to 40 kGy to avoid further contamination during in vitro experiments.

FTIR measurements were conducted to assess any potential changes in the chemical composition of the capsules after sterilization. The results revealed that no significant alterations occurred in the signals, indicating that there were no chemical changes within the capsules. Similarly, careful examination of the capsule morphology demonstrated no noticeable changes in their physical structure.

4.3.2 Growing media

Each cell line requires a specific culture medium tailored to its unique requirements. Therefore, for the cells under study, we utilized the following media:

a. The BJ cell line requires a standard medium known as Eagle's Minimum Essential Medium (EMEM, 30-2003, ATCC). The complete growth medium contains fetal bovine serum (FBS, 30-2020, ATCC) at a final concentration of 10%.
b. The SCLII cell line requires a growth medium known as Dulbecco's Modified Eagle's Medium (DMEM, 10-013-CV, Corning) containing 4.5 g/L glucose, L-glutamine, and sodium pyruvate. The media was supplemented with 10% FBS (35-079-CV, Corning).
c. The 3T3 cell line requires a growth medium known as Dulbecco's Modified Eagle Medium/Nutrient Mixture F-12 (DMEM/F-12, 10-092-CV, Corning) that is a 1:1 mixture of DMEM and Ham's F-12. This formulation combines DMEM's high glucose, amino acids, and vitamin concentrations with F-12's various components. The complete growth medium was supplemented with 10% FBS (35-079-CV, Corning). DMEM/F-12 uses a sodium bicarbonate buffer system and requires a 5–10% CO_2 environment to maintain physiological pH.

4.3.2.1 Cell detachment (passaging)

To obtain a cell suspension, the medium from the culture flask (T25) was aspirated with a sterile pipette. Next, 2-3 mL of PBS, 1X solution without calcium and magnesium (21-040-CV, Corning), were added to the flask to rinse its surface. The PBS solution was then discarded using a new sterile pipette.

To detach the cells from the growth surface, 1-2 mL of 0.25% trypsin with 2.21 mM EDTA (Ethylenediaminetetraacetic acid) and 1X sodium bicarbonate (25-053-Cl, Corning) was directly added to the cell layer, and the flask was incubated for 3-5

minutes in the incubator. After detachment, 1 mL of medium containing FBS was added to the flask to inactivate the trypsin. The cells were then transferred to a 15 mL centrifugal tube and centrifuged for 5 minutes at room temperature at 350 Xg.

Once the cells had settled, the medium was discarded, and 2 mL of fresh medium was added to the cell pellet. The solution was mixed gently.

A portion of the cell suspension was transferred to a new flask with 5 mL of media and incubated for further experiments. The medium was renewed every 2–3 days.

Cell counting

Cell counting was performed by harvesting a specific volume of cell suspension and mixing it with the same volume of 0.4% Trypan Blue Solution (Corning). The cells were then counted in a Neubauer counting chamber using a light microscope (Olympus). The method is based on the concept that dead cells are permeable, take up the dye, and stain blue.

4.3.2.2 Cell culture for viability analysis

Cells were transferred to 96-well plates at a 5 x 10^3 cells/cm^2 density and suspended in 100 µL of growth medium. After initial 24-hour incubation in standard conditions, the growth medium was replaced with 100 µL of medium containing the capsules at a concentration of 1.0 mg/mL and 0.33 mg/mL. The plates were then placed in the incubator. The survivability test was conducted during 24 and 72 hours of contact with the capsules.

4.3.2.3 Viability

The MTT assay was used to assess cell viability. This protocol involves converting the water-soluble thiazolyl blue tetrazolium bromide (MTT reagent) into insoluble formazan by metabolically active cells. After culture, the growth medium was discarded. Cells were incubated with 1mg/mL MTT reagent (21795, Cayman

Chemical) in serum-free MEM with Earle's salts without L-glutamate and phenol red (17-305-CVR, Corning) for 3 hours at 37°C. Formazan crystals were then dissolved in dimethyl sulphoxide (DMSO), an HPLC-grade chemical with CAS number 67-68-5 purchased from POCH (Polska). Absorbance was measured at 570 nm using a microplate reader (iMark, Bio-Rad, Japan), and the Skanlt (software version 5.0) spectrophotometer was used for analysis.

4.3.3 Pretreatment to increase cell-capsule interaction

Cells were pretreated to increase their interactions with capsules. For this purpose, they were gently mixed with capsules for 15, 30, and 60 minutes before 24 incubation.

Initially, capsule suspensions were prepared at a concentration of 1.0 mg/mL and 0.33 mg/mL in the cell culture media. These suspensions were mixed with cells in Eppendorf tubes to achieve a seeding density of 5000 cells per well.

Two controls were included, one of the whole process and the other of the pretreatment to assess cell viability for comparative purposes. After this pretreatment, 100 µL of each pretreated sample was seeded per well and incubated for 24 hours.

After the incubation, the wells were washed twice with PBS to remove any unbound or excess material. Subsequently, the cells were imaged using a fluorescent microscope to visualize the fluorescence signal of capsules distributed on the well surface.

4.3.4 Fixation of cells on glass slides

Sterilized cover glass slides were placed in wells of a 6-well plate. Subsequently, 5000 cells were seeded into each well and incubated for 24 hours. Following

incubation, the medium was exchanged with a 1mg/mL capsule solution. The cells were then incubated for additional 24 hours.

Afterwards, the cell culture was washed with PBS, and the cells were stained by adding 150 µL of a phalloidin-ifluorTM 647 conjugate solution (20555, Cayman Chemical). Cells were stained for 1 hour in darkness at room temperature. The wells were then washed with PBS.

A drop of the mounting solution Eukitt® Quick-hardening mounting medium for microscopy (03989, Sigma Aldrich) was added between the cover slip and the glass slide to mount the fixated cells between the glass slides.

4.3.5 Spheroids cells culture with CS/TPP nano and microcapsules

Cells were seeded as in **Section 4.3.2.2** and manage with the same micro and nanocapsule composition. The 96-well plate used had a functionalized surface that prevented cell adherence to the bottom of the plate. The wells were then imaged.

Subsequently, cells were washed with PBS, and 50 µL of 0.1% formaldehyde solution (Sigma Aldrich) was added to each well. Plates were incubated for 24h at room temperature in darkness. The solution was exchanged with 0.1 % triton-x 100 (Sigma Aldrich) to permeabilize the cells. Plates were incubated for 24h at room temperature in darkness. The spheroids were stained by adding 50 µL of a phalloidin-ifluorTM 647 conjugate solution. The staining procedure was conducted for 1 hour in darkness at room temperature. Each spheroid was placed between the cover slip and the glass slide with the mounting media.

4.3.6 Cell-capsules morphological characterization

Cell morphology was evaluated using an inverted phase contrast microscope (CKX53-FL, Olympus, Japan) equipped with the Orca Spark monochrome camera (Orca Soark, Hamamatsu, Japan). The observations were made for the cell lines

cultured with all the tested compound configurations at the predetermined culture time.

The morphological interactions between the stained cells and fluorescence capsules were observed using a fluorescence microscope (X83 HCS, Olympus, Japan) equipped with a “Coolled PE-300 ultra” light source and cellSens software (Olympus, Japan). The fluorescence capsules were detected using a wavelength of approximately 488 nm, while the cells' cytoskeleton was detected using a wavelength of approximately 647 nm. Before analysis, the wells were washed twice with PBS to remove the excess capsules.

4.4 RESULTS AND DISCUSIONS

4.4.1 Cell morphology

The images of different cell lines were captured using an optical microscope, specifically targeting the central region of each well, as shown in **Figure 4-5**. The SCLII cell line typically exhibits a circular shape and grows in clusters or colonies. On the other hand, the 3T3 cell line is elongated in shape. While the BJ cell line is elongated in shape and a tendency to spread, this can pose challenges in imaging due to the low contrast between the cells and the well surface. All cell lines tend to detach from the surface during division, the shape is globular, which might be confused with microcapsules, but microcapsules are all fluorescent due to FTIC; after division, cells return to the surface. After 72 hours, the surface of the well is highly populated in comparison to 24h incubation.

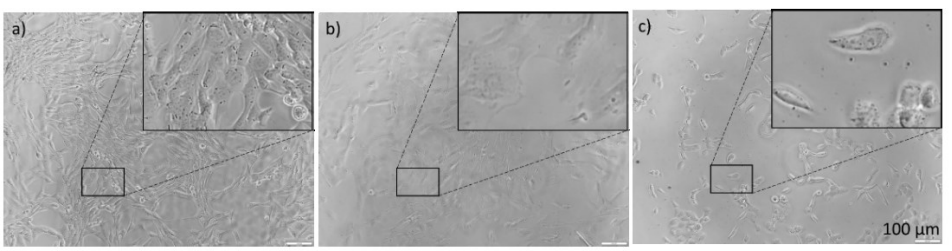

Figure 4-5. Optical images of 5000 a) 3T3 b) BJ and c) SCLII cells after 24-hour incubation.

4.4.2 Mico- and nanocapsule cytotoxic evaluation

Cytotoxicity tests employing MTT assay were used to determine the cell death (e.g., cell lysis), the inhibition of cell growth, colony formation, and other effects on cells caused by medical devices, materials and/or their extracts according to ISO 10993-12, Biological evaluation of medical devices. The MTT results are compared to the control of the procedure as 100 % survivability. Cytotoxic results can be acceptable

over 70 % viability. The concentration of microcapsules and nanocapsules are shown in **Table 4-2** and in **Table 4-1**.

a. Morphology of the cells after exposure to micro and nanocapsules

Before performing the MTT assay, each well was washed with PBS and imaged to contrast any irregularity with the cytotoxic evaluation, but this characterization also provides information about the interaction cell-capsule as shown in **Figure 4-6**.

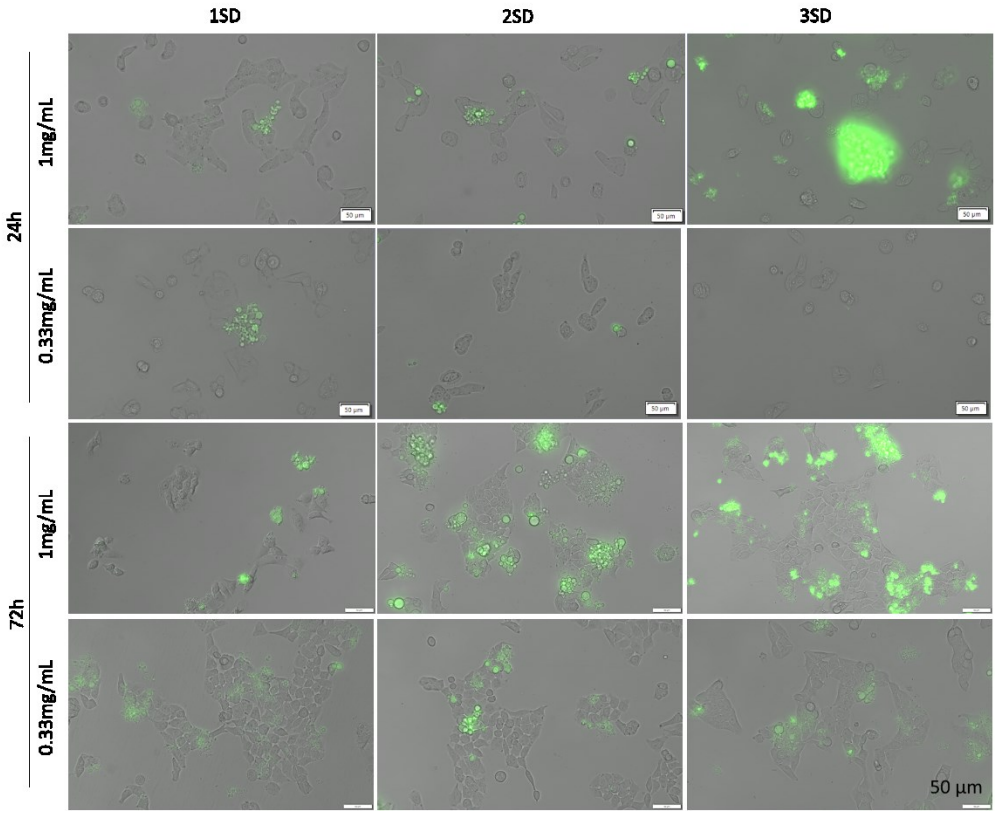

Figure 4-6. SCLII cells observed to the fluorescent microscope after 24 ad 72h incubation with microcapsules.

b. Microcapsule cytotoxic effect on BJ cell line

The BJ and SCLII cell lines were subjected to microcapsules at concentrations of 1 and 0.33 mg/mL in their respective culture media. The findings presented in **Figure 4-7** indicate that, overall, the survivability of the BJ cell line remains unaffected by

the microcapsule treatment. The observed higher survivability rate after 72 hours of incubation, compared to 24 hours, can be attributed to the initial heightened metabolic rate and adaptation of the cells to the presence of foreign bodies in the new media. However, the survivability rate begins to decline over time, indicating a gradual decrease in the cells' response.

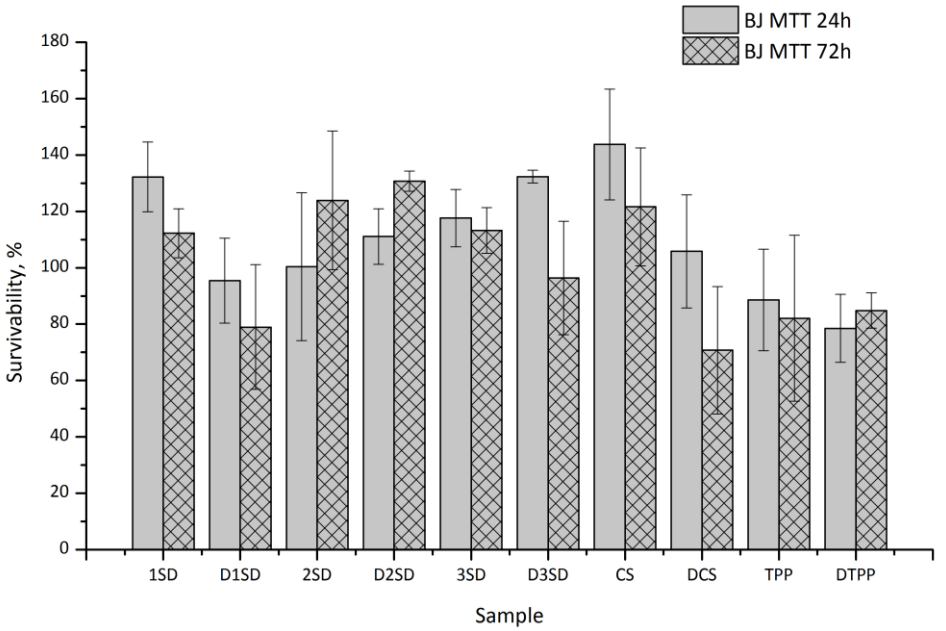

Figure 4-7. The results of the MTT assay on the BJ cell lines treated with 1 mg/mL of microcapsules (1SD, 2SD and 3SD) and raw materials (CS and TPP). Also, dilutions of 0.33 mg/mL of the microcapsules (D1SD, D2SD, D3SD) and raw materials (DCS and DTPP). The cells were incubated for 24 and 72 hours.

The survivability was assessed by comparing absorbances with control samples. The controls were normalized to represent 100% survivability. Consequently, the average survivability was determined using the **equation** (**4-1**):

$$\% \text{ Survivability} = \frac{\bar{A}_{sample}}{\bar{A}_{control}} * 100\% \quad (\mathbf{4\text{-}1})$$

Overall, it seems to exist a synergistic effect of the microcapsules on cell survivability. Additionally, we conducted a control experiment involving only

microcapsules to assess whether they have an impact on increasing the absorbance signal during MTT analysis. The results of this control experiment yielded negative findings, suggesting that the microcapsules themselves do not contribute to an increase in the absorbance signal.

c. Microcapsule cytotoxic effect on SCLII cell line

The results shown in **Figure 4-8** demonstrate that, in general, the SCLII cell line exhibits lower survivability compared to the BJ cell line in **Figure 4-7**, when treated with microcapsules, specifically with TPP at the applied concentrations. Intriguingly, it is observed that the survivability rate is lower after 24 hours of exposure to microcapsules compared to the 72-hour mark. This phenomenon can be attributed to the cells adapting to the new component, which leads to a temporary decrease in survivability.

However, after the 72-hour period, the survivability rate reaches its highest point, indicating that the previous heightened metabolic activity enables the cells to withstand the presence of foreign bodies better. This observation suggests that cells might have adapted and established a more robust response to the microcapsules.

Furthermore, beyond this adaptation period, a consistent and predictable pattern of cell growth in the presence of the new media can be observed, establishing a level of consistency in the cellular response to the microcapsules.

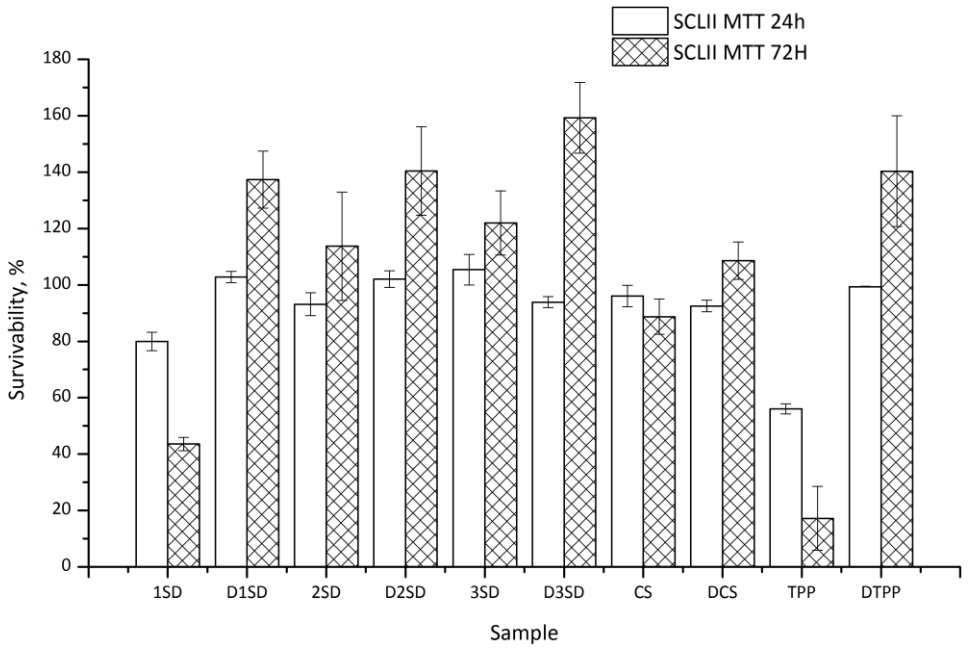

Figure 4-8. The results of the MTT assay on the SCLII cell lines treated with 1 mg/mL of microcapsules (1SD, 2SD and 3SD) and raw materials (CS and TPP). Also, dilutions of 0.33 mg/mL of the microcapsules (D1SD, D2SD, D3SD) and raw materials (DCS and DTPP). The cells were incubated for 24 and 72 hours.

In general, we anticipate a decrease in cell viability due to the attachment of the microcapsule to the cell membrane. We suspect that during the initial 24-hour treatment, ~~c~~ells that come into close proximity with the microcapsules will undergo cell death, while those that manage to survive will continue to proliferate.

a. Nanocapsule cytotoxic effect on 3T3, BJ, and SCLII cell lines

The images in **Figure 4-9** were randomly captured from different wells belonging to the same spot after 24 and 72 hours. It is evident that the fluorescence of the aggregates decreases from 24 to 72 hours of irradiation when the sample is being focused in order to take the image.

In this figure, we can also observe the optical image of BJ cells at both concentrations after 24 hours of incubation. We can observe that the nanocapsules

aggregate. The fluorescence emitted by these aggregates is remarkably intense compared to their size. This enhanced fluorescence can be attributed to the larger quantity of nanocapsules present within the aggregates.

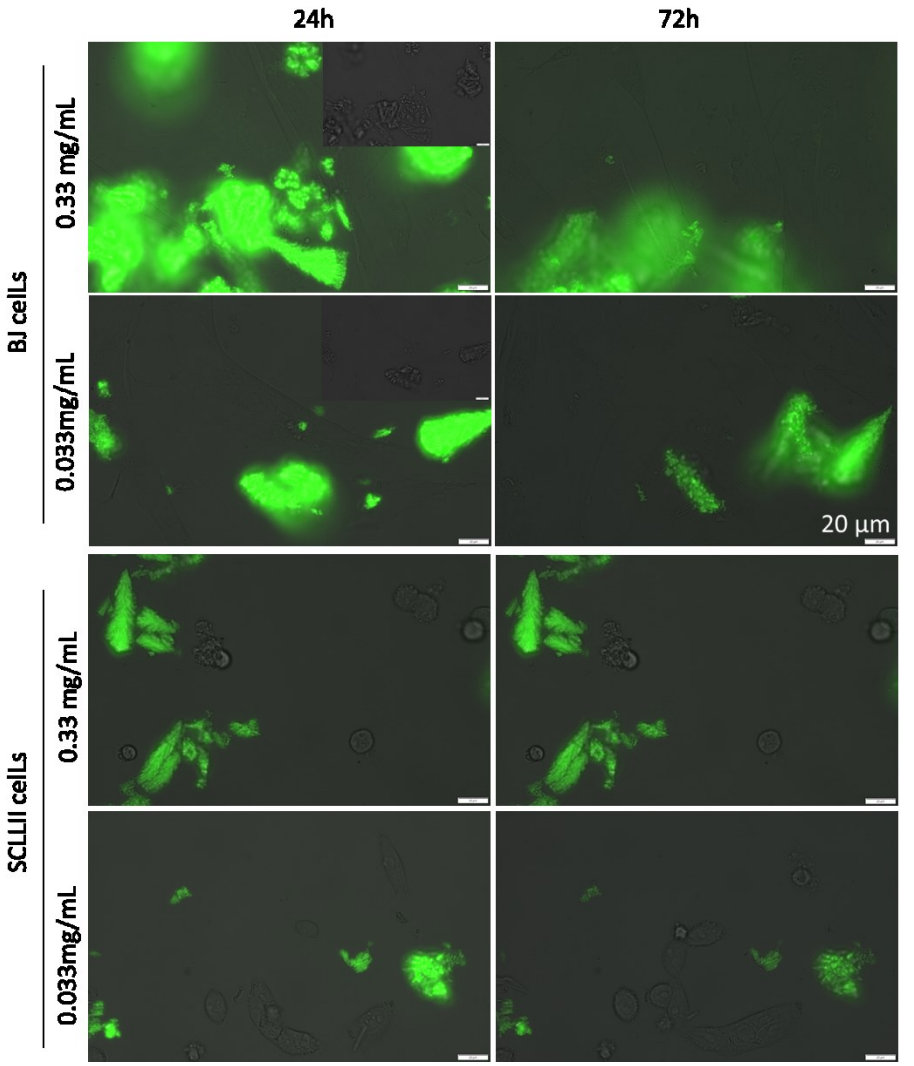

Figure 4-9. BJ and SCLII cells observed under the fluorescent microscope after 24 ad 72h incubation with nanocapsules.

Interestingly, certain areas exhibit a higher concentration of nanocapsule aggregates, such as the BJ cell at a concentration of 0.33 mg/mL. However, due to low contrast, it is challenging to observe these aggregates in BJ cells. Additionally, it

is more challenging to assess BJ cells as they are larger than 50 µm. The larger size of those cells leads to contact with the nanocapsule aggregates. On the other hand, the SCLII cells grow in colonies, resulting in limited contact with the nanocapsules (per cell).

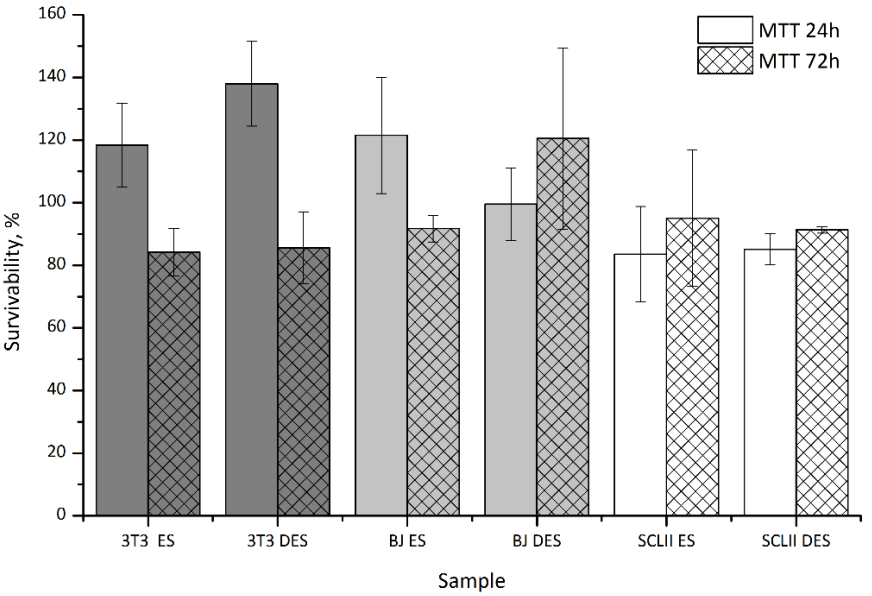

Figure 4-10. The results of the MTT assay on the SCLII and BJ cell lines treated with nanocapsules at two concentrations: 1 and 0.33 mg/mL in media.

All cell lines were exposed to nanocapsules at concentrations of 0.33 and 0.033 mg/mL in their respective media. The survivability of the cells was measured after 24 and 72 hours, and the results are shown in **Figure 4-10**. Overall, the nanocapsules showed no signs of cytotoxicity. As expected, the 3T3 cell line demonstrated remarkable resilience to adaptation to the new media, characterized by increased viability during the initial 24 hours due to the induction of high metabolic activity to survive. However, after 72 hours, a noticeable decrease in viability became apparent due to the return to normal enzymatic activity.

On the other hand, the BJ cell line exhibited the same behavior as 3T3 cell line. Notably, the viability of the SCLII cell line remained unaffected during the treatment at both doses.

4.4.3 Interaction of cells with micro and nanocapsules

Various approaches were employed to determine whether the capsules effectively attach to the cell membrane. It is worth noting that in vitro experiments involve extrapolated microenvironments that differ from *in vivo* conditions, primarily due to the controlled environment necessary to support cell viability and proliferation. In typical in vitro setups, cells are cultured on 2D or flat surfaces, which deviates from the complex in vivo environments they experience.

In this context, certain challenges arise. The media surrounding the cells remains unclear, and the capsules tend to fall downward due to gravity. It becomes a matter of luck for a capsule to land on top of a cell, potentially leading to an incorrect conclusion regarding capsule attachment. To address this, we implemented a strategy to enhance capsule-cell contact through a pretreatment that involved intermittently shaking of the cell suspension every 15 minutes during the initial incubation period. The initial incubation period involved three groups, each being incubated for different periods: 15, 30, and 60 minutes. Following this, the cells-capsules were seeded in a 96-well plate and allowed to incubate for 24 hours. This procedure aimed to promote longer interaction between the capsules and the cells and higher surface area contact, enabling a more accurate assessment of capsule attachment before studying cell proliferation.

a. Morphology of cell-microcapsules interaction after pretreatment

This study aimed to qualitatively evaluate the morphological interaction cell-capsule of 3T3 (**Figure 4-11**), BJ (**Figure 4-12**), and SCLII (**Figure 4-13**) cells to pretreatment before incubation using macro (SD) and nano (ES) capsules. Initially, 3T3 cells were used for their resistance to mechanical stress as preliminary experiments. After

incubation and washing, we still observe the tendency of capsules to form aggregates, and later the other cell lines underwent the same pretreatment.

We observe some affinity for all cells to attach to the capsules, but especially BJ cells, with their spreading behavior, showed higher retention of capsules compared to 3T3 and SCLII cells.

Most of the microcapsules were found near the SCLII cell membrane. However, clear conclusions regarding the attachment of microcapsules to the cells remain challenging. Further investigations are necessary to shed light on this aspect. The current data does not provide relevant information for concluding, as the microcapsules are significantly larger in size, making it unlikely for them to form a strong attraction by the cells.

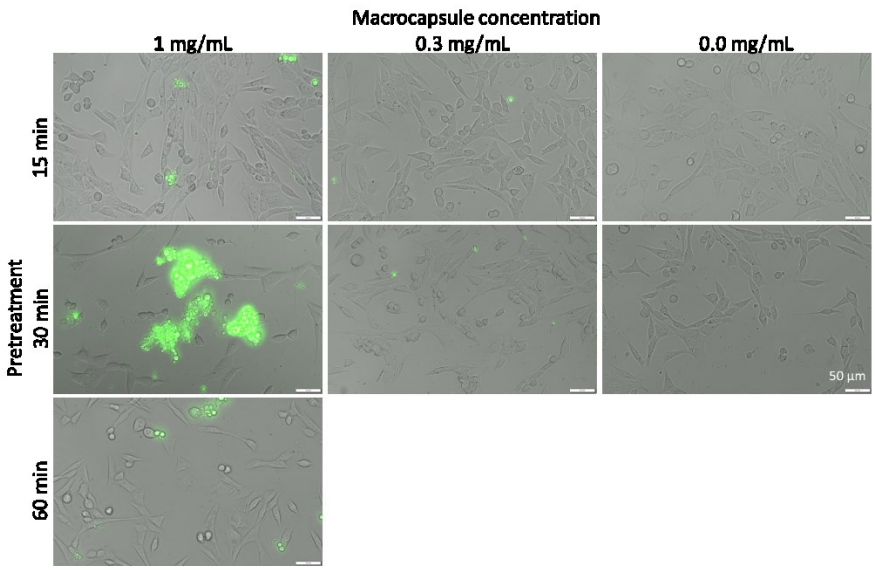

Figure 4-11. Images of 3T3 cell line observed at fluorescent microscope after 24h incubation with 2SD microcapsules.

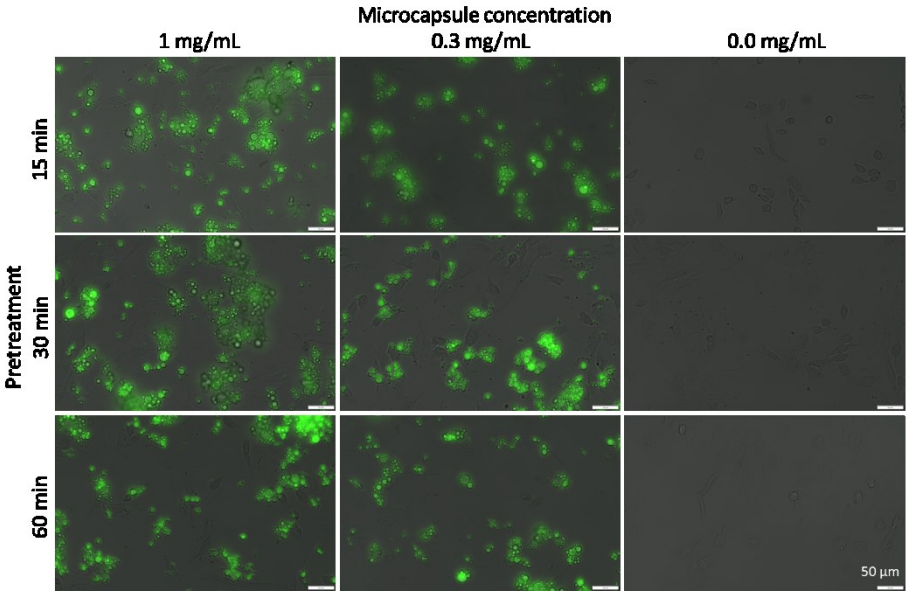

Figure 4-12. Images of BJ cell line observed at fluorescent microscope after 24h incubation after pretreatment with 2SD microcapsules.

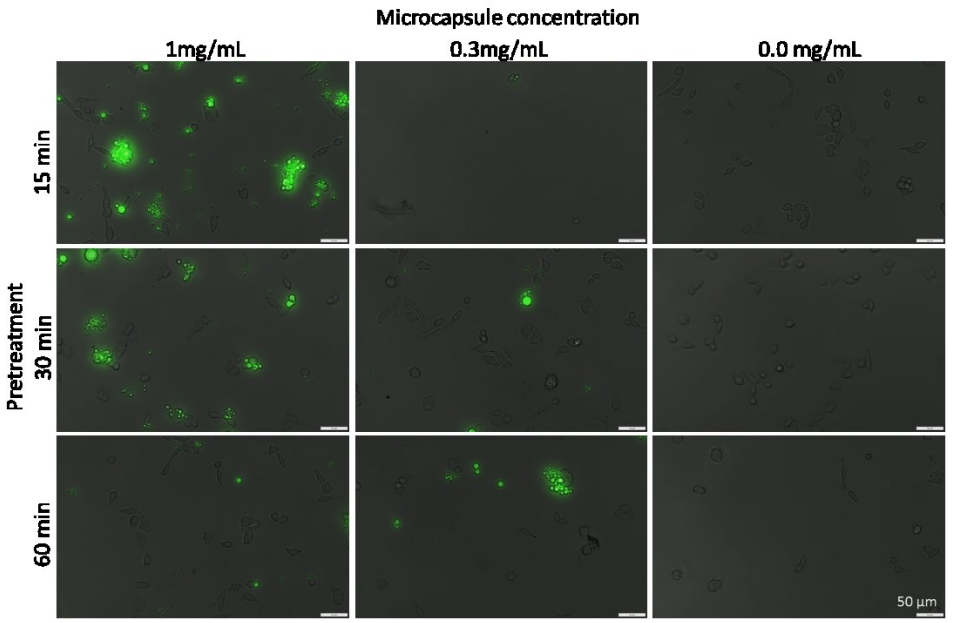

Figure 4-13. Images of SCLII cell line observed at fluorescent microscope after 24h incubation with 2SD microcapsules.

We investigated the potential absorption of small (D <2 µm) microcapsules by cells. We labeled the cells shown in red. Through this approach, our objective was to ascertain the location of the microcapsules, whether they were found inside or outside the cells.

This experiment has revealed that the microcapsules possess moisture, which impacts the mounting media and causes the microcapsules to move slightly away from the cells, as shown in **Figure 4-14**. Consequently, we recognized the need to enhance the experimental setup to investigate whether the capsules attach to the cells.

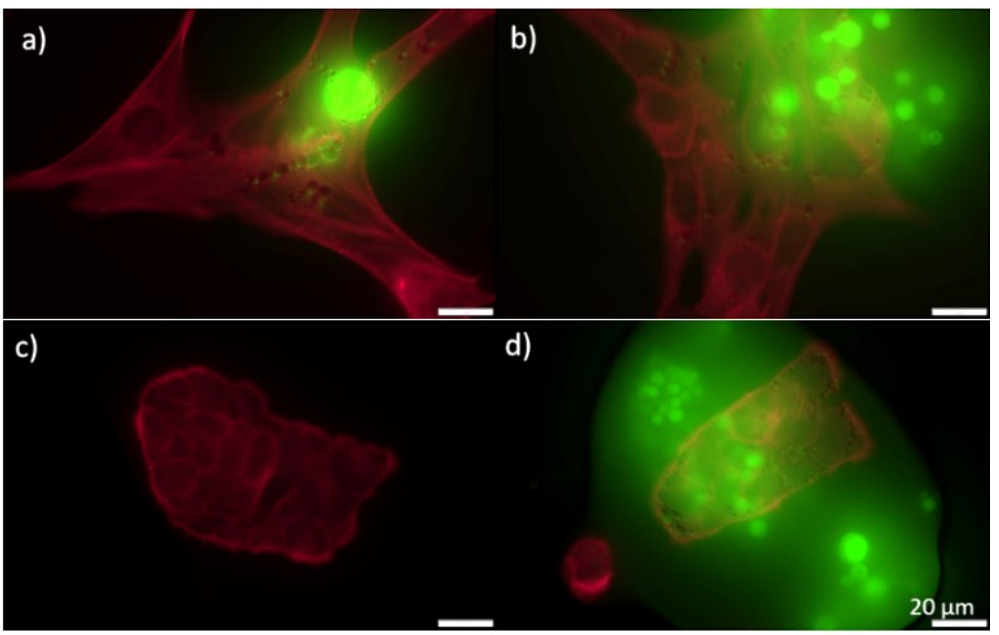

Figure 4-14. Fluorescent images of stained a, b) 3T3 and c, d) SCLII cell lines after 24h incubation with microcapsules.

b. Morphology of cell-nanocapsules interaction after pretreatment

Experiments were repeated as the same in section **4.4.3a** in order to evaluate the interaction cells with nanocapsules. Aggregates of nanocapsules were observed near both BJ and SCLII cells. Notably, there was a general increase in the number of

nanocapsules with prolonged pretreatment in both cases. However, it was still evident that BJ cells surroundings (**Figure 4-15**) had a higher presence of nanocapsules compared to SCLII cells (**Figure 4-16**).

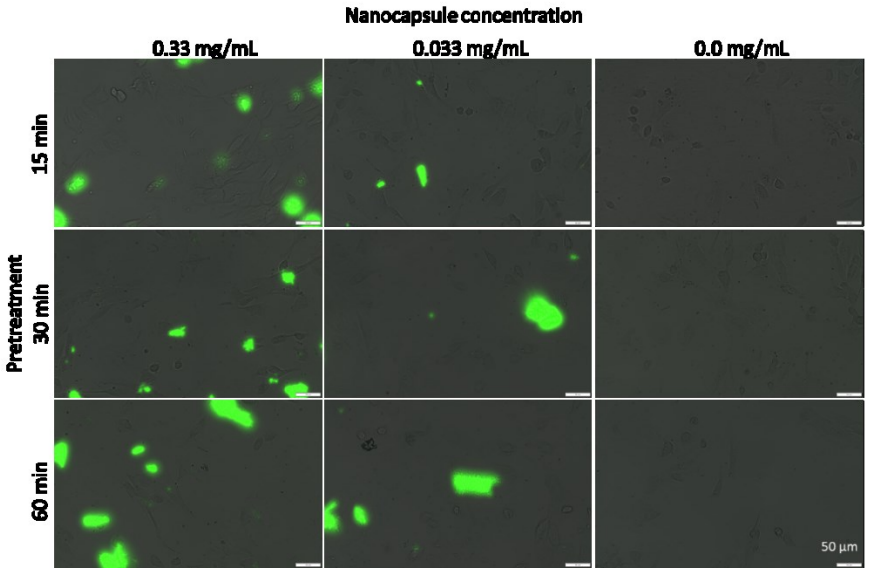

Figure 4-15. Images of BJ cell line observed at fluorescent microscope after 24h incubation after pretreatment with nanocapsules.

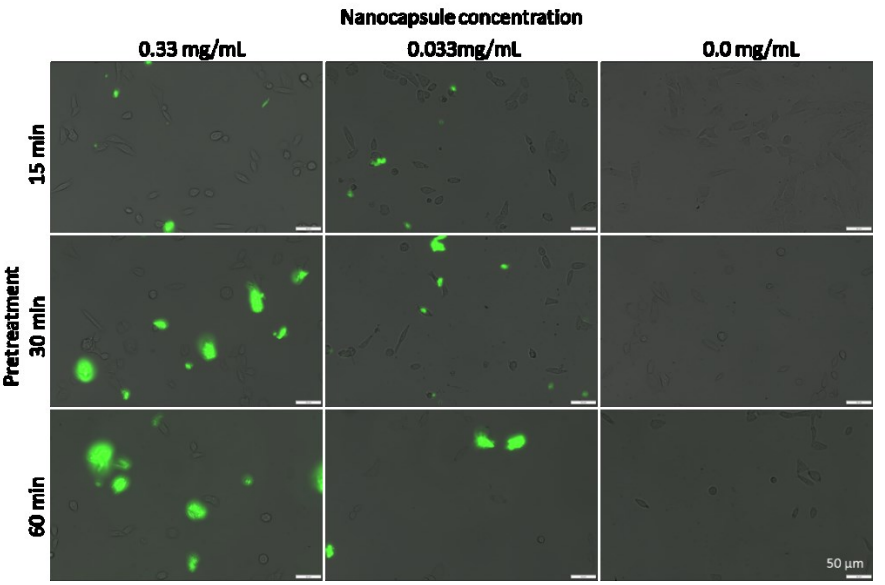

Figure 4-16. Images of SCLII cell line observed at fluorescent microscope after 24h incubation after pretreatment with nanocapsules.

c. Cytotoxic effect of the pretreatment to increase cell-capsule contact

During regular incubation, the microcapsules tended to precipitate on the surface of the well, resulting in limited contact with the cells. To address this issue, the objective of this experiment was to enhance cell-microcapsule interaction through mechanical agitation at different intervals (15, 30, and 60 minutes) prior to the incubation treatment for the MTT assay.

The MTT assay results can be observed in **Figure 4-17**. Two control groups were used to compare the results: one representing cell survivability without any treatment and the second representing the control group for the pretreatment. In the pretreatment control, it was observed that SCLII cells were more susceptible to mechanical stress, while BJ and 3T3 cells exhibited acceptable survivability. Notably, normal cells showed survivability rates of up to 90%.

When cells were pretreated with microcapsules to increase cell-capsule interaction, several key findings were observed:

The survivability of 3T3 and BJ cells decreased with longer pretreatment times using a concentration of 1 mg/mL of microcapsules. However, as the dose of microcapsules decreased, survivability also decreased. Interestingly, after 60 minutes, survivability increased again, indicating a potential adaptation to mechanical stress.

The use of 1 mg/mL of microcapsules promoted the survivability of SCLII cells, but at lower doses, survivability increased after 60 minutes of pretreatment.

These findings suggest that the duration and concentration of microcapsule pretreatment can impact cell survivability, with potential adaptive responses observed. Further investigation is needed to better understand the underlying mechanisms and optimize the conditions for enhancing cell-microcapsule interaction in future experiments.

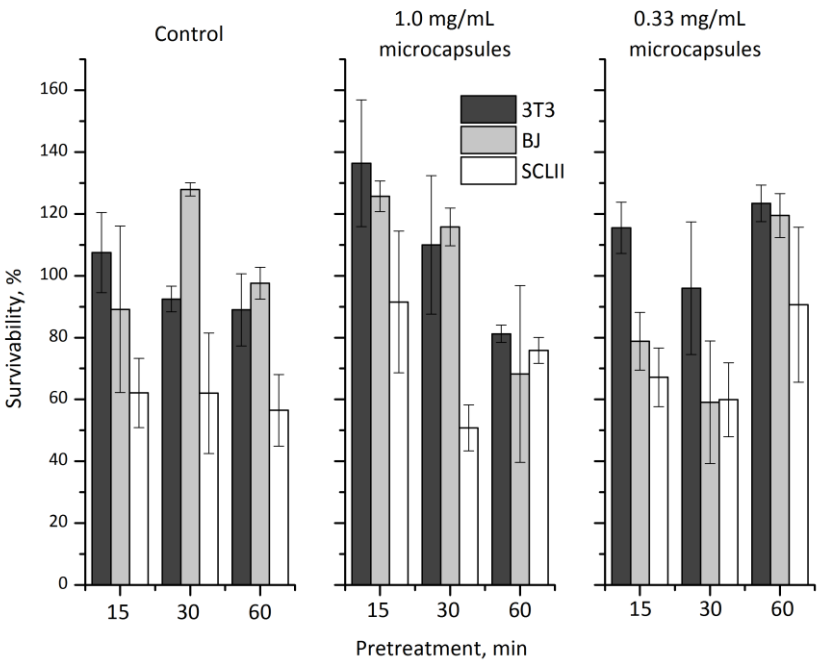

Figure 4-17. MTT assay after pretreatment to increase contact cell-microcapsule at concentration 1 mg/mL (SD) and 0.33 mg/mL (DSD) after 24h incubation.

In contrast, when the pretreatment was conducted using nanocapsules (**Figure 4-18**) the BJ control group exhibited higher survivability against mechanical stress. For both doses, the survivability of BJ cells during the 15 and 30 minutes of treatment mirrored that of the controls. However, after 60 minutes of pretreatment, the survivability rate of BJ cells increased. Intriguingly, the survivability of SCLII cells interacting with 0.03 mg/mL of nanocapsules was high, displaying a similar behavior to the high dose. This observation suggests that a low dose of nanocapsules may enhance the production of growth factors, thereby promoting increased survivability. Further investigation is needed to fully understand the underlying mechanisms responsible for this phenomenon.

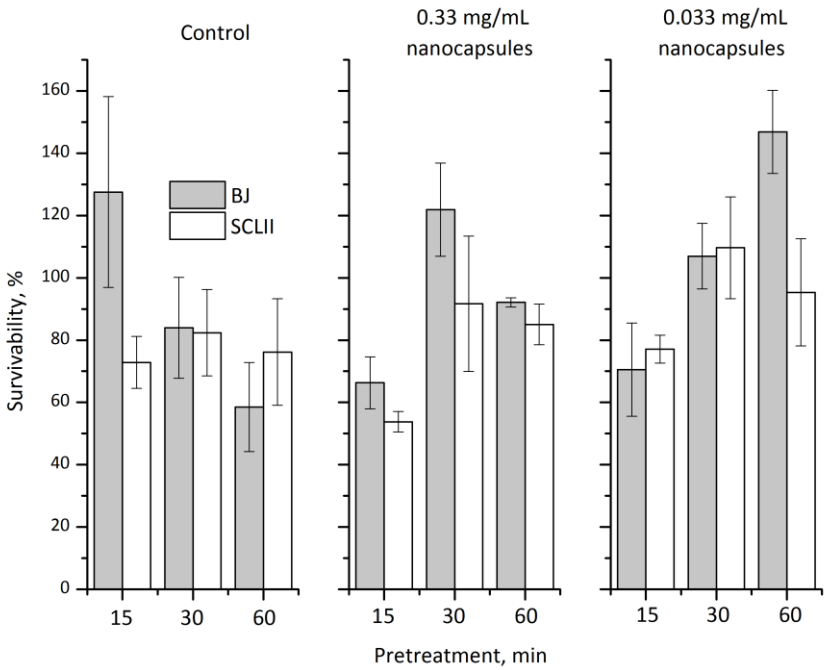

Figure 4-18. MTT assay after pretreatment to increase contact cell-nanocapsule at concentrations 0.33 mg/mL (ES) and 0.033 mg/mL (DES).

4.4.3.1 Real‑time cell growth during incubation with capsule.

BJ and SCLII cell lines were seeded following the procedure described in section **4.3.2.2.** Cells were incubated during imaging with the fluorescent microscope. Images were taken each hour during 72h in order to follow the behavior of the cells in the presence of the nano (ES) and microcapsules (SD). Microcapsules were specifically chosen as they exhibit a distinct individual appearance, which is easier to analyze than the aggregated form of nanocapsules. Moreover, even in cases where individual nanocapsules are present, the optical resolution of the microscope could decrease the level of detail of the nanocapsules due to the methodology applied to focus.

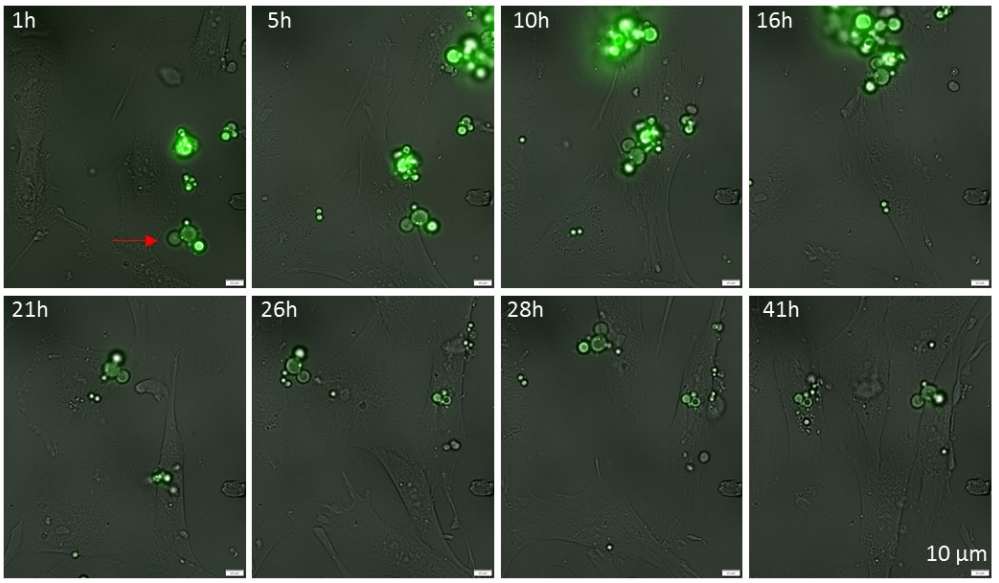

Figure 4-19. Representative image of real-time analysis of BJ cells incubated with 0.03 mg/mL of SD microcapsules.

Upon analyzing the videos generated from the 72 images, we made several significant observations. Both BJ and 3T3 cells were observed to carry aggregates of capsules on their surface while they proliferated and moved. Some videos even revealed where cells attempted to remove these aggregates, but they adhered firmly to the cells (capsules in image 1h with a red arrow of **Figure 4-19**). Interestingly, when the cells moved across the surface of the well, they tried to avoid the aggregates. However, in some videos shows cells that come near the aggregates, resulting in the aggregates sticking to the cells. During the 72 hours of observation, 3T3 and BJ cells continue living and reproducing, as we observe in some images of **Figure 4-19**.

On the contrary, the behavior of SCLII cells in the presence of the capsules presented a different scenario. The mobility of SCLII cells was significantly reduced, and their primary focus was on reproduction and the formation of cell clusters. Consequently, the interaction between SCLII cells and the capsules was considerably reduced due to poor mobility. In cases where SCLII cells encountered the capsules, diverse outcomes were observed following cell reproduction. The cell-capsule

interaction exhibited two scenarios: either they adhered to the SCLII cells or remained in close proximity to them (SCLII cells observed in image 1h a) and b) of **Figure 4-20**). These interactions allowed the cells to continue their life cycle and undergo reproduction. However, it was notable that after the reproduction process, these cells eventually perished within 72h, as depicted in **Figure 4-20**.

Several additional observations were made when clusters of cells interacted with the capsules. It was noticed that cells that had some form of contact with the capsules appeared to be in a state of cell death after division. However, the clusters of cells surrounding the death cell seemed to absorb it, possibly utilizing it to sustain their own survival or just absorbed it due to proximity. Notably, in certain videos, it was evident that the clusters released cells that appeared to be in a state of cell death, indicating that these cells might have perished due to their contact with the capsules.

In further experiments, a combination of 2500 BJ cells and 2500 SCLII cells were seeded together, with each cell type receiving half of their respective media. In the control group, it was observed that BJ cells displayed high mobility, while SCLII cells exhibited minimal mobility. When BJ cells encountered SCLII cells, their membranes adhered to each other, resulting in two distinct scenarios.

In the first scenario, SCLII cells started to expand as a response to the action of BJ cells, which expanded to drag and move across the surface of the well. The behavior of the SCLII cells began to resemble that of the BJ cells during 72h observation.

In the second scenario, the SCLII cells were released from contact with BJ cells, and after one hour, they underwent cell death. The SCLII cells that remained isolated continued to increase in size without undergoing reproduction until reaching cell death.

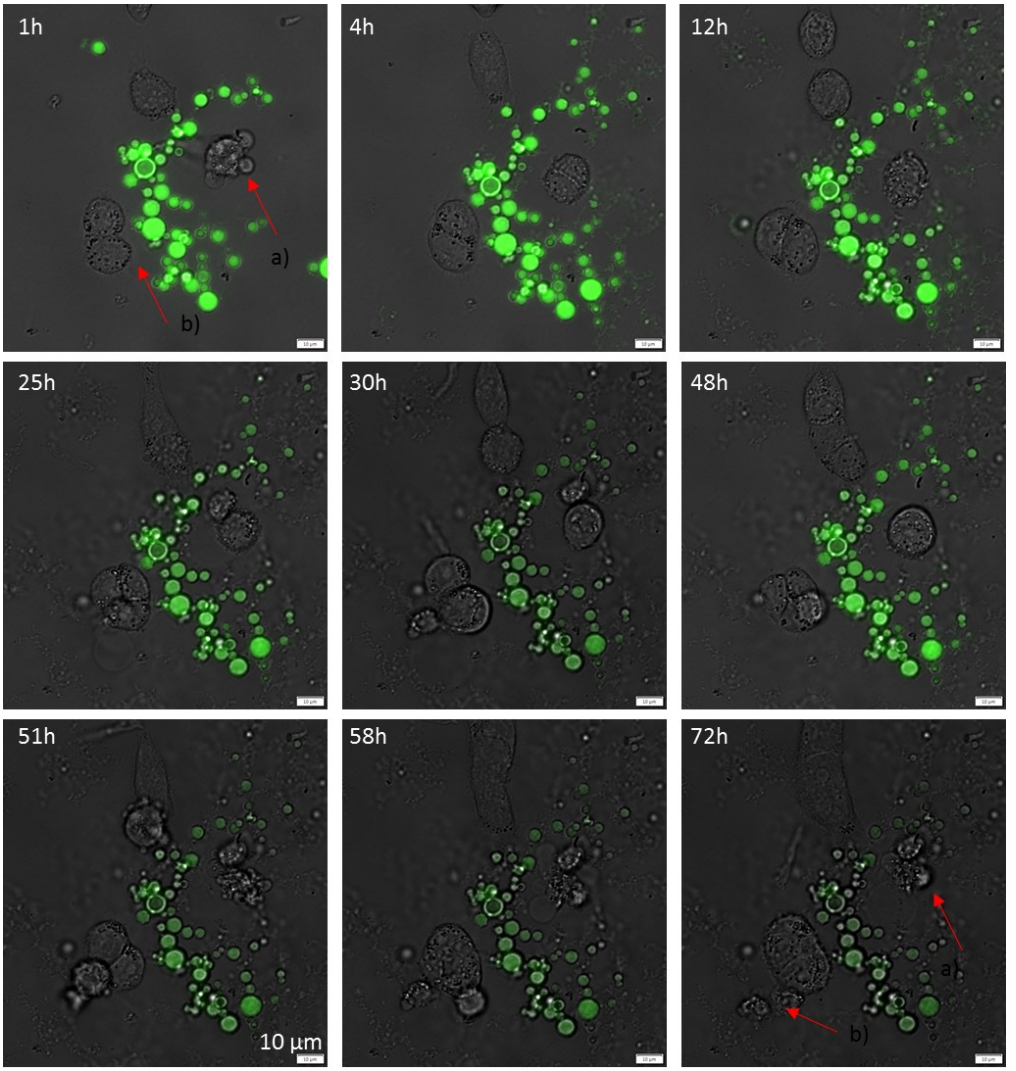

Figure 4-20. Representative of a fluorescent image of real-time incubation of SCLII with 0.3 mg/mL microcapsules.

When microcapsules were introduced to the combination of BJ and SCLII cell culture, a similar pattern of behavior was observed. The capsules attached to the BJ cells and moved along with them. In this case, the SCLII cells had more contact with the microcapsules. However, after a while, the SCLII cells with contact with capsules and those without contact eventually experienced cell death.

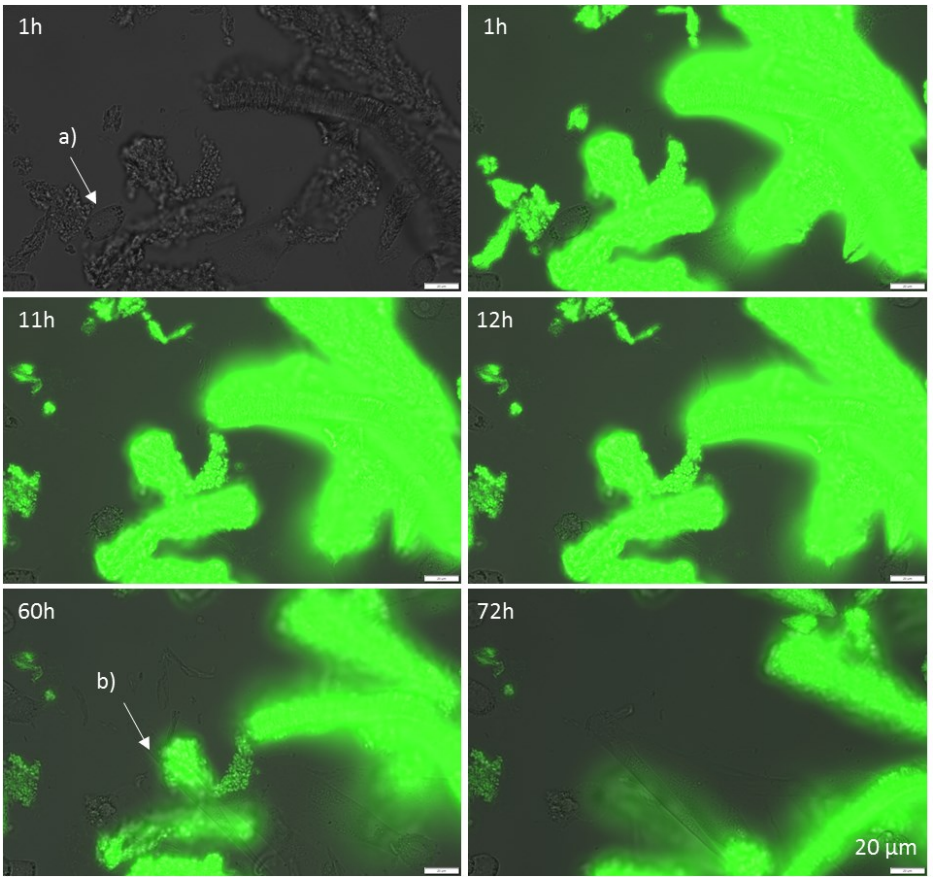

Figure 4-21. SCLII and BJ cells were cultured together with 0.3 mg/mL of nanocapsules.

In **Figure 4-21** we present two images captured at the 1-hour mark. The image from the left shows the optical view without fluorescence, while the image on the right incorporates fluorescence. Notably, the aggregates of nanocapsules exhibit a layered appearance, likely due to the removal of the silicon wafer by blade casting the nanocapsules.

At 1 hour, we observe the exposure of cells to nanocapsules. Firstly, a single SCLII cell (labeled as a) can be seen alone near the aggregates of nanocapsules. However, after 11 hours, abnormalities in the cell membrane become evident, and by 12 hours, the cell has perished.

At 60 hours, a BJ cell (labeled as b) with low contrast, is observed. This BJ cell is seen moving in the direction indicated by the arrow, and there is a noticeable displacement of nanocapsules in the direction of the BJ cell. This observation highlights that the BJ cell possesses enough strength to either attract the nanocapsules or displace them through its own movement.

4.4.3.2 Spheroids cell culture with nanocapsules

In contrast, cell culture as spheroids in a three-dimensional (3D) system provides a more realistic simulation of the in vivo microenvironment. Within spheroids, cells reproduce while floating, resulting in a more homogeneous contact with their surroundings compared to cells grown on flat surfaces (2D). This approach offers a valuable alternative for studying capsule-cell interactions in a manner that closely mimics the in vivo conditions (Eelco Fennema, 2013; Franziska Sambale, 2015).

a. Morphology of the control for cells growth as spheroids

A total of 5000 cells were seeded into each well of a 96-well plate. Over time, the cells proliferated and formed spheroids composed of clustered cells. It was observed that the cells tended to grow predominantly along the border of the well, likely due to enhanced mobility in that area, as observed in **Figure 4-22**.

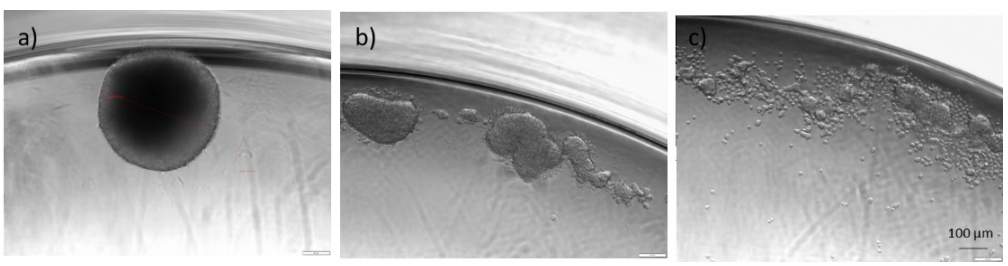

Figure 4-22. Optical images of spheroids of a) 3T3, b) BJ, and c) SCLII after 24h, 24h, and 96 hours incubation, respectively.

b. Spheroid interaction with nanocapsules

The smallest spheroids observed in **Figure 4-23** exhibit diameters ranging from 99 to 148 nm, corresponding to the SCLII cell line. We noticed that the morphology of SCLII cells is comparatively smaller compared to the other cell lines investigated. The spheroids formed by BJ cells range from 130 to 140 nm, while those of 3T3 cells measure between 456 and 512 nm. It is worth noting that the 3T3 spheroids were grown for an additional 48 hours compared to the others.

Furthermore, the images obtained from the SCLII spheroids reveal the presence of PBS (phosphate-buffered saline) crystals. Additionally, the nanocapsules demonstrate partial adhesion to the spheroids, which supports the hypothesis of this thesis to develop a layer of nanocapsules around the cancer cells. Notably, the spheroids continue to grow even after the introduction of nanocapsules, which is a remarkable finding.

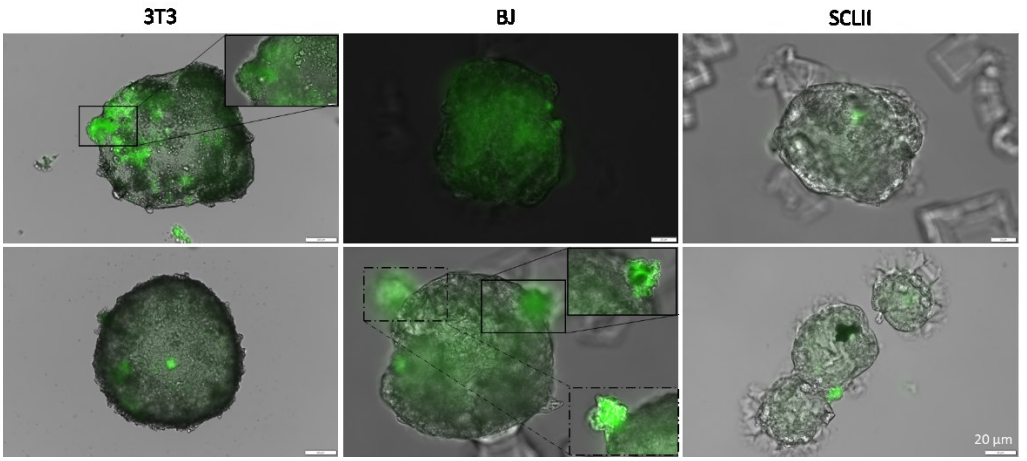

Figure 4-23. Incubation of 24h of the different cell lines with 0.3 mg/mL nanocapsules.

4.5 CONCLUSIONS

In the in vitro experiments involving BJ and SCLII cell lines and the CS/TPP nanocapsules and microcapsules, several important findings emerged related to the impact on cell viability, the cellular interaction. The effects on SCLII cells by the presence of BJ, the capsule attachment and movement and the morphology and aggregation of capsules.

Impact on cell viability: The 3T3, BJ, and SCLII cell lines exhibit a remarkable survivability rate of over 70% when treated with CS/TPP nanocapsules and microcapsules for 24 and 72h incubation. Even when subjected to mechanical stress to enhance cell-capsule interaction, these cells demonstrate a high level of resilience, highlighting the robustness of the capsules and their compatibility with the cell lines.

Cellular Interaction: In a 2D cell growth system, the interaction between cells and capsules is unclear. When capsules are introduced to the cells, they fall due to gravity, resulting in random encounters between the capsules and cells.

When the BJ and SCLII cells met the nanocapsules, a clear interaction was observed. The nanocapsules adhered to the cells or were near them, leading to various conclusions, including cell expansion, mitosis, and cell death. The presence of nanocapsules seemed to influence cellular behavior and fate.

The utilization of micro and nanocapsules in contact with spheroids has proven to be a promising approach in the realm of 3D cell growth systems. The attachment of the capsules to the spheroids is remarkable, mimicking in vivo conditions and enhancing the physiological relevance of the model. Furthermore, the cells within the 3D model have demonstrated resilience and maintained their health even after prolonged exposure to the capsules. These findings underscore the potential of micro and nanocapsules as a valuable tool for studying cell behavior and interactions in a more realistic and dynamic environment, paving the way for

advancements in tissue engineering, drug delivery, cancer treatment, and regenerative medicine.

Effects on SCLII cells by the presence of BJ: The SCLII cells expanded and exhibited similar behavior to BJ cells, which have higher mobility. However, this expansion was not sustainable, and after a certain time, the SCLII cells started to exhibit abnormal membrane activity and eventually died. In the other scenario, SCLII cells remained alone and continued to increase in size without undergoing reproduction, ultimately leading to cell death.

Capsule attachment and movement: The capsules were found to attach to BJ cells, indicating a binding or affinity between the cells and the capsules. Additionally, the movement of the BJ cells was observed to cause displacement of the capsules. This suggests that the BJ cells possess enough force or attraction to influence the positioning and movement of the nanocapsules.

Morphology and aggregation of capsules: The nanocapsules tended to aggregate, forming aggregates. These aggregates showed layered structures when nanocapsules were removed from the silicon wafer, indicating the arrangement of the nanocapsules after collection. Microscopic images of the microcapsules revealed individual capsules and aggregated forms, with individual capsules offering better resolution than the aggregated ones.

In summary, the experiments demonstrated the interaction between the CS/TPP nanocapsules and microcapsules with BJ and SCLII cell lines, highlighting the influence of the capsules on cellular behavior, viability, and mobility. These findings contribute to a better understanding of the cellular response to these drug delivery carriers and pave the way for further exploration of their potential applications in cancer therapy.

5. GENERAL CONCLUSIONS

"Science is not only a discipline of reason

but also, one of romance and passion."

_Stephen Hawking

Chapter 2

Microcapsule production using a spray drier resulted in a broad size distribution and optimizing parameters such as nozzle size and atmospheric gas could reduce the size distribution. Temperature control was crucial to prevent membrane cracks and degradation of microcapsule integrity.

CS/TPP microcapsules exhibited stability across a wide range of pH values, thanks to the presence of the TPP crosslinker. In contrast, chitosan capsules were pH-sensitive and prone to dissolution at low pH values due to increased electrostatic repulsion between polymer chains.

The surface charge of CS/TPP microcapsules was pH-dependent, with enhanced dispersion stability at low pH values. The presence of folic acid (FA) further increased the surface charge, improving dispersion stability. The pH-dependent surface charge had implications for the microcapsules' behavior in different environments and their potential use in targeted drug delivery.

The release behavior of FA from CS/TPP microcapsules varied in different buffer solutions. Higher release rates were observed in phosphate buffer solution, suggesting greater susceptibility of cationic FA to release. In lactate buffer solution, the microcapsules retained their swollen state, resulting in a lower release rate of FA.

Chapter 3

Nanocapsules were successfully produced using electrospray with a transparent CS solution, resulting in globular-shaped nanocapsules with a narrow size distribution suitable for pharmaceutical applications.

The addition of TPP to the nanocapsules led to crosslinking between CS and TPP, forming a distinct layer. Nanocapsules exposed to water did not show layer formation, highlighting the role of TPP in the crosslinking process.

The production of crosslinked CS/TPP particles from microemulsions showed agglomeration and spider web-shaped material, but particles collected from the periphery exhibited smaller sizes due to the drying effect of electrospray.

Analysis using FTIR revealed a lower degree of crosslinking between CS and TPP in electrosprayed particles compared to spray-dried particles. The presence of OH^- ions affected the stability of CS/TPP complexes, leading to a higher degree of cleavage. Mixing CS and TPP solutions during electrospray was suggested to enhance crosslinking.

A coaxial electrospray approach was developed to achieve homogeneous and crosslinked nanocapsules. Optimization of the Taylor cone shape, protrusion, and nozzle configuration improved stability and crosslinking. The resulting nanocapsules exhibited spherical morphology and prolonged stability in solution.

Chapter 4.

The investigation of the biological activity of nano- and microcapsules with BJ, 3T3, and SCLII cell lines provided valuable insights into their potential applications in the field of biomedical research. The utilization of CS/TPP capsules demonstrated a significant impact on cellular behavior, particularly in promoting enhanced cell viability during cell-capsule attachment. While the capsules do not characteristically

differentiate cells, it is worth noting that incorporating biomarkers can enhance specificity in targeting. The compatibility of the capsules with the tested cell lines, as evidenced by the observed cellular responses, suggests their potential utility in various biomedical applications, including tissue engineering and regenerative medicine. Further studies and optimization of these nano- and microcapsules are warranted to fully explore their potential, thereby paving the way for the development of advanced biomedical technologies that can positively impact healthcare and therapeutic interventions.

BIBLIOGRAPHY

A. J. Hijano, I. G. (2015). Periodic emission of droplets from an oscillating electrified meniscus of a low-viscosity, highly conductive liquid. *PHYSICAL REVIEW E, 91*, 013011-1, 013011-12. doi:DOI: 10.1103/PhysRevE.91.013011

A. M. Gañan-Calvo, J. D. (1997). Current and droplet size in the electrospraying of liquids. Scaling Laws. *Journal of Aerosol Science, 28*(2), 249-275.

Agnes Aruna John, S. K. (2017). Folic acid decorated chitosan nanoparticles and its derivatives for the delivery of drugs and genes to cancer cells. *CURRENT SCIENCE, 8*(25), 1530-1542.

Alessandro F. Martins, D. M. (2012). Chitosan/TPP microparticles obtained by microemulsion method applied in controlled release of heparin. *International Journal of Biological Macromolecules, 51*, 1127-1133. doi:http://dx.doi.org/10.1016/j.ijbiomac.2012.08.032

Andréia Lange de Pinho Neves, ,. C. (2014). Factorial design as tool in chitosan nanoparticles development by ionic gelation technique. *Colloids and Surfaces A: Physicochemical and Engineering Aspects, 445*(20), 34-39. doi:https://doi.org/10.1016/j.colsurfa.2013.12.058

Anna Lesniak, A. S.-M. (2013). Nanoparticle Adhesion to the Cell Membrane and Its Effect on Nanoparticle Uptake Efficiency. *Journal of the American Chemical Society, 135*, 1438−1444. doi:dx.doi.org/10.1021/ja309812z

Ashraf Abdelkhaliq, M. v. (2018). Impact of nanoparticle surface functionalization on the protein corona and cellular adhesion, uptake and transport. *Journal of Nanobiotechnology, 16*(70), 1-13. doi:https://doi.org/10.1186/s12951-018-0394-6

Barbara Muz, P. d. (2015). The role of hypoxia in cancer progression, angiogenesis, metastasis, and resistance to therapy. *Dove Medical press, 3*, 83-92. doi:http://dx.doi.org/10.2147/HP.S93413

Begoña Almería, T. M. (2011). A multiplexed electrospray process for single-step synthesis of stabilized polymer particles for drug delivery. *Journal of Controlled Release, 154*, 203–210. doi:10.1016/j.jconrel.2011.05.018

Berta Nogueiro Estevinho, F. R. (2013). Microencapsulation with chitosan by spray drying for industry applications- A review. *Trends in Food Science & Technology, 31*, 138e155. doi:http://dx.doi.org/10.1016/j.tifs.2013.04.001

Bingdi Chen, W. L. (2016). targeting negative surfaces charges of cancer cells by multifunctional nanoprobes. *Theranostics, 6*(11), 1886-1898. doi:10.7150/thno.16358

Bo Wang, T. O. (2008). Coacervation Technique as an Encapsulation and Delivery Tool for Hydrophobic Biofunctional Compounds. En A. M. Alexandru Mihai Grumezescu, *Role of Materials Science in Food Bioengineering* (págs. 235-261). Elsevier Inc. doi:http://dx.doi.org/10.1016/B978-0-12-811448-3.00007-3

Bodnár, E. G.-L. (2018). Polymer solution electrospraying: A tool for engineering particles and films with controlled morphology. *Journal of Aerosol Science, 125*, 93–118. doi:DOI:10.1016/j.jaerosci.2018.04.012

Bryant Garret D., N. a. (2008). Cell Encapsulation in Biodegradable Hydrogels for Tissue Engineering Applications. *TISSUE ENGINEERING: Part B, 14*(2), 149-165.

Brynn N. Sundberg, A. F. (2018). Coaxial Electrospray Ionization for the Study of Rapid In-source Chemistry. *American Society for Mass Spectrometry, 29*, 2023Y2029. doi:DOI: 10.1007/s13361-018-2004-0

Carolina de las Heras Alarcón, S. P. (2005). Stimuli responsive polymers for biomedical applications. *Chemical Society Reviews, 34*, 276–285. doi:10.1039/b406727d

Chen, Q. L. (2017). Chitosan–PVA monodisperse millimeter-sized spheres prepared by electrospraying reduce the thromboembolic risk in hemorrhage control. *Journal of Materials Chemistry B,, 5*(20), 3686–3696.

Christophe Roca, B. C. (2012). Production of yeast chitin–glucan complex from biodiesel industry byproduct. *Process Biochemistry, 47* , 1670–1675.

Chul Ho Park, J. L. (2009). Electrosprayed Polymer Particles: Effect of the Solvent Properties. *Journal of Applied Polymer Science, 114*, 430–437.

Daijiro Shno, A. K. (2015). Amine effect on phenylboronic acid complex with glucose under physiological pH in aqueous solution. *Journal of Biomaterials Science, Polymer Edition, 7*(8), 697-705,. doi:10.1163/156856296X00462

Daniele R. Nogueira-Librelotto, L. E. (2016). Chitosan-tripolyphosphate nanoparticles functionalized with a pH-responsive amphiphile improved the in vitro antineoplastic effectsof doxorubicin. *Colloids and Surfaces B: Biointerfaces, 147*, 326–335. doi:http://dx.doi.org/10.1016/j.colsurfb.2016.08.014

Daniele R. Nogueira-Librelotto, L. E. (2020). pH-Sensitive chitosan-tripolyphosphate nanoparticles increase doxorubicin-induced growth inhibition of cervical HeLa tumor cells by apoptosis and cell cycle modulation. *Colloids and Surfaces B: Biointerfaces*. doi:https://doi.org/10.1016/j.colsurfb.2020.110897

Dan-Lei Yang, R.-K. L.-X. (2024). Micro-sized nanoaggregates: Spray-drying-assisted fabrication and applications. *Particuology, 85*, 22e48. doi:https://doi.org/10.1016/j.partic.2023.03.013

Dazhi Wang, Z. A. (2022). Numerical modeling and analysis of coaxial electrohydrodynamic jet printing. *Scientific Reports, 12*(1924), 1-17. doi:https://doi.org/10.1038/s41598-022-05596-y

Devika R. Bhumkar, a. V. (2006). Studies on Effect of pH on Cross-linking of Chitosan With Sodium Tripolyphosphate: A Technical Note. *American Association of Pharmaceutical Scientists PharmSciTech, 7*(2), E1-E6.

Eelco Fennema, N. R. (2013). Spheroid culture as a tool for creating 3D complex tissues. *Trends in Biotechnology, 31*(2), 108-115.

Esmaeili, F. A.-M. (2021). Parameters influencing size of electrosprayed chitosan/HPMC/TPP nanoparticles containing alendronate by an artificial neural networks model. *Journal of Electrostatics, 112*, 10359.

Eun Seok Gil, S. M. (2004). Stimuli-reponsive polymers and their bioconjugates. *Progress in Polymer Science, 29*, 1173–1222. doi:doi:10.1016/j.progpolymsci.2004.08.003

F. Di Mario, P. R. (2008). Chitin and chitosan from Basidiomycetes. *International Journal of Biological Macromolecules, 43*, 8–12. doi:doi:10.1016/j.ijbiomac.2007.10.005

Faezeh Bagheri-Tar, M. S. (2007). Preparation of Polyetherimide Nanoparticles by an Electrospray Technique. *Ind. Eng. Chem. Res.*, 3348–3357.

Francisca Villanueva-Flores, A. C.-L. (2019). Understanding cellular interactions with nanomaterials: Towards a rational design of medical nanodevices. *Nanotechnology in press*, 1-40. doi:https://doi.org/10.1088/1361-6528/ab5bc8

Francisca Villanueva-Flores, A. C.-L. (2020). Understanding cellular interactions with nanomaterials: towards a rational design of medical nanodevices. *Nanotechnology, 31*, 1-20. doi:https://doi.org/10.1088/1361-6528/ab5bc8

Franziska Hirschhaeuser, U. G.-K. (2011). Lactate: A Metabolic Key Player in Cancer. *American Association for Cancer Research*, 6921-6925. doi:10.1158/0008-5472.CAN-11-1457

Franziska Sambale, A. L. (2015). Three dimensional spheroid cell culture for nanoparticle safety testing. *Journal of Biotechnology*, 1-10.

Fwu-Long Mi, S.-S. S.-B.-F.-T.-T. (1999). Chitosan–Polyelectrolyte Complexation for the Preparation of Gel Beads and Controlled Release of Anticancer Drug. II. Effect of pH-Dependent Ionic Crosslinking or Interpolymer Complex Using Tripolyphosphate or Polyphosphate as Reagent. *Journal of Applied Polymer Science, 74*(5), 1037-1319. doi:https://doi.org/10.1002/(SICI)1097-4628(19991031)74:5<1093::AID-APP6>3.0.CO;2-Copen_in_newISSN0021-8995

Fwu-Long Mi, S.-S. S.-T.-B. (1999). Kinetic Study of Chitosan-Tripolyphosphate Complex Reaction and Acid-Resistive Properties of the Chitosan-Tripolyphosphate Gel Beads Prepared by in-Liquid Curing Method. *Journal of Polymer Science: Part B: Polymer Physics,, 37*, 1551–1564.

Fwu-Long Mi, S.-S. S.-Y.-T.-T.-F. (1999). Chitosan–Polyelectrolyte Complexation for the Preparation of Gel Beads and Controlled Release of Anticancer Drug. I. Effect of Phosphorous Polyelectrolyte Complex and Enzymatic Hydrolysis of Polymer. *Journal of Applied Polymer Science, 74*(7), 1607-1879. doi:https://doi.org/10.1002/(SICI)1097-4628(19991114)74:7<1868::AID-APP32>3.0.CO;2-N

Gamero-Castaño, M. &. (2019). The minimum flow rate of electrosprays in the cone-jet mode. *Journal of Fluid Mechanics*, 553–572.

H.H. Kim, .. N.-C. (2014). Polarity effectontheelectrohydrodynamic(EHD)spray of water. *Journal ofAerosolScience*, 98–114. doi:http://dx.doi.org/10.1016/j.jaerosci.2014.06.002

Hamid Reza Naghibi Beidokhti, R. G. (2016). Preparation, Characterization, and Optimization of Folic Acid-Chitosan-Methotrexate Core-Shell Nanoparticles by Box-Behnken Design for Tumor-Targeted Drug Delivery. *American Association of Pharmaceutical Scientists*, 1-15. doi:10.1208/s12249-015-0445-3

Hang Thu Ta, C. R. (2008). Injectable chitosan hydrogels for localised cancer therapy. *Journal of Controlled Release, 126*, 205–216. doi:doi:10.1016/j.jconrel.2007.11.018

Helene Jonassen, A.-L. K. (2012). Stability of Chitosan Nanoparticles Cross-Linked with Tripolyphosphate. *Biomacromolecules, 13*, 3747−3756. doi:dx.doi.org/10.1021/bm301207a

Hongliang Du, M. L. (2015). The design of pH-sensitive chitosan-based formulations for gastrointestinal delivery. *Drug Discovery Today*, 1-8. doi:https://doi.org/10.1016/j.drudis.2015.03.002

Hun Min Lee, M. H. (2017). Fluorescent Property of Chitosan Oligomer and Its Application as a Metal Ion Sensor. *Marine drugs, 15*(105), 1-8. doi:doi:10.3390/md15040105

Ilaria Silvestro, I. F. (2020). Preparation and Characterization of TPP-Chitosan Crosslinked Scaffolds for tissue engineering. *Materials, 13*(3577), 1-15. doi:doi:10.3390/ma13163577

J. M. López-Herrera, A. B. (2004). An Experimental Study of the Electrospraying of Water in Air at Atmospheric Pressure. *American Society for Mass Spectrometry., 15*, 253–259. doi:doi:10.1016/j.jasms.2003.10.018

J.M. López-Herrera, M. H.-C.-C. (2023). Effects of geometry in the operation of coaxial electrosprays. *Journal of Aerosol Science, 167*, 106075. doi:https://doi.org/10.1016/j.jaerosci.2022.106075

Jaworek, A. (2008). Electrostatic micro- and nanoencapsulation and electroemulsification: A brief review. *Journal of Microencapsulation, 27*(7), 443–468. doi:DOI: 10.1080/02652040802049109

Jelena Filipović-Grčïć, B. P. (2003). Spray-dried carbamazepine-loaded chitosan and HPMC microspheres: preparation and characterisation. *Journal of pharmacy and pharmacology*, 921-931. doi: https://doi.org/10.1211/0022357021503

Joan Rosell-Llompart, J. G. (2018). Electrosprays in the cone-jet mode: from Taylor cone formation to spray development. *Journal of Aerosol Science*. doi:https://doi.org/10.1016/j.jaerosci.2018.04.008

Jose M. López-Herrera, M. A.-C. (2020). A numerical simulation of coaxial electrosprays. *Journal of Fluid Mechanics, 885*, A15-1-23. doi:doi:10.1017/jfm.2019.880

Juan D. Giraldo, V. H.-R. (2019). Chitosan–tripolyphosphate bead: the interactions that govern its formation. *Polymer Bulletin, 76*, 3879–3903. doi:https ://doi.org/10.1007/s00289-018-2574-9

Jung, J. H.-N. (2013). Use of electrosprayed Sophora flavescens natural-product nanoparticles for antimicrobial air filtration. *Journal of Aerosol Sci*, 185−193.

Kleine-Brueggeney, H. Z.-G. (2015). A rational approach towards the design of chitosan-based nanoparticles obtained by ionotropic gelation. *Colloids and Surfaces B: Biointerfaces, 135*(1), 99-108. doi:https://doi.org/10.1016/j.colsurfb.2015.07.016

Kultida Songsurang, N. P. (2011). Electrospray Fabrication of Doxorubicin-Chitosan-Tripolyphosphate Nanoparticles for Delivery of Doxorubicin. *Arch Pharm Res*, 583-92.

Kumar, M. N. (2000). A review of chitin and chitosan applications. *Reactive and Functional Polymers, 46*(1), 1-27. doi:https://doi.org/10.1016/S1381-5148(00)00038-9

Leonardo M.B. Ferreira, A. M. (2020). Design of chitosan-based particle systems: A review of the physicochemical foundations for tailored properties. *Carbohydrate Polymers*, 1-20. doi:https://doi.org/10.1016/j.carbpol.2020.116968

Li Tang, N. P. (2013). Size-Dependent Tumor Penetration andin VivoEfficacy of monodisperse Drug−Silica Nanoconjugates. *Molecular pharmaceutics, 10*, 883−892Downloaded via UNIV ROVIRA I VIRGILI on July 6, 2023 at 08:24:47 (UTC).See https://pubs.acs.org/sharingguidelines for options on how to legitimately share published articles. doi:dx.doi.org/10.1021/mp300684a

López-Herrera J. M., H. M.-C.-C. (2023). Effects of geometry in the operation of coaxial electrospray. *Journal of Aerosol Science, 167*(106075), 1-9. doi:https://doi.org/10.1016/j.jaerosci.2022.106075

Loscertales, J. F. (1994). The current emitted by higly conducting Taylor cones. *Journal of Fluid Mechanics*, 155-184.

M. Goldman, A. G. (1985). The corona discharge, its properties and specific uses. *Pure and Applied Chemistry, 57*(9), 1353–1362. doi:https://doi.org/10.1351/pac198557091353

M.N. Khalid, F. A. (2002). Water state characterization, swelling behavior, thermal and mechanical properties of chitosan based networks. *European Journal of Pharmaceutical Sciences, 15*, 425–432.

Mandeep Kaloti, H. B. (2010). Kinetics of coacervation transition versus nanoparticle formation in chitosan–sodium tripolyphosphate solutions. *Colloids and*

Surfaces B: Biointerfaces, 81, 165–173. doi:doi:10.1016/j.colsurfb.2010.07.006

Mauro Sousa de Almeida, E. S.-B.-F.-R. (2021). Understanding nanoparticle endocytosis to improve targeting strategies in nanomedicine. *Chemical Society Reviews, 50*, 5397–5434. doi:10.1039/d0cs01127d

Meghdad Kamali Moghaddam, S. M. (2015). Micro/nano-encapsulation of a phase change material by coaxial electrospray method. *Iran Polym J, 24*, 759–774. doi:DOI 10.1007/s13726-015-0364-x

Min Huang, Z. M.-Y. (2002). Uptake of FITC-Chitosan Nanoparticles by A549 Cells. *Pharmaceutical Research, 19*(10), 1488-1494.

Mitchell Jones, M. K. (2020). Crab vs. Mushroom: A Review of Crustacean and Fungal Chitin in Wound Treatment. *Marin drugs, 18*(64), 1-23. doi:10.3390/md18010064

Mohammed Eddya, B. T.-H. (2020). A comparison of chitosan properties after extraction from shrimp shells by diluted and concentrated acids. *Heliyon*, 1-17. doi:https://doi.org/10.1016/j.heliyon.2020.e03486

Morteza Bahram, N. M. (2016). Chapter 2. An Introduction to Hydrogels and Some Recent Applications. En S. B. Majee, *Emerging Concepts in Analysis and Applications of Hydrogels* (págs. 9-31). India: IntechOpen.

Muñoz, A. J. (2021). *Production of Homogeneous Particles by Controlled Neutralization of Electrosprays.* Tarragona, Cataluña, Spain: Universitat Rovira i virgili.

Naghibi Beidokhti, H. R. (2017). Preparation, Characterization, and Optimization of Folic Acid-Chitosan-Methotrexate Core-Shell Nanoparticles by Box-Behnken Design for Tumor-Targeted Drug Delivery. *AAPS PharmSciTech*, 115–129.

Narayan Bhattarai, H. R. (2005). PEG-grafted chitosan as an injectable thermosensitive hydrogel for sustained protein release. *Journal of Controlled Release, 103*, 609–624.

Natarajan Raghunand, a. R. (2000). pH and drug resistance in tumors. *Drug Resistance Updates, 3*, 39-47. doi:10.1054/drup.2000.0119,

Natarajan Raghunand, B. P. (2003). Tumor acidity, ion trapping and chemotherapeutics II. pH-dependent partition coefficients predict importance of ion trapping on pharmacokinetics of weakly basic chemotherapeutic agents. *Biochemical Pharmacology, 66*, 1219–1229.

Nathan D. Donahue, H. A. (2019). Concepts of nanoparticle cellular uptake, intracellular trafficking, and kinetics in nanomedicine. *Advanced Drug Delivery Reviews, 143*, 68–96. doi:https://doi.org/10.1016/j.addr.2019.04.008

Nienke M. Eijkelboom, A. P. (2023). Particle structure development during spray drying from a single droplet to pilot-scale perspective. *Journal of Food Engineering, 337*, 111222. doi:https://doi.org/10.1016/j.jfoodeng.2022.111222

Noelia Campillo, B. F. (2019). Differential Oxygenation in Tumor Microenvironment Modulates Macrophage and Cancer Cell Crosstalk: Novel Experimental Setting and Proof of Concept. *Frontiers in Oncology, 9*, 1-12.

Pacheco, Y. P. (2019). *Master´s thesis, CHITOSAN CHARACTERIZATION AND APPLICATION AS A MATERIAL FOR FUTURE CANCER CELL ENCAPSULATION.* Tarragona, Spain: URV.

Park, K. G. (2005). preparation and Characterization of Drug-Loaded Chitosan–Tripolyphosphate Microspheres by Spray Drying. *DRUG DEVELOPMENT RESEARCH, 64*, :114–128. doi:https://doi.org/10.1002/ddr.10416

Pasquale Sacco, S. P. (2016). Insight into the ionotropic gelation of chitosan using tripolyphosphate and pyrophosphate as cross-linkers. *International Journal of Biological Macromolecules, 92*, 476-483. doi:https://doi.org/10.1016/j.ijbiomac.2016.07.056

Paul Kebarle, a. U. (2009). ELECTROSPRAY: FROM IONS IN SOLUTION TO IONS IN THE GAS PHASE, WHAT WE KNOW NOW. *Mass Spectrometry Reviews, 28*, 898– 917. doi:DOI 10.1002/mas

Pengfei Lu, V. M. (2021). The extracellular matrix: A dynamic niche in cancer progression. *Journal of Cell Biology., 196*(4), 295-406. doi:http://doi.org/10.1083/jcb.201102147

Peppino Mirabelli, L. C. (2019). Cancer Cell Lines Are Useful Model Systems for Medical Research. *Cancers (Basel), 11*(8), 1098.

Peter Vaupel, F. R. (1989). Blood Flow, Oxygen and Nutrient Supply, and Metabolic Microenvironment of Human Tumors: A Review. *CANCER RESEARCH, 49*, 6449-6465.

Petra Mazancová, V. N. (2018). Dissociation of chitosan/tripolyphosphate complexes into separate components upon pH elevation. *Carbohydrate Polymers, 192*, 104–110. doi:https://doi.org/10.1016/j.carbpol.2018.03.030

Philipp Seydel, J. B. (2006). Modeling Particle Formation at Spray Drying Using Population Balances. *Drying Technology, 24*, 137–146. doi:DOI: 10.1080/07373930600558912

Piotr Owczarz, P. Z. (2018). Rheo-Kinetic Study of Sol-Gel Phase Transition of Chitosan Colloidal Systems. *Polymers, 10*(47), 1-14. doi:10.3390/polym10010047

Piotr Owczarz, P. Z. (2018). Rheo-Kinetic Study of Sol-Gel Phase Transition of Chitosan Colloidal Systems. *Polymers, 10*(47), 2-14. doi:10.3390/polym10010047

Pokharkar, D. R. (2006). Studies on Effect of pH on Cross-linking of Chitosan With Sodium Tripolyphosphate: A Technical Note. *AAPS PharmSciTech, 7*(2), 1-6.

Qi Zhao Wang, X. G. (2006). Protonation constants of chitosan with different molecular weight and degree of deacetylation. *Carbohydrate Polymers, 65*, 194–201.

R. Harris, E. L.-A. (2011). Chitosan nanoparticles and microspheres for the encapsulation of natural antioxidants extracted from Ilex paraguariensis. *Carbohydrate Polymers, 84*, 803–806. doi:doi:10.1016/j.carbpol.2010.07.003

Rajasree Shanmuganathan, T. N. (2019). Chitosan nanopolymers: An overview of drug delivery against cancer. *International Journal of Biological Macromolecules*, 727–736. doi:https://doi.org/10.1016/j.ijbiomac.2019.02.060

Rawal Tejal, S. P. (2018). Chitosan nanoparticles as a promising approach for pulmonary delivery of bedaquiline. *European Journal of Pharmaceutical Sciences*, 1-50. doi:10.1016/j.ejps.2018.08.038

Rinaudo, M. (2006). Chitin and chitosan: Properties and applications. *Progress in Polymer Science, 31*(7), 603-632. doi:https://doi.org/10.1016/j.progpolymsci.2006.06.001

Rolim, D. R.-L. (2016). Chitosan-tripolyphosphate nanoparticles functionalized with a pH-responsive amphiphile improved the in vitro antineoplastic effects of doxorubicin. *Colloids and Surfaces B: Biointerfaces*, 1-35. doi:http://dx.doi.org/doi:10.1016/j.colsurfb.2016.08.014

S. Islam, M. A. (2017). Chitin and Chitosan: Structure, Properties and Applications in Biomedical Engineering. *Journal of Polymers and the Environmen, 25*, 854–866. doi:DOI 10.1007/s10924-016-0865-5

Samah A Loutfy, H. M.-D. (2016). Synthesis, characterization and cytotoxic evaluation of chitosan nanoparticles: in vitro liver cancer model. *Advances in Natural Sciences: Nanoscience and Nanotechnology, 7*, 1-9. doi:doi:10.1088/2043-6262/7/3/035008

Shameek Vats, M. A. (2021). Stable Electrospinning of Core-Functionalized Coaxial Fibers Enabled by the Minimum-Energy Interface Given by Partial Core−Sheath Miscibility. *Langmuir, 37*, 13265−13277. doi:https://doi.org/10.1021/acs.langmuir.1c01824

Shaoling Zhang, K. K. (2010). One-step preparation of chitosan solid nanoparticles by electrospray deposition. *International Journal of Pharmaceutics, 397*, 211–217. doi:10.1016/j.ijpharm.2010.07.007

Shreya Thakkar, D. S. (2020). Tumor microenvironment targeted nanotherapeutics for cancer therapy and diagnosis: A review. *Acta Biomaterialia, 101*, 43–68.

Tannock, V. V. (1997). Influence of low pH on cytotoxicity of paclitaxel, mitoxantrone and topotecan. *British Joumal of Cancer, 75*(8), 1167-1172.

Taylor, G. (1964). Disintegration of water drops in an electric field. *Proceedings of the Royal Society A: Mathematical, Physical and Engineering Sciences, 280*(1382), 383–397. doi:https://doi.org/10.1098/rspa.1964.0151

Tiyaboonchai, W. (2003). Chitosan Nanoparticles : A Promising System for Drug Delivery. *Naresuan University Journal, 11*(3), 51-66.

V. Vukovic, a. I. (1997). Influence of low pH on cytotoxicity of paclitaxel, mitoxantrone and topotecan. *British Joumal of Cancer, 75*(8), 1167-1172.

Vladimir Gogvadze, B. Z. (2010). The Warburg effect and mitochondrial stability in cancer cells. *Molecular Aspects of Medicine, 31*, 60–74. doi:10.1016/j.mam.2009.12.004

Wittaya Julklang, B. G. (2015). Effect of process parameters on energy performance of spray drying with exhaust air heat recovery for production of high value particles. *Applied Energy, 151*, 285–295. doi:http://dx.doi.org/10.1016/j.apenergy.2015.04.069

Xavier Montané, A. B.-V. (2020). Encapsulation for Cancer Therapy. *Molecules, 25*(1605), 1-25. doi:10.3390/molecules25071605

Xiao Dong Xu, S. X. (2015). Warburg Effect or Reverse Warburg Effect? A Review of Cancer Metabolism. *Oncology Research and Treatment, 38*, 117–122. doi:10.1159/000375435

Xingzhen Zhanga, X. Y. (2016). Tumor targeting strategies for chitosan-based nanoparticles. *Colloids and Surfaces B: Biointerfaces, 148*, 460–473. doi:http://dx.doi.org/10.1016/j.colsurfb.2016.09.020

Xu, Y. &. (2007). Electrosprayed bovine serum albumin-loaded tripolyphosphate cross-linked chitosan capsules: Synthesis and characterization. *Journal of Microencapsulation, 24*(2), 143–151.

Yasumasa Kato, S. O. (2013). Acidic extracellular microenvironment and cancer. *Cancer Cell International*, 1-8.

Yixiang Xu, M. A. (2008). Electrosprayed bovine serum albumin-loaded tripolyphosphate cross-linked chitosan capsules: Synthesis and characterization. *Journal of Microencapsulation*, 143–151.

Yu Zhang, M. Y. (2008). Zeta potential: a surface electrical characteristic to probe the interaction of nanoparticles with normal and cancer human breast epithelial cells. *Biomedical Microdevices, 10*, 321–328. doi:10.1007/s10544-007-9139-2

Yuan Gao, Y. B.-W.-S. (2015). Tuning Microparticle Porosity during Single Needle Electrospraying Synthesis via a Non-Solvent-Based Physicochemical Approach. *Polymers, 7*, 2701–2710. doi:10.3390/polym7121531

Yuhang Cai, ,. Y. (2014). Formation and dissolution of chitosan/pyrophosphate nanoparticles: Is the ionic crosslinking of chitosan reversible? *Colloids and Surfaces B: Biointerfaces, 115*, 100-108. doi:https://doi.org/10.1016/j.colsurfb.2013.11.032

Zahir., S. H. (2013). Effect of Zeta Potential on the Properties of Nano-Drug Delivery Systems - A Review (Part 2). *Tropical Journal of Pharmaceutical Research, 12*(2), 265-273. doi:http://dx.doi.org/10.4314/tjpr.v12i2.20

Zeng-liang Zhan, L.-j. L.-r.-h.-c. (2020). Preparation and properties of chitosan-based microspheres by spray drying. *food science & nutrition technology*, 1933–1941. doi:10.1002/fsn3.1479

UNIVERSITAT
ROVIRA i VIRGILI